Linearization Techniques to Suppress Optical Nonlinearity

A Thesis Submitted for the Degree of Doctor of Philosophy

In

Wireless Communication Networks

By

Farbod Tabatabai

Supervisor

Professor: Hamed. S. Al-Raweshidy

School of Engineering & Design
Brunel University

September 2008

Linearization Techniques to Suppress Optical Nonlinearity

School of Engineering & Design
Brunel University

September 2008

Student's Name: Farbod Tabatabai

Signature of Student: _____

Declaration: I have read and I understand the dissertation guidelines on plagiarism and cheating, and I certify that this submission fully complies with these guidelines.


بسم الله الرحمن الرحيم

ABSTRACT

This thesis is shown the implementation of the linearization techniques such as feed-forward and pre-distortion feedback linearization to suppress the optical components nonlinearities caused by the fibre and semiconductor optical amplifier (SOA).

The simulation verified these two linearization techniques for single tone direct modulation, two tone indirect modulation and ultra wideband input to the optical fibre. These techniques uses the amplified spontaneously emission (ASE) noise reduction in two loops of SOA by a feed-forward and predistortion linearizer and is shown more than 6dB improvement. Also it investigates linearization for the SOA amplifier to cancel out the third order harmonics or inter-modulation distortion (IMD) or four waves mixing. In this project, more than 20 dB reductions is seen in the spectral re-growth caused by the SOA. Amplifier non-linearity becomes more severe with two strong input channels leading to inter-channel distortion which can completely mask a third adjacent channel. The simulations detailed above were performed utilizing optimum settings for the variable gain, phase and delay components in the error correction loop of the feed-forward and Predistortion systems and hence represent the ideal situation of a perfect feed-forward and Predistortion system. Therefore it should be consider that complexity of circuit will increase due to amplitude, phase and delay mismatches in practical design.

Also it has describe the compatibility of Software Defined Radio with Hybrid Fibre Radio with simulation model of wired optical networks to be used for future research investigation, based on the star and ring topologies for different modulation schemes, and providing the performance for these configurations.

ACKNOWLEDGMENTS

First, I would like thank my advisor Prof. Hamed S. Al-Raweshidy, for providing constant encouragement, valuable advice, and an enjoyable working environment during my Ph. D. studies.

I would like to express particular gratitude to Toktam Nezakati my lovely wife for the love, encouragement, and unending support.

DEDICATION

I dedicate this work to my Wife

ABBREVAIATIONS

16-QAM	16-Quadrature Amplitude Modulation
2G	Second Generation
3G	Third Generation
64-QAM	64-Quadrature Amplitude Modulation
AGC	Automatic Gain Control
AM	Amplitude Modulation-Subcarrier Multiplexing
AM	Amplitude Modulation
AM/AM	Amplitude Modulation to Amplitude Modulation
AM/PM	Amplitude Modulation to Phase Modulation
AM-SCM	Amplitude Modulation-Subcarrier Multiplexing
ASE	Amplified Spontaneous Emission
ASIC	Application Specific Integrated Circuit
ATM	Asynchronous Transfer Mode
ATT	Attenuator
BBI	Balance Bridge Interferometer
BER	Bit Error Rate
BL	Bit rate distance product
BPF	Band Pass Filter
BPSK	Binary Phase Shift Keying
CATV	Cable Television
CBS	Central Base Station
CD	Compatible Disk
CDMA	Code Division Multiple Access
CDMA	Code Division Multiple Access
CMOS	Complementary Metal Oxide Semiconductor
CS	Central Station
CW	Continuous Wave
DFB	Distributed Feedback
DFB	Distributed Feedback Laser
DSP	Digital Signal Processing
E/O	Electrical to Optical
EVM	Error Vector Magnitude
FAR	Flexible Architecture Radio
FBG	Fiber Bragg Grating
FCC	Federal Communications Commission
FDM	Frequency Division Multiplexing
FDMA	Frequency Division Multiple Access
FP	Fabry Perot
FPGA	Field Programmable Gate Array
FWHM	Full Width at Half Maximum
FWM	Four Wave Mixing
GPRS	General Packet Radio Service

GSM	Global System for Mobile Communication
GSM	Global System Mobile
GVD	Group Velocity Dispersion
HD2	Second Harmonic Distortion
HD3	Third Harmonic Distortion
HFR	Hybrid Fibre Radio
I/Q	In phase/Quadrature Phase
IEEE	Institute of Electric and Electronic Engineering
IF	Intermediate Frequency
IM	Inter Modulation
IM3	Third Order Inter Modulation
IMD	Inter Modulation Distortion
IP3	Third Order Intercept Point
IR-UWB	Impulse Radio-Ultra Wide Band
ITU	International Telecommunication Union
LAN	Local Area Network
LNA	Low Noise Amplifier
LO	Local Oscillator
LUT	Look up Table
MAN	Metropolitan Area Network
MONET	Multi-Wavelength Optical Network
MQW-EA	Multi Quantum Well-Electro Absorption
MST	Multi Standard Radio
MZM	Mach-Zehnder Modulator
ND:YAG	Neodymium-Doped Yttrium Aluminium Garnet
NZDSFs	Nonzero Dispersion Shifted Fibres
O/E	Optical to Electrical
OFDM	Orthogonal Frequency Division Multiple
OH	Hydroxyl
OPDFB	Optical Predistortion Feedback
OSNR	Optical Signal to Noise Ratio
OSSB+C	Optical Signal Sideband with Carrier
PA	Power Amplifier
PD	Predistortion
PN	Pseudo Random Noise
PONs	Passive Optical Networks
PPM	Part per Million
PRBS	Pseudo Random Binary Sequence
PSK	Phase Shift Keying
QAM	Quadrature Amplitude Modulation
QPSK	Quadrature Phase Shift Keying
RF	Radio Frequency
RIN	Relative Intensity Noise
RMS	Root Mean Square
RoF	Radio over Fibre
RZ	Return Zero

SBR	Signal to Background Noise Ratio
SC	Subcarrier
SDH	Synchronous Digital Hierarchy
SDR	Software Defined Radio
SMF	Single Mode Fibre
SNR	Signal to Noise Ratio
SOA	Semiconductor Optical Amplifier
SPM	Self Phase Modulation
TAT-8	8th Transatlantic Telephone Cable
TCP-IP	Transmission Control Protocol-Internet Protocol
TD	Time Delay
TDM	Time Division Multiplexing
TDMA	Time Division Multiple Access
TEF	Transverse Electric Field
TMF	Transverse Magnetic Field
TW	Travelling Wave
TWT	Travelling Wave Tube
UWB	Ultra Wide Band
VCO	Voltage Control Oscillator
WAN	Wide Area Network
WCDMA	Wideband Code Division Multiple Access
WDM	Wavelength Division Multiplexing
WDM	Wavelength Division Multiplexer
WDMA	Wavelength Division Multiplexing Access
WGR	Wave Guide-Grating Router
WIMAX	Worldwide Interoperability for Microwave Access
XPM	Cross Phase Modulation

Mathematical and Greece Symbols

α	Line width enhancement factor
α_{int}	Internal losses
β	Propagation constant
β_c	Enhancement factor
Γ	Radiation confinement factor
δ_x	Power penalty for mth channel
η_m	Quantum efficiency
$\Delta\theta(t)$	Phase difference
λ_1	1st Channel Frequency Wave length
λ_2	2nd Channel Frequency Wave length
λ_{FWM1}	$2\lambda_1 - \lambda_2$ FWM1 Wave length
λ_{FWM2}	$2\lambda_2 - \lambda_1$ FWM2 Wave length
μ	Mean of the Gaussian distribution
π	Pi constant
σ	Standard deviation
σ_g	Differential Gain
σ_m	Cross sectional area
τ	Effective spontaneous carrier lifetime
$\Delta\tau$	Error path delay
τ_c	Carrier life time
ϕ	Unsaturated device phase delay
$\Delta\phi$	Phase difference
ϕ_c	Phase of the carrier
φ	phase
$\Delta\varphi(t)$	Signal phase change
ψ_m	Phase lag
ω	angular frequency
ω_c	carrier frequency
ω_j	Carrier frequency of the jth channel
Ω_{jk}	Beat Frequency
ω_m	Modulation frequency
A	Gain of the main amplifier
a	Distortion component
A_1	Field gain at quiescent point
A_F	Amplitude of the FWM component
A_j	Amplitude of the jth signal
B	beta
B_N	nth order of Bessel polynomial

B_r	Bit rate
c	Speed of light
C_1	Coupling factor
C_2	Coupling factor
c.c.	Complex Conjugate
d_F	Degeneracy factor
DV_{in}	Detected Input Signal
DV_{out}	Detected Output Signal
$E(t)$	Normalized optical field signal
e_A	Field output from the amplifier
e_d	Distorted optical field
e_{error}	Error signal
E_{in}	Amplitude optical field
e_{in}	Input electric field
E_{sat}	Saturation energy
f_c	Cut off frequency
F_n	Noise figure
fw_b	Normalized 3db band width
G	Gain
G_0	Unsaturated field gain
g_0	Unsaturated gain coefficient
$G_{FP}(v)$	Amplification factor of Fabry Perot interferometers
h	Plank's constant
$h(\tau)$	Total Integrate Gain
I	Incident optical power
$i(t)$	Electrical current
I_{ch}	Current at each channel
I_D	Decision threshold
$I_{k-out}(t)$	Amplitude of output signal
$i_s(t)$	Photo current
$i_{th}(t)$	Thermal noise current
$i_{sh}(t)$	Shot noise current
I_x	Crosstalk contribution
L	Cavity length
L_{eff}	Effective length
M	Number of Channel
N	Carrier population
N_0	The value of N required of transparency
N_1	Atomic Population for the Ground State

N_2	Atomic Population for the Excited State
N_b	Steady state value at the bias current
n_m	Small changes occurring
N_{sh}	Power spectral density
$p(t)$	Ideal Gaussian pulse wave form
P_{ch}	Single channel input power
p_m	Power in the mth channel
P_S	Saturation power
q	Electric charge
$Q(t)$	Electrical input signal
$Q_{k-out}(t)$	Amplitude of output signal
R	Normalized Amplitude of output signal
r	responsibility
R_1	Facet reflectivity
R_2	Facet reflectivity
R_m	Photo detector responsively
$s(t)$	Pulse train
SC	Sub carrier
SF	Symmetry factor
T	Pulse repetition interval
T_{mn}	Filter transmittivity for channel n
T_w	Global parameter time window
V_e	Error Signal
v_g	Group velocity
$v_I(t)$	I quadrature component
V_{in}	Input Signal
Δv_L	Longitudinal mode
v_m	Cavity resonance frequency
V_{nl}	Nonlinear transfer function
V_{out}	Output Signal
$v_Q(t)$	Q quadrature component
V_{ref}	Linear Phase and Amplitude Adjusted of V_{in}

Contents

List of Figures

List of Tables

List of Publications

Patents

1) U.S. Patent Application No. 11,845,606, entitled “Radio Frequency Power Combining”
2) US Provisional Patent Application No: 61223156, entitled “Feed-Forward Linearization Technique to Suppress the Non-Linearity Distortion in Semiconductor Optical Amplifier”
3) US Provisional Patent Application No: 61223296, entitled “Noise reduction with the use of Optical Predistortion Feedback Linearization Technique”

Journals

1) F. Tabatabai, H. S. Al-Raweshidy, “Feed-Forward Linearization Technique for Reducing Non-Linearity in Semiconductor Optical Amplifier,” *J. Lightw. Technol.*, Vol.25, No. 9, pp.2667-2674, Sep. 2007.
2) F. Tabatabai, H. S. Al-Raweshidy, “Feed-Forward Linearization Technique for Impulse Radar Ultra Wideband over Fiber,” *IET Microw. Antennas Propag.*, Vol.3, Issue 7, pp.1060-1068, Oct. 2009.

Conferences

1) F. Tabatabai, H. S. Al-Raweshidy, “Reducing Nonlinearity for Impulse Radar Ultra Wideband over Fibre using Analogue Feedback linearization”, APMC2008, Hong Kong
2) F. Tabatabai, H. S. Al-Raweshidy, “Optical Predistortion Feedback Linearization for suppressing the Nonlinearity in Optical Amplifier”, APMC2008, Hong Kong
3) F. Tabatabai, H. S. Al-Raweshidy, “Feed-Forward Linearization for Fibre

Optic Application using Semiconductor Optical Amplifier", APMC2007, Thailand

4) F. Tabatabai, H. S. Al-Raweshidy, "Linearity Improvement for Impulse Radar Ultra Wideband over Fibre", APMC2007, Thailand

5) F. Tabatabai, H. S. Al-Raweshidy, "C and Ka-Band Wide Bandpass Filter Using LTCC Technology", APMC2007, Thailand

6) F. Tabatabai, H. S. Al-Raweshidy, **"**Performance Evaluation for WLAN and UWB Using Radio over Fibre", EUMW2006, Manchester

CHAPTER 1

INTRODUCTION

1.1 Motivation

The optical signals require linear processing in modern optical architectures and this includes the optical amplifier in the optical link. In addition to linearity, the optical amplifier must also be power efficient, and cost efficient. This thesis is shown the implementation of the linearization techniques such as Feed-Forward and Pre-Distortion Feedback linearization to suppress the optical components nonlinearities caused by the fibre and semiconductor optical amplifier. Also it describes the compatibility of these linearization techniques with multi-standard over fibre with simulation model of wired optical networks to be used for future research investigation. The optical networks are based on the star and ring topologies for different modulation schemes, and providing the performance for these configurations.

1.2 Research Challenges (contribution)

The most important aspect of this project is based on wired infra structure. Radio over Fibre (RoF) provides an excellent link for high bandwidth communication. On the other hand, when the wireless link co-exists with the RoF link especially in a multi user environment a nonlinear distortion of the RoF link, due to the laser and optical amplifier, becomes the primary concern.

The project investigates the non-linearity and noise cancellation produced by fibre and semiconductor optical amplifier (SOA). Two techniques from the electrical domain is adapted and applied in the optical domain. The two linearization techniques are known as the Feedforward and Predistortion Feedback linearization. These techniques are explained in chapter 4.

These techniques applied for the different RF sources such as continuous wave (CW) and ultra wideband (UWB). Also four different modulation schemes based on orthogonal frequency division multiplex (OFDM) are multiplexed and amplified by SOA, then the feedforward linearization technique is applied, which is shown a great distortion reduction in chapter 5. The main contribution is shown below with dedicated chapter:

- Acceptable Linearity by harmonic cancellation (chapter 4)
- Acceptable Linearity by ASE cancellation (chapter 4)
- Analogue Feed-Forward linearization for improving linearity in optical amplifier (chapter 4)
- Analogue Predistortion Feedback linearization for improving linearity in optical amplifier (chapter 4)
- Performance of the Multicarrier Signals over Fiber (chapter 5)
- Analogue Feed-Forward linearization for improving linearity in WDM (chapter 5)

1.3 Organization of Thesis

Chapter 1: This section will give an overview to the project object and also a brief description to each chapter.

Chapter 2: Provides a review of relevant to this research topic. Practically, the literature review contains an overview of linearization problem in optical domain as

well as a brief description of developed techniques for linearizing the distortion in optical domain. Further more research challenges and contributions are mentioned.

Chapter 3: Provides a theoretical background and an overview of the history and definition of SOA, also an explanation to the SOA distortions. The SOA characterization is also is explained in this chapter.

Chapter 4: Main contribution of thesis in this chapter gives an explanation on linearization techniques. Laser and SOA cause amplified spontaneous emission (ASE) noise to the signal and also due to using multi wavelengths, four-wave mixing will exist. The main aim of this thesis is to investigate linearization of SOA using feed-forward and predistortion feedback linearization schemes to improve linearity and reduce the nonlinear distortion such as noise and four wave mixing cancellation associates with SOAs.

Chapter 5: A Wavelength Division Multiplexing (WDM) systems has been explained in this chapter. In order to ensure full flexibility in the usage and combination of current and future radio and fibre optic components, range of possible architectures will be considered in this chapter. Different modulation schemes such as binary phase shift keying (BPSK), quadrature phase shift keying (QPSK), 16 quadrature amplitude modulation (16-QAM) and 64 quadrature amplitude modulation (64-QAM) at 3.5 GHz will be considered, and a wavelength is dedicated for each of them. The multiplex wavelength is transmits and sent over fibre. At the receiver following the photo detector filters are uses to recover modulated signals. The simulation model is mainly based on the star topology. The objective is to design and optimize the system's performance by investigating the effect that the fibre will have on the system and compare the results with the linearized signal.

Chapter 6: Conclude the thesis and gives further suggestion and discussions for future works is mentioned.

CHAPTER 2

Background and Literature Review

2.1 Introduction

Radio-over-Fiber (RoF) systems are widely used for wireless communication networks and various linearization techniques have been created to reduce the nonlinear distortions generated by the use of semiconductor optical amplifier. Wavelength conversion by the four-wave mixing (FWM) effect in SOAs typically has a poor efficiency. For practical applications, the signal to background noise ratio (SBR) and the wavelength conversion range of an SOA based on FWM converters must be considerably improved [1]. The feed-forward technique is superior since it offers a large improvement in the third-order inter-modulation (IM3) components and reduces intensity noise. Pre-distortion with diodes is a simple approach, but it offers little improvement in IM3 components than the feed-forward technique [2]. Moreover, these techniques need complex control circuits to handle the temperature variation during the operation and these circuits consume a lot of power [3]. There is a strong demand for a linearizer that has a simple optical circuit configuration, a simple control circuitry, and a large improvement in IM3 components [4]. This thesis mostly investigates a RoF system with a feed-forward and predistortion linearizer to suppress the FWM and reduce the amplified spontaneous emission (ASE) noise of the system.

Today, modern communication systems use optical fibre. Hence, it is possible to transmit more data at higher data rates and preserve the quality of the signal without loss of information. In optical communication systems, digital modulation schemes where the information is carried are accessed by various systems such as time division

multiple access (TDMA), code division multiple access (CDMA) and orthogonal frequency division multiple (OFDM). In optical systems, a wide range of band-width can be used for communication; this makes optical communication popular in modern communication systems. However, the resulting signal has a high envelope peak-to-average ratio (crest factor) and linear power amplifiers with high back-off power are required in order not to degrade the quality of the signal. Linear power amplifiers that have a high back-off power and a high third order intercept point (IP3) give rise to the problem of efficiency [5]. In order to increase the linearity performance of the system, various linearization techniques such as pre-distortion, envelope elimination and restoration, Cartesian feedback, and feed-forward are used. Among these methods, feed-forward has a better linearization performance and provides a more wide-band stable operation since there is no feedback path whereas it has the limitation of efficiency [6].

The operation of the feed-forward circuit is based on the subtraction of two equal signals with subsequent cancellation of the error signal in the amplifier output spectrum, and it contains two cancellation loops. The first loop is the carrier cancellation loop, which extracts the distortion products, and the second loop is the error cancellation loop, which amplifies the distortion products and subtracts the distortion components from the main amplified signal. The amplifier used in this loop is called the error amplifier and it must be sufficiently linear in order not to introduce extra distortion products. Amplitude, phase, and delay mis-matches are the main constraints on the linearization performance of the feed-forward, and its efficiency is limited by the third intercept point (IP3) of the main and error amplifiers, losses of the couplers and delay compensators. For a complete feed-forward system with two power amplifiers and couplers, a similar closed-form expression which relates the

linearity performance to the parameters of the linearizer and signal characteristics may be required. Using such a tool system parameters can be optimized for optimum efficiency and a given linearity performance [5].

Also for the first time the application of optical predistortion feedback (OPDFB) is proposed to linearize the overall optical amplifier response so that spectral re-growth of the amplified optical modulated signal can be avoided. There is strong demand for a linearizer that has a simple optical circuit configuration, a minimal control circuit, and a large improvement in IM3 components. This thesis also investigates a simple and low cost method using OPDFB linearization to suppress the FWM and reduce the ASE noise due to the semiconductor optical amplifier used in Radio-over-Fiber (RoF) systems.

A promising technique to remove the drawbacks of the RF linearization technique is, predistortion (PD). The PD based on error feedback correction is a powerful linearization technique because the error correction is insensitive to amplifier variations, such as temperature, supply voltage, and device variations, as well as nonlinear characteristics of the PA. Among the PD linearization techniques, the lookup table (LUT)-based PD has been widely used because it is relatively simple and easily implemented to build the inverse function of PAs. In the PD algorithms that provide the inverse function of the amplitude and phase distortions (AM/PM) generated by the PAs, the basic and most important issue is that the estimation error. The difference between the desired and the estimated values, should reach the minimum value for a given input signal.

Most of the work that has been done on the linearization in optical domain were applied for laser linearization, to the best knowledge of the author there is no work on

optical amplifier using feedforward and predistortion techniques. In this chapter some of the works that have been done on laser linearization is presented.

2.2 Optical Linearization Techniques

The demonstration of an external modulator was illustrated in [7] using an auxiliary externally modulated laser and the second output port of the main balanced bridge interferometer (BBI) modulating device in order to derive the error signal. A practical implementation of the feedforward method is shown in Fig. 2.1. Gain units and delay lines are included, the comparators are realized as a broad-band 180 RF hybrids and the optical correction signals are injected by means of fibre-optic couplers. As explained below, the auxiliary lasers must be of the distributed feedback laser (DFB) type and tuned to a wavelength different from the solid laser wavelength to prevent coherent interference, and are driven by their respective RF drivers.

When a dual output BBI modulator is used as in the figure, feedforward correction must be applied to each output separately, doubling the amount of broad-band circuitry. In order to take advantage of all available optical power, both output ports of the combining couplers are used, thus there are four output fibres, which reduces the power per fibre, for a given Nd:YAG laser source.

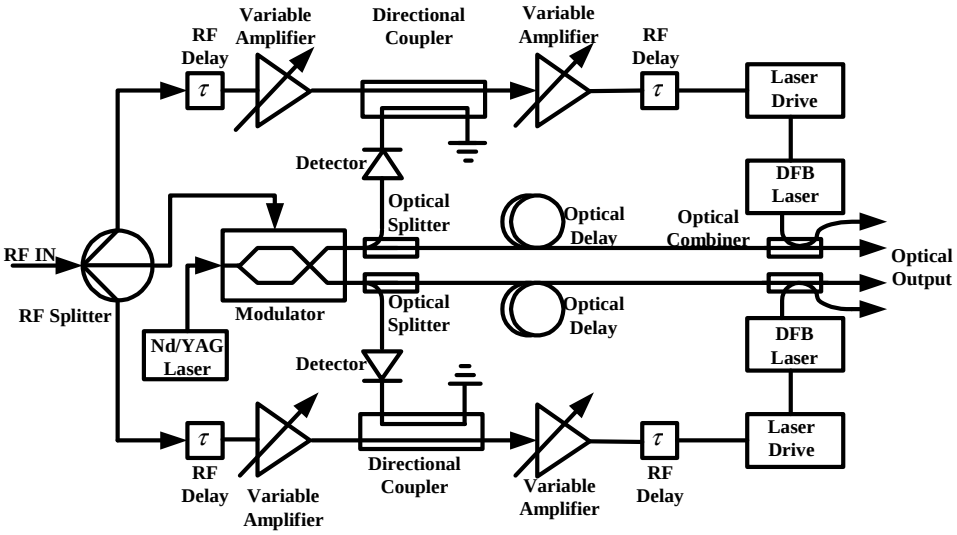

Figure 2.1 Feedforward linearization [7]

Feedforward scheme to eliminate harmonic distortion and reduce laser relative intensity noise (RIN) presented in [8] is utilized to meet CATV specifications with noisy but low-cost Fabry-Perot lasers. The optical feedforward transmitter consists of two loops (Fig.2.2). Loop #1 creates the error signal for linearization. Loop #2 conditions the error signal and converts it to light. The primary signal and the error components are combined and travel down the fibre at slightly different wavelengths. To reduce the noise created by optical reflections optical isolators were connected to the laser outputs. Without isolators the measured noise was found to be periodic with frequency and varied greatly with the quality of optical splices. In loop #1 the input signal is split between the primary laser and an RF variable amplitude and delay arm. The RF arm consists of a variable delay unit, a delay line and attenuators. The output of the primary laser was split through a 50:50 optical coupler between an optical receiver and optical delay line. The optical receiver was specially designed to provide a broadband a low-noise output signal. A 180 degree phase shift was included with the optical receiver. Although the 50:50 optical coupler reduces the available optical

power on the network, this isn't seen as a problem since Fabry-Perot lasers with output powers in excess of 25 mW are commercially available. The high coupling ratio, on the other hand, was necessary to avoid high amplification ratios for the RF amplifiers behind the detector of the first loop. The signals of the optical receiver and the variable amplitude and delay were subtracted using a power combiner. The output of the power combiner ideally should consist only of nonlinear products and the detected noise of the primary laser. The phasor sum at the combiner output includes the nonlinear products and the differences in the phase and amplitude of the two arms of the loop, the cancellation of the fundamental components is not complete. Broadband amplitude and phase matching of the two arms of the loop is not a trivial problem and can dramatically limit the performance of the transmitter.

In loop #2, the error signal passes amplifier and a delay line prior to modulating the second laser. A power amplifier is used in the amplitude and phase matching arm (in front of laser#2) to minimize the potential for additional distortion. The output of the optical delay line and error signal were combined with a 73:27 optical coupler and fed into the network. In the test circuit, instead of the network we have connected the receiver through a short length of fibre. In this receiver diode the error signal, the inverted nonlinear products as well as the inverted noise, and the output of the primary laser, the fundamentals plus the nonlinear products and noise of the primary laser, are vector summed and ideally cancel. It is demonstrated that an average of l0 dB noise reduction can be achieved over a frequency range of up to 400 MHz. The disadvantage of this technique is to converting the signal twice to optical and back to electrical. Also in the second loop laser no 2 has to be linear to achieve acceptable noise reduction.

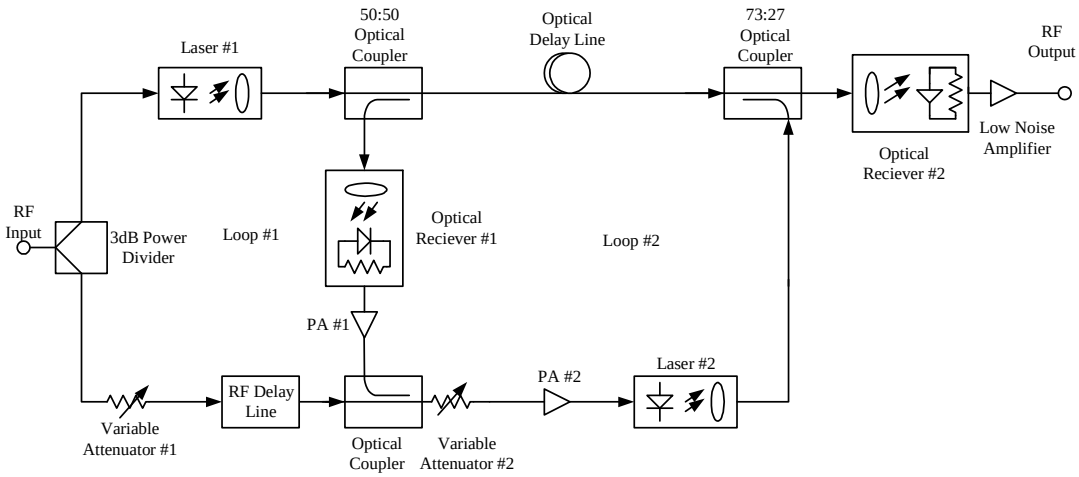

Figure 2.2 Optical Feedforward Transmitter [8]

An amplitude modulation-subcarrier multiplexing (AM-SCM) optical transmitter based on external modulation with multi quantum well - electroabsorption (MQW-EA) modulator has been illustrated in [9]. Figure 2.3 shows the experimental setup constructed for 42 channels AM transmission. At the optical splitter (a) one part (fractional power ratio α) of the light output from the modulator is split and after O/E conversion, only the error signal (i.e. signal distortion and noise) is output by the electrical subtracter (b) as the difference from the original frequency-division-multiplex (FDM) signal. A DFB laser (the second DFB laser) is modulated by the error signal. At the optical coupler (c) the light output is combined (coupled power ratio β) in anti-phase with the main signal light output from the modulator. This eliminates the signal distortion in the main signal light. This method is also the same as previous one has the same problems.

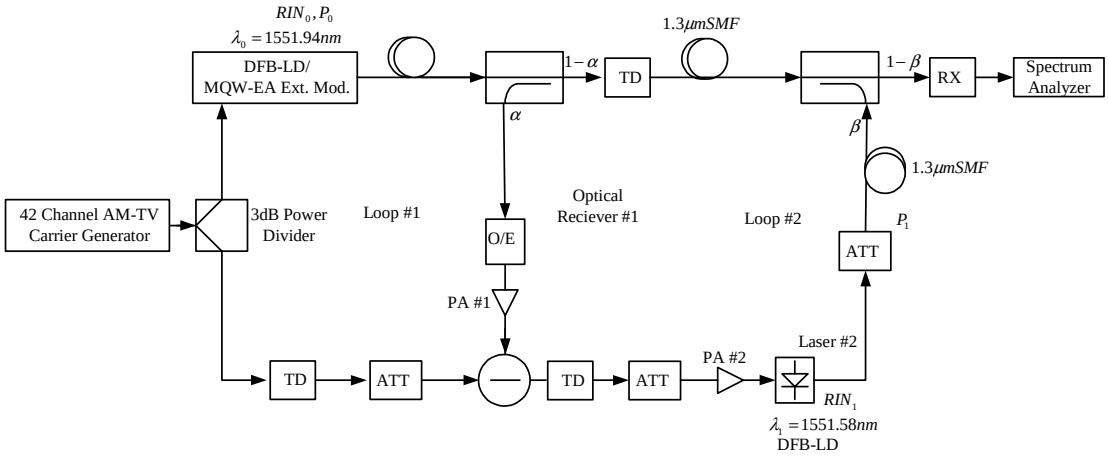

Figure 2.3 The experimental setup for 42 channels AM optical transmitter. TD: time delay, ATT: attenuator. Notations of the other symbols are shown in the text [9]

Figure 2.4 shows the block diagram of a typical externally modulated fibre-optic transmitter with parametric linearity feedback control. The linearizer has an arcsine transfer function that is the inverse of the raised cosine transfer function of the modulator. The purpose of the local feedback loop is to stabilize the transmitter against long term drifts of the modulator bias point or circuit component values. Such variations may be caused by thermal drift or device degradation.

The arcsine circuit presented in [10] generates odd harmonics that cancel those of the modulator biased at the quadrature point. Traditionally, such circuits have been realized using diodes or bipolar transistors, taking advantage of their exponential transfer characteristics to generate odd-order harmonics. Field-effect devices, such as CMOS, have been shunned due to inadequate high-frequency trans-linear performance and lack of suitable circuit architecture [10].

Two-tone IMP3 measurement of an experimental fibre-optic link employing the linearization circuit shows 14 dB improvement of the link SFDR at 1 GHz from 85 to 99 dBc/Hz .

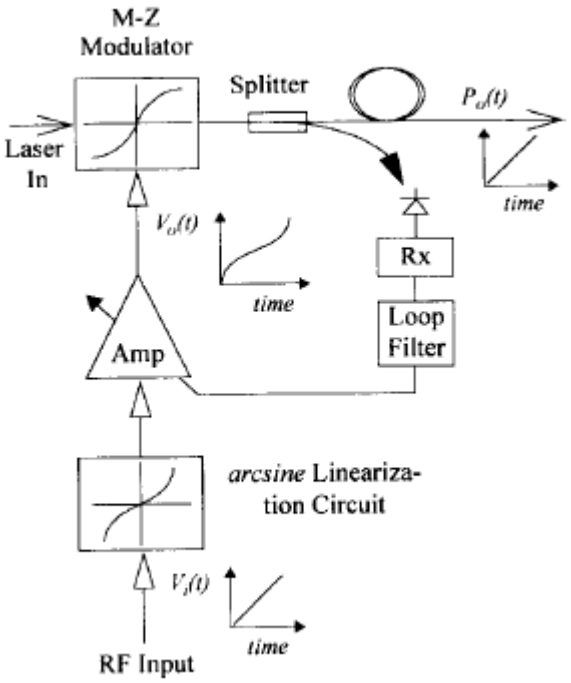

Figure 2.4 Typical linearized externally modulated fibre-optic transmitter with parametric feedback control [10]

Figure 2.5 shows a linearized link illustrated in [11] that uses a commercial lithium niobate MZ modulator with a single travelling-wave RF electrode and a single bias electrode. The MZ simultaneously modulates two wavelengths, and a wavelength division multiplexer (WDM) routes the modulated carriers to separate detectors whose outputs are combined in an RF hybrid coupler.

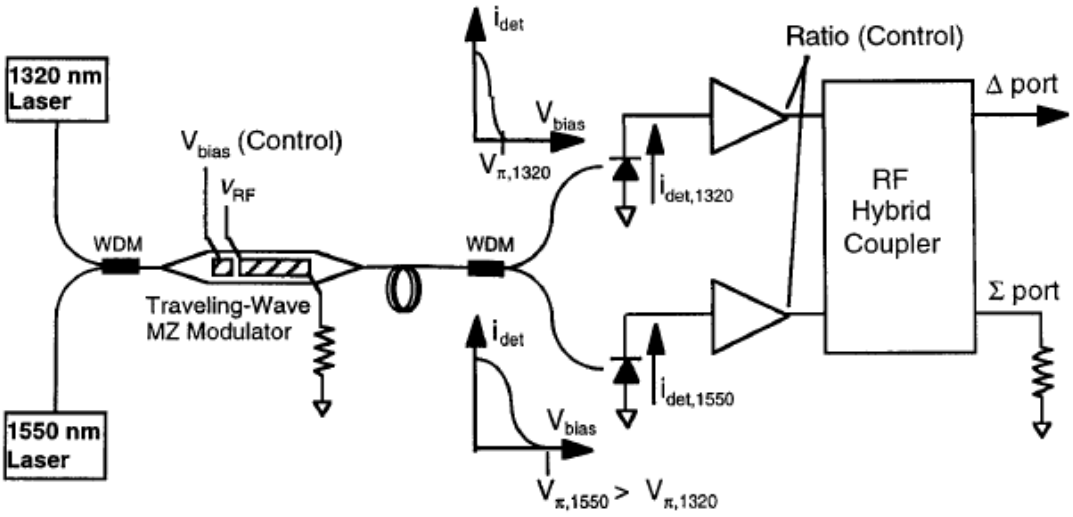

Figure 2.5 Two-wavelength broadband linearization architecture Second- and third-order distortion are simultaneously minimized by control of the modulator bias and the ratio of signal powers carried by the two optical wavelengths [11]

The simulator an ideal predistorter configuration has illustrated in [12]. The circuit consists of two parts: a linear part (a time delay line) and a nonlinear part. The latter is further on subdivided into second-order and third-order paths. Portions of the RF-input signal are extracted to feed both the quadratic-law $(X^2)$and cubic-law (X^3) generators. The two generated correction signals, with amplitude and phase suitably adjusted through a chain of shaping block, are then recombined with the original delayed RF-signal and sent to the laser. In this way the circuit can simultaneously compensate second- and third-order distortions. To feed and recombine the linear and non-linear paths of the predistorter, 10 dB and 3 dB splitters/combiners have been adopted. The (X^2)-device can be realized with a couple of diodes in push-push configuration, fed with two 180- degree shifted inputs. To have a large operational frequency range a differential amplifier has been used to realize the input 180 degrees phase-shift. The (X^3)-device can be also realized with a couple of diodes, but in a push-pull configuration and with no input phase-shift. The functionality of the

shaping chains is to generate correction signals having the same amplitudes of the distortion components generated by the laser, in a frequency range as wide as possible.

To this aim two LNAs have been inserted after the nonlinear generators to adjust the amplitude level of the drawn correction signals, which suffer an overall attenuation of about 30 dB due to the input and output splitters and combiners; a fine control on the amplitude level can be assured by variable attenuators. Also a fine phase-adjustment stage, to match the laser harmonic phase variations, has been inserted in both the non-linear paths. Finally, frequency-tilt shaping networks have been implemented to let the correcting signals match the laser HD2 and HD3 curves in the whole operational band.

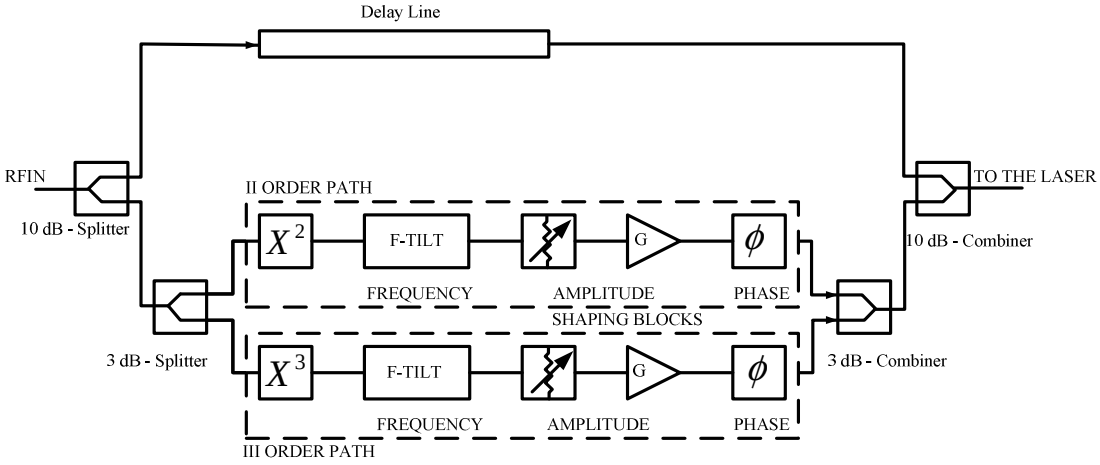

Figure 2.6 pre-distorter schematic [12]

The down-conversion and simultaneous linearization of microwave frequency signals using photonic in-phase and quadrature detection with digital demodulation has illustrated in [13]. Suppression of third-order inter-modulation products by 20 dB is obtained.

Figure 2.7 illustrates the experimental test system. A two-tone microwave test signal is generated by combining the outputs from two independent frequency synthesizers. Typically, test frequencies *f*1, *f*2, in the vicinity of 10 GHz have been used, although the technique has demonstrated up to 18 GHz. The two microwave signal paths are isolated to ensure that any spurious inter-modulation products are suppressed by >80 dB. The two-tone signal is applied to the optical carrier via a broadband phase modulator. The second phase modulator, which is used to apply the microwave down-conversion reference frequencies. Two frequencies are used: The first, referred to as the ½LO, is at approximately half the frequency of the test signals to be down-converted and is generated directly by a microwave frequency synthesizer at $f_0/2$. The second, f_0 referred to as the local oscillator (LO), is obtained by doubling the ½LO and amplifying. Variable attenuators and a variable delay are provided for optimizing the down-conversion efficiency.

The *I*/*Q* demodulated power spectrum is nearly distortion-product free with a signal-to-spur ratio improvement of approximately 20dB. However, there is external LO circuitry required for this technique.

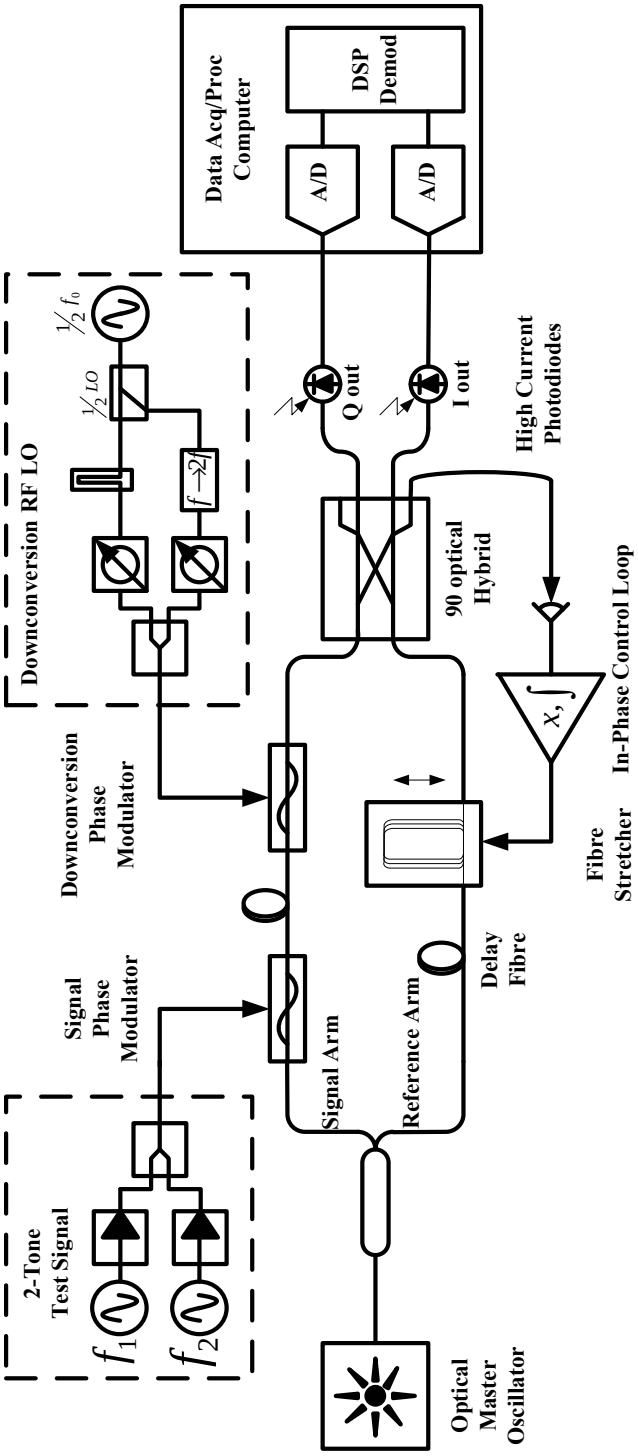

Figure 2.7 Experimental test link, consisting of a homodyne interferometer configured for optical quadrature (Q) and in-phase (I) outputs for digital linearization. Full I/Q photonic down conversion of the phase-modulated X-band test signals is implemented via simultaneous phase modulation at a nearby reference frequency $(f_0 \approx 10GHz)$ and its first sub-harmonic [13]

The linearization technique with the capability to support baseband transmission is schematically shown in Fig. 2.8 and illustrated in [14], and is based on the removal of the optical components in the vicinity of the optical carrier generated from the optical single sideband with carrier (OSSB+C) modulator. The optical carrier is split into two paths: one where the OSSB+C signal is generated, and the other remaining un-modulated. At the output of the modulator, the optical carrier and the nearby components are removed using a narrowband fibre Bragg grating (FBG).

The filtered signals are then recombined with the optical carrier from the other path with its phase and amplitude adjusted to optimize the received signals. The optical carrier removed from the top arm can be re-used to transmit baseband data for serving other access networks such as passive optical networks (PONs). A proof-of-concept experiment was carried out based on Fig.2.8 for the transmission of three unequally spaced RF tones at 27.5, 27.505 and 27.52 GHz, and a baseband data at 2.5 Gb/s.

Experimental results is shown more than 9 dB improvement in the carrier to interference ration of the three tone RF signals with simultaneous error free 2.5 Gb/s baseband transmission. The carrier re-use scheme is quantified as a function of total RF channels, amplitude and channel spacing. It is found that as the number of RF channels increases at a fixed total input RF power, the baseband performance improves with RF channel spacing. But the improvement is not high enough on this technique; it must be more than 20 dB IMD reduction to consider it as a high performance linearization technique.

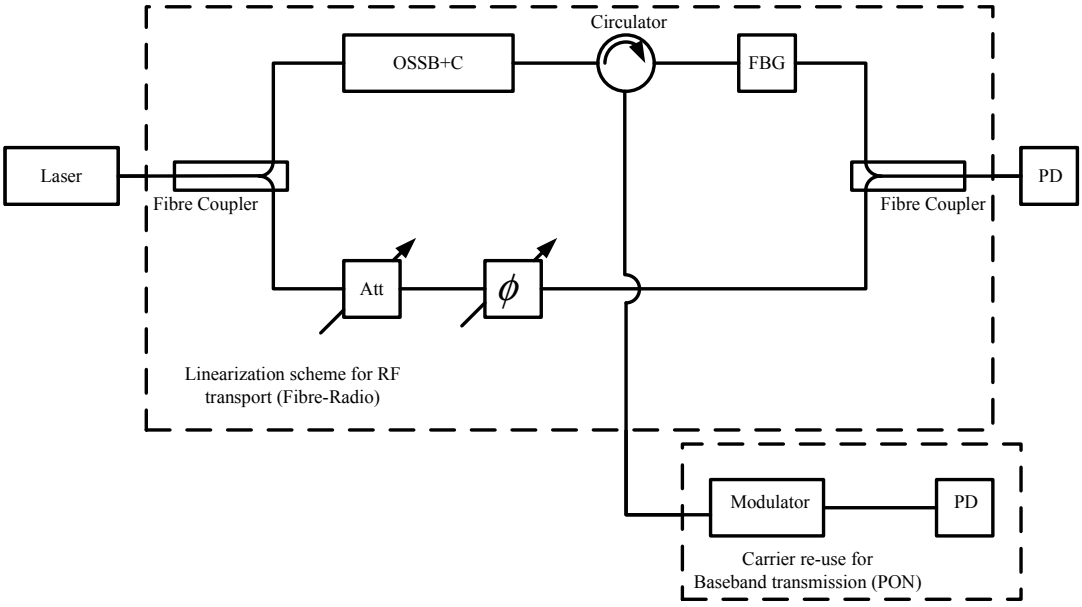

Figure 2.8 Schematic of proposed linearization technique with simultaneous baseband transmission [14]

2.3 Summary

This chapter has described the optical linearization techniques, which they are mostly applied to the laser. The demonstration of an external modulator was illustrated using an auxiliary externally modulated laser and the second output port of the main BBI modulating device in order to derive the error signal. In order to take advantage of all available optical power, both output ports of the combining couplers were used, thus there are four output fibres, which reduces the power per fibre. Feedforward scheme to eliminate harmonic distortion and reduce laser RIN presented is utilized to meet CATV specifications with noisy but low-cost Fabry-Perot lasers. The disadvantage of this technique is to converting the signal twice to optical and back to electrical. An AM-SCM optical transmitter based on external modulation with MQW-EA modulator has been illustrated. The externally modulated fibre-optic transmitter with parametric linearity feedback control has also been illustrated. Then the linearizer that has an arcsine transfer function which is the inverse of the raised cosine transfer function of

the modulator. Field-effect devices, such as CMOS, have been shunned due to inadequate high-frequency trans-linear performance and lack of suitable circuit architecture. Next the down-conversion and simultaneous linearization of microwave frequency signals using photonic in-phase and quadrature detection with digital demodulation was illustrated. The *I*/*Q* demodulated power spectrum is nearly distortion-product free with a signal-to-spur ratio improvement of approximately 20dB. However, there is external LO circuitry required for this technique. Finally the linearization technique with the capability to support baseband transmission was shown schematically, and is based on the removal of the optical components in the vicinity of the optical carrier generated from the OSSB+C modulator. But the improvement is not high enough on this technique; it must be more than 20 dB IMD reduction to consider it as a high performance linearization technique.

CHAPTER 3

Semiconductor Optical Amplifier

3.1 Introduction

All lasers act as amplifiers close to but before reaching threshold, and semiconductor lasers are no exemption. Indeed, research on SOAs started soon after the invention of semiconductor lasers in 1962. However, it was only during the 1980s that SOAs were developed for practical applications, motivated largely by the lightwave systems [15]-[19]. Although, with the advent of the doped-fibre and Raman amplifiers, SOAs are rarely used for fibre-loss compensation in lightwave systems, they are often used for signal processing. This section focuses on the characteristics of SOAs and their applications.

3.2 Amplifier Design

Optical amplifier without feedback is called travelling-wave (TW) amplifier, which emphasize that the amplified signal travels in the forward direction only. Semiconductor lasers can be used as amplifiers when biased below threshold, but multiple reflections at the facets must be included. Such amplifiers are called Fabry Perot FP amplifiers. The amplification factor is obtained by using the standard theory of FP interferometers and is given by [39]:

$$G_{FP}(\nu) = \frac{(1-R_1)(1-R_2)G(\nu)}{(1-G\sqrt{R_1R_2})^2 + 4G\sqrt{R_1R_2}\sin^2\left[\pi(\nu-\nu_m)\big/\Delta\nu_L\right]} \qquad (3.1)$$

Where R_1 and R_2 are the facet reflectivities, ν_m represents the cavity-resonance frequencies given by $2\beta L = 2m\pi$ or $\nu = \nu_m = mc\big/2\bar{n}L$, and $\Delta\nu_L$ is the longitudinal-

mode spacing, or the free spectral range, of the FP cavity. The single-pass amplification factor $G = \exp(gL)$ corresponds to that of a travelling wave (TW) amplifier when gain saturation is negligible; G_{FP} reduces to G when $R_1 = R_2 = 0$.

The amplifier bandwidth is determined by the sharpness of the FP resonance. One can calculate the amplifier bandwidth from the detuning $v - v_m$ for which G_{FP} drops by 3 dB from its peak value. The result is given by [39]:

$$\Delta v_A = \frac{2v_L}{\pi} \sin^{-1}\left(\frac{1 - G\sqrt{R_1 R_2}}{\left(4G\sqrt{R_1 R_2}\right)^{1/2}} \right) \tag{3.2}$$

To achieve a large amplification factor, $G\sqrt{R_1 R_2}$ should be quite close to 1. As seen from Eq. (3.2), the amplifier bandwidth is a small fraction of the free spectral range of the FP cavity (typically, $\Delta v_L \approx 100GHz$ and $\Delta v_A < 10GHz$). Such a small bandwidth makes FP amplifiers unsuitable for most lightwave systems.

Travelling-wave operation of SOAs can be realized if the reflection feedback from the end facets is suppressed. A simple way to reduce the reflectivity is to coat both facets with an antireflection coating. However, the residual reflectivity of the coated facet must be extremely small (<0.1%) for an SOA to act as a travelling-wave amplifier. Furthermore, the minimum reflectivity depends on the amplifier gain itself. One can estimate that the minimum reflectivity depends on the amplifier gain itself. The tolerable value of the facet reflectivity can be estimates by considering the maximum and minimum values of G_{FP} from Eq. (3.1) near a cavity resonance. It is easy to verify that their ratio is given by:

$$\Delta G = \frac{G_{FP}^{\max}}{G_{FP}^{\min}} = \left(\frac{1 + G\sqrt{R_1 R_2}}{1 - G\sqrt{R_1 R_2}} \right)^2 \tag{3.3}$$

If ΔG exceeds 3 dB, the amplifier bandwidth is set by the activity resonances rather than by the gain spectrum. To keep $\Delta G < 2$, the facet reflectivities should satisfy the condition:

$$G\sqrt{R_1 R_2} < 0.17 \qquad (3.4)$$

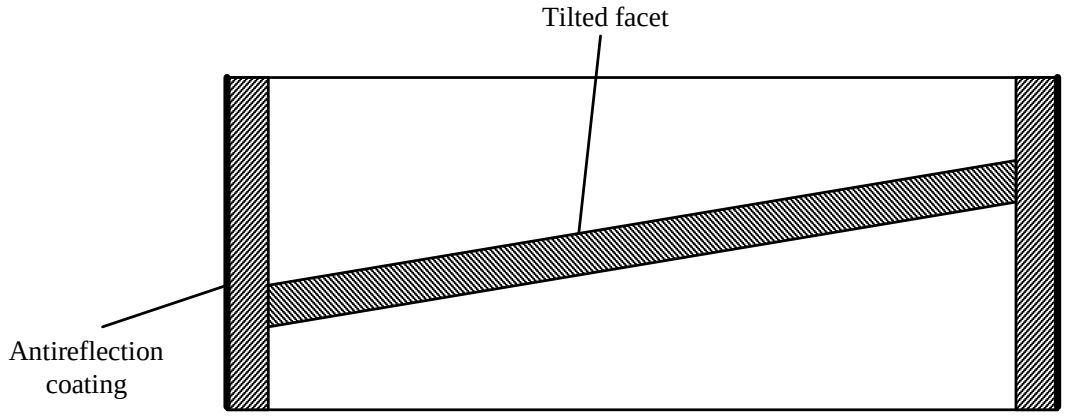

(a)

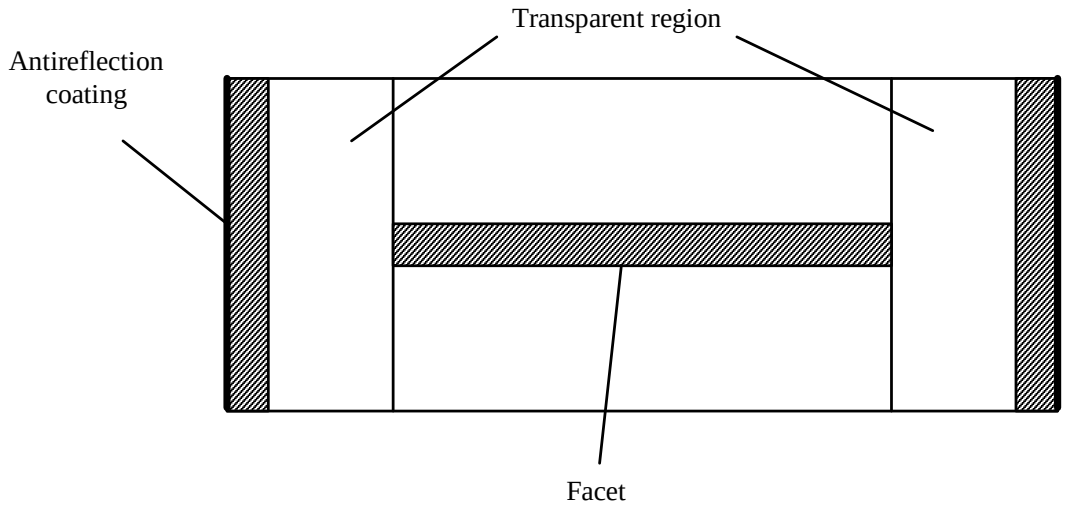

(b)

Figure 3.1 (a) Tilted-stripe, and (b) buried-facet structures for nearly TW semiconductor optical amplifiers

It is customary to characterize the SOA as a TW amplifier when Eq. (3.4) is satisfied. An SOA designed to provide a 30-dB amplification factor (G=1000) should have facet reflectivities such that $\sqrt{R_1 R_2} < 1.7 \times 10^{-4}$

Considerable effort is required to produce antireflection coatings with reflectivities less than 0.1%. Even then, it is difficult to obtain low facet reflectivities in a predictable and regular manner. For this reason, alternative techniques have been developed to reduce the reflection feedback in SOAs. In one method, the active region stripe is tilted for the facet normal, as shown in Fig.3.1 (a). Such a structure is referred to as the angle-facet or tilted-stripe structure [20]. The reflected beam at the facet is physically separated from the forward beam because of the angled facet. Some feedback can still occur, as the optical mode spreads beyond the active region in all semiconductor laser devices. In practice, the combination of an antireflection coating and the tilted stripe can produce reflectivities below 10^{-3} (as small as 10^{-4} with design optimization). In an alternative scheme shown in Fig.3.1 (b), a transparent region is inserted between the active the active-layer ends and the facets [21], where optical beam spreads before arriving at the semiconductor-air interface. The reflected beam spreads even further on the return trip and does not couple much light into the thin active layer. Such a structure is called buried-facet or window facet structure and has provided reflectivities as small as 10^{-4} when used in combination with antireflection coatings.

3.3 Amplifier Characteristics

The amplification factor of SOAs is given by Eq. (3.1). Its frequency dependence results mainly from the frequency dependence of $G(v)$, when condition (3.4) is

satisfied. The measured amplifier gain exhibits ripples reflecting the effects of residual facet reflectivities.

To discuss gain saturation, the carrier rate equation is used and given by [39]:

$$\frac{dN}{dt} = \frac{1}{q} - \frac{N}{\tau_c} - GP \tag{3.5}$$

Expressing the photon number in terms of the optical power, this equation can be written as:

$$\frac{dN}{dt} = \frac{I}{q} - \frac{N}{\tau_C} - \frac{\sigma_g (N - N_0)}{\sigma_m h\nu} P \tag{3.6}$$

where τ_C is the carrier lifetime, σ_g is the differential gain, σ_m is the cross-sectional area of the waveguide mode, and the N_0 is the value of N required at transparency. The carrier population N changes with injection current I and the signal power P. In the case of a CW beam or pulses much longer than τ_C, the steady-state value of N is obtained by setting $dN/dt = 0$ in Eq. (3.5). When the solution is substituted in net rate of stimulated emission G the optical gain is found to saturate as:

$$g = \frac{g_0}{1 + P/P_s} \tag{3.7}$$

where the small-signal gain g_0 is given by:

$$g_0 = (\Gamma \sigma_g / V)(I\tau_C / q - N_0) \tag{3.8}$$

And the saturation power P_S is defined as:

$$P_S = h\nu\sigma_m / (\sigma_m \tau_C) \tag{3.9}$$

Typical values of P_S are in the range of 5-10 mW.

The noise figure F_n of SOAs is larger than the minimum value of 3 dB for several reasons. The dominant contribution comes from the spontaneous-emission factor (or population-inversion factor) n_{SP}, which is obtained from:

$$n_{sp} = N_2/(N_2 - N_1) \tag{3.10}$$

where N_1 and N_2 are the atomic populations for the ground state and excited states respectively.

After replacing N_2 and N_1 by N and N_0, respectively in Eq.(3.10), an additional contribution, results from internal losses (such as free-carrier absorption or scattering loss), which reduce the available gain from g to $g - \alpha_{\text{int}}$. The noise figure can be written as [17]:

$$F_n = 2\left(\frac{N}{N - N_0}\right)\left(\frac{g}{g - \alpha_{\text{int}}}\right) \tag{3.11}$$

Typical values of F_n for SOAs fall in the range of 5-7 dB.

3.4 Practical Issues

Although SOAs were used before 1990 for compensating fibre losses in optical communication systems [22], they suffer from several drawbacks that make their use as in-line amplifiers impractical. A few among them are polarization sensitivity, inter-channel crosstalk, a relatively high noise figure, and large coupling losses occurring as the signal is coupled into and out of an SOA. For this reason, they have been rarely used commercially for this purpose. This may however change as SOAs also being pursued for metropolitan-area networks as a low-cost alternative to fibre amplifiers. We focus on the undesirable features of SOAs in this subsection.

An undesirable characteristic of SOAs is their polarization sensitivity. The amplifier gain G differs for the TE and TM modes by as much as 5-8 dB simply because

both G and σ_g are different for the two orthogonally polarized mode. This feature makes the amplifier gain sensitive to the polarization state of the input beam, a property undesirable for lightwave systems in which the state of polarization changes with propagation along the fibre (unless fibres are used). Several schemes have been devised to reduce the polarization sensitivity [21], [23]-[27]. In one scheme, the amplifier is designed such that the width and the thickness of the active region are comparable. Again difference of less than 1.3 dB between TE and TM polarizations has been realized by making the active layer $0.26\,\mu m$ thick and $0.4\,\mu m$ wide [21]. Another scheme makes use of a large-optical-cavity structure; a gain difference of less than 1 dB has been obtained with such a structure [23].

Several other schemes reduce the polarization sensitivity by using two amplifiers or two passé through the same amplifier. Figure 3.2 shows three such configurations. In Figure 3.2 (a), the TE-polarized signal in one amplifier becomes TM-polarized in the second amplifier, and vice versa. If both amplifiers have identical gain characteristics, the twin amplifier configuration provides signal gain that is independent of signal polarization. A drawback of the series configuration is that residual facet reflectivities lead to mutual coupling between the two amplifiers. In the parallel configuration shown in Figure 3.2 (b), the incident signal is split into a TE- and a TM-polarized signal, each of which is amplified by separate amplifiers. The amplified TE and TM signals are then combined to produce the amplified signal with the same polarization as that of the input beam [24]. The double-pass configuration of Figure 3.2 (c) passes the signal through the same amplifier twice, but the polarization is rotated by 90° between the two passes [25]. Since the amplified signal propagates in the backward direction, a 3-dB fibre coupler is needed to separate it from the incident

signal. Despite a 6-dB loss occurring at the fibre coupler 3dB for the input signal and 3dB for the amplified signal), this configuration provides high gain from a single amplifier, as the same amplifier supplies gain on the two passes.

Although SOAs can be used to amplify several channels simultaneously, they suffer from a fundamental problem related to their relatively fast response. Ideally, the signal in each channel should be amplified by the same amount.

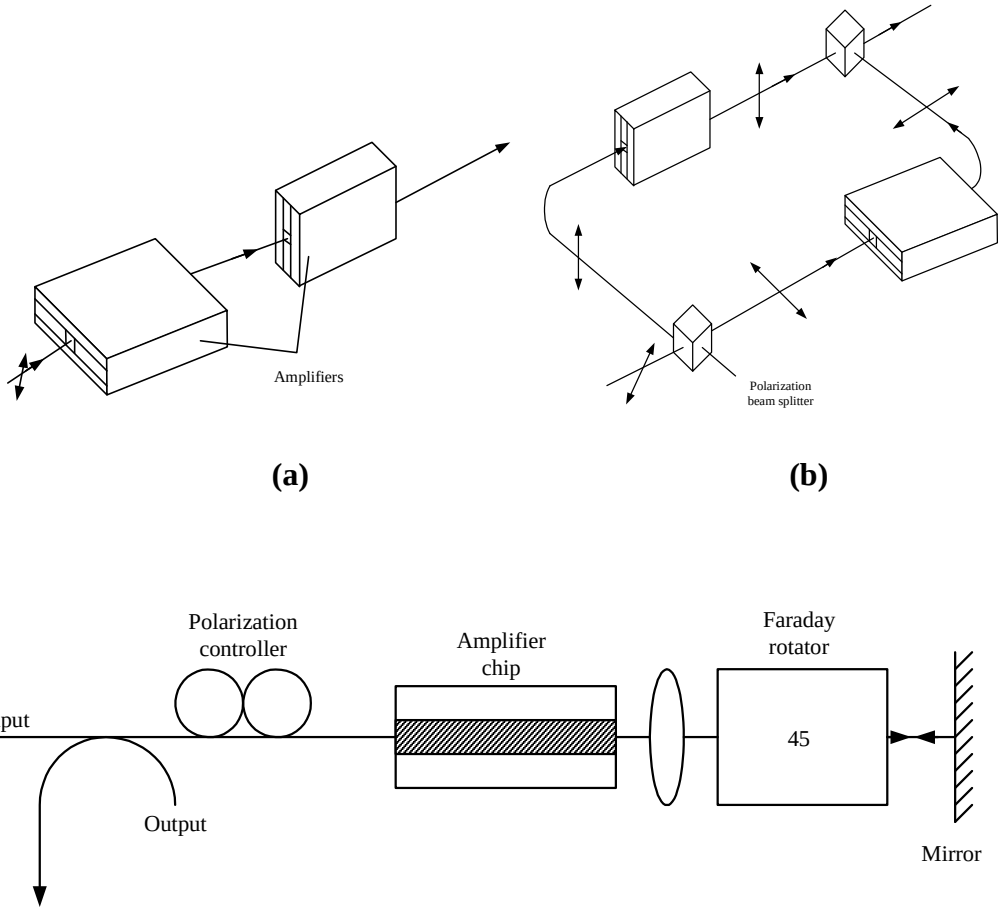

Figure 3.2 Three configurations used to reduce the polarization sensitivity of semiconductor optical amplifiers: (a) twin amplifiers in series; (b) twin amplifiers in parallel; and (c) double pass through a single amplifier

In practice, several nonlinear phenomena in SOAs induce inter-channel crosstalk, an undesirable feature that should be minimized for practical lightwave systems. Two

such nonlinear phenomena are cross-gain saturation and four-wave-mixing (FWM). Both of them originate from the stimulated-emission term in Eq. (3.6). In the case of multi-channel amplification, the power P in this equation is replaced with:

$$P = \frac{1}{2}\left|\sum_{j=1}^{M} A_j \exp\left(-i\omega_j t\right) + c.c.\right|^2 \tag{3.12}$$

Where c.c. stands for the complex conjugate, M is the number of channels, A_j is the amplitude, and ω_j is the carrier frequency of the j th channel. Because of the coherent addition of individual channel fields, Eq. (3.12) contains time-dependent terms resulting from beating of the signal in different channels, that is:

$$P = \sum_{j=1}^{M} P_j + \sum_{j=1}^{M}\sum_{k\neq j}^{M} 2\sqrt{P_j P_k}\cos\left(\Omega_{jk} t + \phi_j - \phi_k\right) \tag{3.13}$$

Where $A_j = \sqrt{P_j}\exp\left(i\phi_j\right)$ was assumed together with $\Omega_{jk} = \omega_j - \omega_k$. When Eq. (3.13)) is substituted in Eq. (3.6), carrier population is also found to oscillate at the beat frequency Ω_{jk}. Since the gain and the refractive index both depend on N, they are also modulated at the frequency Ω_{jk};such a modulation creates gain index gratings, which induce inter-channel crosstalk by scattering a part of the signal from one channel to another. This phenomenon can also be viewed as FWM [28]. FWM can occur even for widely spaced channels through intra-band nonlinearities [29] occurring at fast time scales (<1 ps).

The origin of cross-gain saturation is also evident from Eq. (3.13). The first term on the right side shows that the power P in Eq. (3.7) should be replaced by the total power in all channels. Thus, the gain of a specific channel is saturated not only by its own power but also by the power of neighbouring channels, a phenomenon known as cross-gain saturation. The cross-gain saturation is undesirable in WDM systems since

the amplifier gain changes with time, depending on the bit pattern of neighbouring channels. As a result, the amplified signal appears to fluctuate more or less randomly. Such fluctuations degrade the effective SNR at the receiver. The inter-channel crosstalk occurs for any channel spacing or the modulation format. It can be avoided by reducing the channel powers so that the SOA operates in the unsaturated regime [30]-[33].

3.5 SOA as a Nonlinear Device

The same nonlinear effects that limit the usefulness of SOAs in lightwave systems as an optical amplifier also render them quite useful for nonlinear signal processing (while amplifying the signal simultaneously). SOAs can be used for all-optical switching, FWM, wavelength conversion, and logic operations, and thus constitute an important active component of lightwave technology [34]-[37]. SOAs are not only extremely compact (active volume $< 1 mm^3$), they can also be integrated monolithically with other devices on the same chip. Since they additionally provide amplification, SOAs allow features such as fan-out and cascadability, both of which are general requirements for large-scale photonic circuits.

The most important feature of SOAs is that they exhibit a strong carrier-induced third nonlinearity with effective values of $n_2 \approx 10^{-9}\, cm^2/W$ [38] that are seven orders of magnitude larger than that of silica fibres. Although this nonlinearity does not respond on a femto second time scale, it is fast enough that it can be used to make devices operating at bit rate as fast as $40\, Gb/s$. The origin of this nonlinearity lies in gain saturation and the fact that any change in the carrier density affects not only the optical gain but also the refractive index within the active region of an SOA.

A simple way to understand the nonlinear response of an SOA is to consider what happens when a short optical pulse is launched into it. The amplitude $A(z,t)$ of the pulse envelope inside the SOA evolves as [38]:

$$\frac{\partial A}{\partial z}+\frac{1}{v_g}\frac{\partial A}{\partial t}=\frac{1}{2}(1-i\beta_c)gA \tag{3.14}$$

where v_g is the group velocity, g is the gain, and carrier-induced index changes are included through the line-width enhancement factor β_c. The time dependence of g is governed by Eq. (3.6), which can be written in simple form, as:

$$\frac{\partial g}{\partial t}=\frac{g_0-g}{\tau_c}-\frac{g|A|^2}{E_{sat}} \tag{3.15}$$

Where the saturation energy E_{sat} is defined as:

$$E_{sat}=h\nu(\sigma_m/\sigma_g) \tag{3.16}$$

and g_0 is given by Eq. (3.8). Typically, $E_{sat}\approx 1pJ$.

Equations (3.14) and (3.15) govern amplification of optical pulses in SOAs. They can be solved analytically for pulses whose duration is short compared with the carrier lifetime $(\tau_p \langle\langle \tau_C)$. The first term on the right side of Eq. (3.15) can then be neglected during pulse amplification. By introducing the reduced time $\tau = t - z/v_g$ together with $A=\sqrt{P}\exp(i\phi)$, Eqs, (3.14) and (3.15) can be written as [38]:

$$\frac{\partial P}{\partial z}=g(z,\tau)P(z,\tau), \tag{3.17}$$

$$\frac{\partial \phi}{\partial z}=-\frac{1}{2}\beta_C\, g(z,\tau), \tag{3.18}$$

$$\frac{\partial g}{\partial \tau}=g(z,\tau)P(z,\tau)/E_{sat}\,, \tag{3.19}$$

Equation (3.17) can easily be integrated over the amplifier length L to yield:

$$P_{out}(\tau) = P_{in}(\tau)\exp[h(\tau)],$$

Where $P_{in}(\tau)$ is the input power and $h(\tau)$ is the total integrated gain defined as:

$$h(\tau) = \int_0^L g(z,\tau)dz, \tag{3.20}$$

If Eq. (3.19) is integrated over the amplifier length after replacing gP by $\partial P/\partial z$, $h(\tau)$ satisfied [23]:

$$\frac{dh}{d\tau} = -\frac{1}{E_{sat}}[P_{out}(\tau) - P_{in}(\tau)] = -\frac{P_{in}(\tau)}{E_{sat}}(e^h - 1), \tag{3.21}$$

Equation (3.21) can easily be solved to obtain $h(\tau)$. The amplification factor $G(\tau)$ is related to $h(\tau)$ as $G = \exp(h)$ and is given by:

$$G(\tau) = \frac{G_0}{G_0 - (G_0 - 1)\exp[-E_0(\tau)/E_{sat}]}, \tag{3.22}$$

Where G_0 is the unsaturated amplifier gain and $E_0(\tau) = \int_{-\infty}^{\tau} P_{in}(\tau)d\tau$ is the partial energy of the input pulse defined such that $E_0(\infty)$ equals the input pulse energy E_{in} .

The solution (3.22) shows that the amplifier gain is different for different parts of the pulse. The leading edge experiences the full gain G_0 as the amplifier is not yet saturated. The trailing edge experiences the least gain since the whole pulse has saturated the amplifier gain. As seen from Eq. (3.22), gain saturation leads to a time-dependent phase shift across the pulse. This phase shift is found by integrating Eq. (3.18) over the amplifier length and is given by:

$$\phi(\tau) = -\frac{1}{2}\beta_C \int_0^L g(z,\tau)dz = -\frac{1}{2}\beta_C h(\tau) = -\frac{1}{2}\beta_C \ln[G(\tau)] \tag{3.23}$$

Since the pulse modulates its own phase through gain saturation, this phenomenon is referred to as saturation-induced self-phase modulation [37]. The frequency chirp is related to the phase derivative as:

$$\Delta\nu_C = \frac{1}{2\pi}\frac{d\phi}{d\tau} = \frac{\beta_C}{4\pi}\frac{dh}{d\tau} = -\frac{\beta_C P_{in}(\tau)}{4\pi E_{sat}}[G(\tau)-1] \qquad (3.24)$$

where Eq. (3.21) was used.

Self-phase modulation and the associated frequency chirp are similar to the phenomena that occur when an optical pulse propagates through a fibre.

Just as in optical fibres, the spectrum of the amplified pulse broadens and contains several peaks of different amplitudes [39].

3.6 Summary

A brief introduction to SOA was discussed in this chapter. Semiconductor optical amplifiers are amplifiers which use a semiconductor to provide the gain medium. These amplifiers have a similar structure to Fabry-Perot laser diodes but with anti-reflection design elements at the end faces. Also the amplifier characteristic and practical issues, such as non-linearities and FWM were explained. SOAs can be used for all-optical switching, FWM, wavelength conversion, and logic operations, and thus constitute an important active component of lightwave technology.

CHAPTER 4

Optical Linearization Technique

4.1 Introduction

Actual and incipient communication systems require higher linear amplification in their transmitters. The aim of this chapter lies in compilation and description of the linearization technique. The three major linearization techniques in electrical domain are explained. Then the implementation of the Feedforward and Predistortion linearization techniques is illustrated in optical domain. It is shown the linearization of the semiconductor optical amplifier distortion, such as ASE and FWM cancellation.

Contrary to expectations, linearization techniques are not as novel as they seem to be. In fact, some of them were proposed before the transistor was used as an amplifier device, mainly in analogue AM broadcasting.

In recent years, the need for higher efficiency has resulted in specific efforts to best use the electromagnetic spectrum. The quest for higher efficiency involved high linear amplification and consequently, efficiency reductions. This has culminated in an ongoing research on linearization techniques focused on higher frequencies, bandwidths and efficiency rates.

The classification of linearization techniques, according to one of the most generalized tendency, can be divided into two groups. In the first group an input signal is amplified while distortion components are generated. The aim of these techniques is to cancel distortion by modifying the input signal or directly subtracting it from the output signal.

These linearization techniques are:

- Feedback
- Pre-distortion
- Feed-forward

4.2 Feedback Linearization

4.2.1 RF Feedback

This technique is based on the standard feedback scheme used in low frequency amplification and control systems (Fig.4.1). The gain G of the system defined in terms of the main amplifier A and the feedback gain B is given as:

$$G = \frac{A}{1 + BA} \qquad (4.1)$$

In the feedback loop distortion reduces with the gain factor, so a trade-off must be made between them.

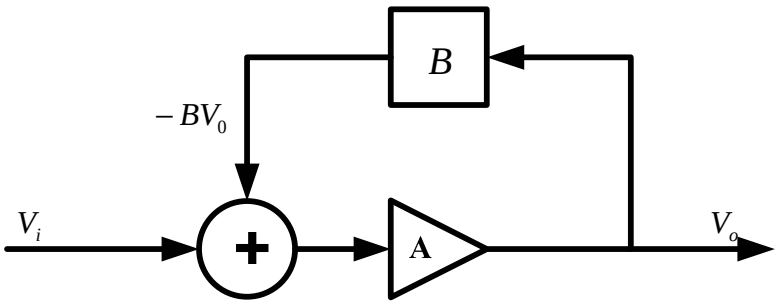

Figure 4.1 Feedback basic architecture

One of the inherent disadvantages of this technique is the stability, so it is impossible to assure a proper functionality against component aging. Another disadvantage is the bandwidth reduction due to the feedback loop delay. These limitations initiated the emergence of new architectures based on the same concept, but comparing the low frequency signals instead of the RF signal. Those new techniques require demodulation of the amplified signal, so the implementation is more complicated.

4.2.2 Envelope Feedback

This linearization technique corrects the amplitude distortion of the output signal and compensates the gain variation of the main amplifier. As shown in Fig.4.2, both input and output are detected and compared using a differential amplifier that simultaneously the output of which is used to control the main amplifier.

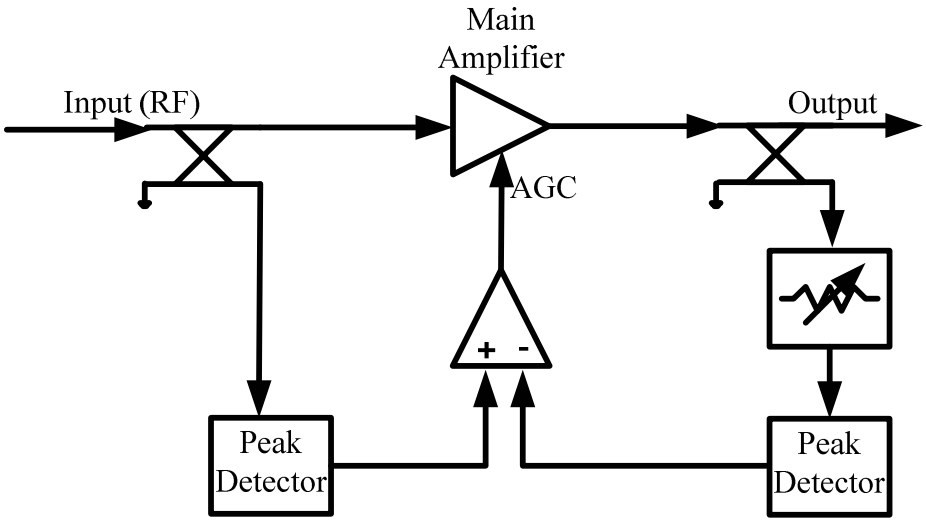

Figure 4.2 Envelope feedback architecture

To reduce instabilities and distortion the peak detectors must have a high dynamic range and a bandwidth twice that of amplified signal.

This technique improves the output amplitude but at the cost of increased phase error, thus is usually used with linear amplifiers.

4.2.3 Envelope and Phase Feedback

As the name suggests, phase unbalances are also rectified, though precision and bandwidth requirements are still mandatory see Fig.4.3.

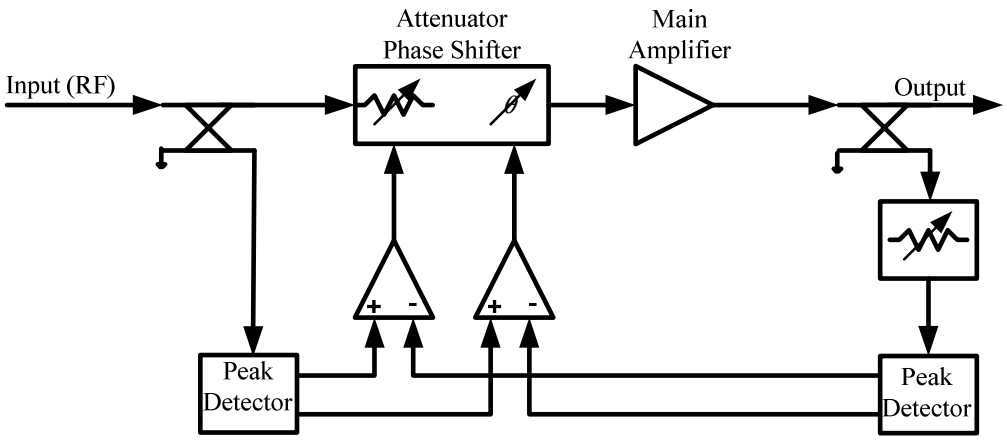

Figure 4.3 Envelope and phase feedback architecture

4.2.4 Polar Loop

The Polar Loop is an alternative technique for both amplitude and a phase adjustment that uses intermediate frequency (IF) instead of the RF signal (Fig.4.4).

In this case, the phase and amplitude of the input and output signals are compared. Amplitude is used to adjust AGC while phase comparison is employed to control a voltage control oscillator (VCO).

The linearity characteristics of these feedback amplifiers are good. However, the design and the component selection are critical because of their influence on the frequency conversion process, the linearity performance and the unbalances of the signal comparators [40].

The bandwidth of the differential amplifiers is also critical. The output phase detector bandwidth must be 5 to 10 times higher than the bandwidth of the envelope detector. Otherwise, distortion components will be outside the phase detector range, therefore will be impossible to carry out subtraction.

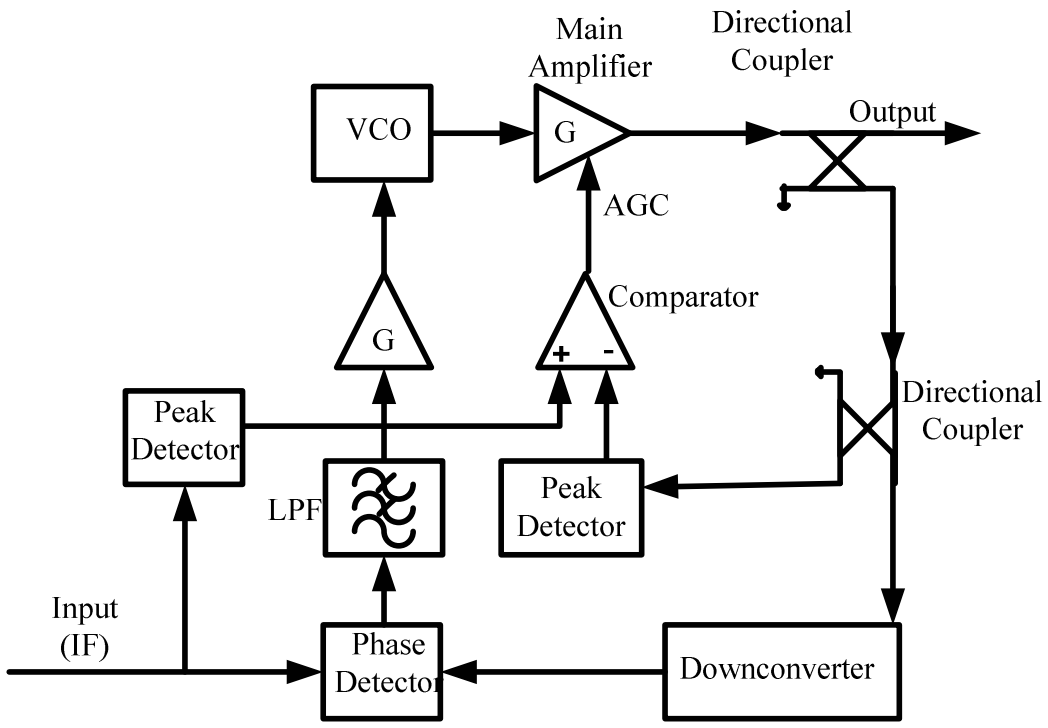

Figure 4.4 Polar loop architecture

4.2.5 Cartesian Loop

The Cartesian Loop developed by Petrovic and Smith [1], but, It was not an interesting linearization technique until the digital systems were developed and the I/Q baseband signals were digitally generated. Nowadays, this technique is suitable for single carrier applications and is the most promising of all Feedback techniques [41-44]. The basic scheme is shown in Fig.4.5, where there is no comparison between the input and output amplitude and phase magnitudes, but output signal demodulation results in a critical step such as stability that must be carefully done. The input signal is required in in-phase and quadrature (I/Q) format. This is applied to a summing amplifier (usually known as the ‘error amplifier’) where it is compared to the feedback signal. The output of the ‘error amplifier’ is applied to an up-converter to generate an RF signal that is then amplified by a power amplifier. A sample of the output of the amplifier is taken, generally using a directional coupler; this is down-converted and applied to the error amplifier. This forms the closed loop system, such

that as long as the feedback path does not introduce distortion, the system will attempt to correct the signal at the output to match the I/Q input signal applied to the error amplifier.

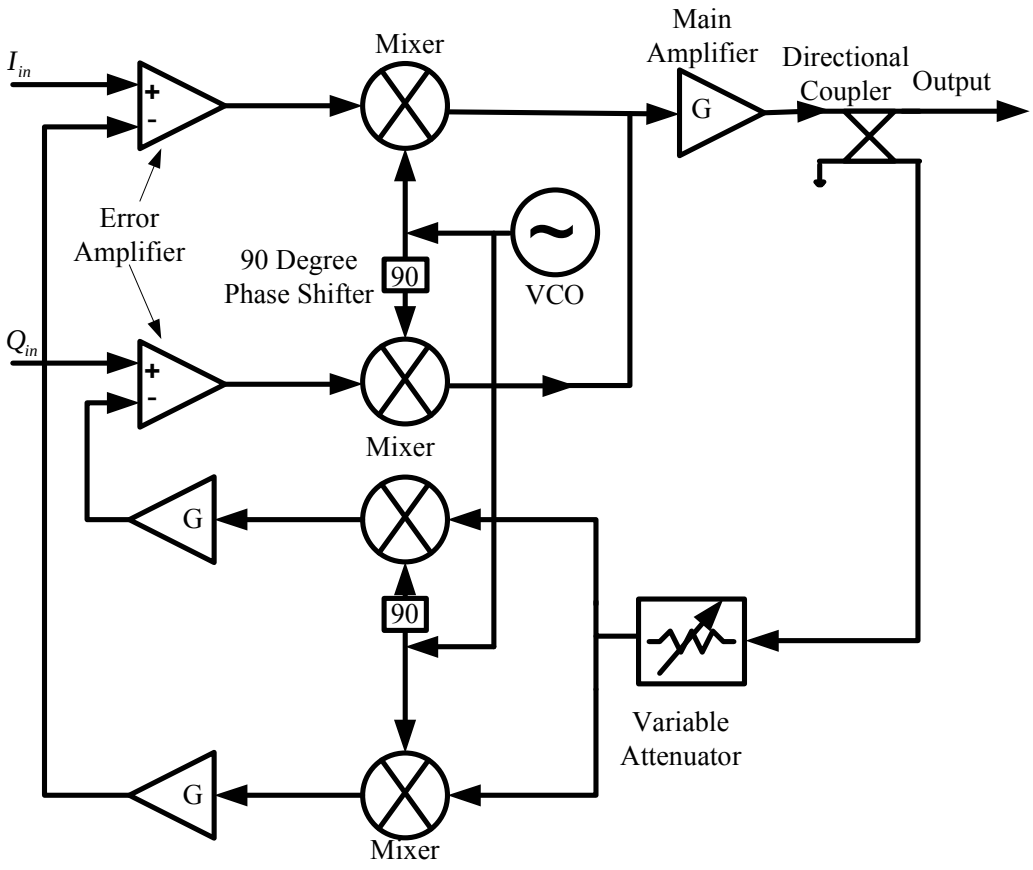

Figure 4.5 Cartesian loop architecture

Despite the implementation difficulties, the Cartesian Loop technique is widely standardized, among other things, owing to the low production costs. The linearization improvement depends on the gain and bandwidth characteristics of the differential amplifiers and, above all, on the linearity of the demodulator device. The Application Specific Integration Circuits (ASIC) developed for Feedback amplifiers open up new possibilities in the Digital Signal Processing (DSP) field. Despite the increase of production costs, DSP based devices allow the use of simultaneous linearization techniques, i.e., Cartesian Loop together with Predistortion techniques, improving the overall linearity.

Ideally, this technique achieves 20 dB to 45 dB cancellation levels of the inter-modulation with 35% to 65% efficiency rates. Really, those values get worse as the

signal bandwidth achieves, theoretically, a 20 dB distortion cancellation. This is the reason that this technique is not suitable for wideband signals and it is usually used in TDMA and FDMA narrow band single carrier applications.

4.3 Predistortion Linearization

The Predistortion linearization technique, as it name suggests, modifies the input signal according to the non linearity characteristics of the main amplifier transfer function. The basic architecture is shown in Fig.4.6.

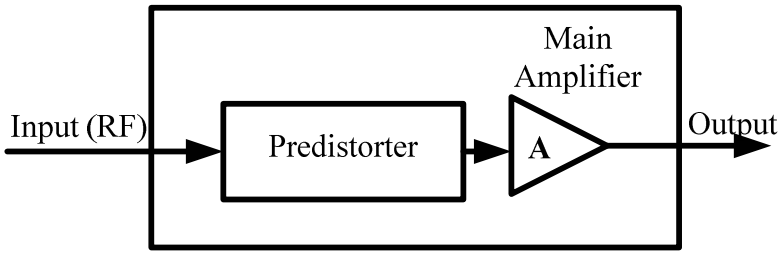

Figure 4.6 Predistortion architecture

The open loop architecture turns the Predistortion technique into an unconditionally stable system. The input signal can be predistorted in a constant way or dynamically with feedback loops. The former is, though much simpler, but ineffective against environmental changes and aging effects.

In the next subsections, three particular Predistortion techniques are summarized:

- RF Predistortion
- Envelope Predistortion
- Baseband Predistortion

4.3.1 RF Predistortion

This technique is regularly used in high power amplifiers [45] and often together with other linearization techniques. It entails inserting one or more nonlinear devices Predistortion devices-between the input signal and the main amplifier Fig.4.6. The transfer function of the distortion signal of the Predistortion device must be exactly opposite to the transfer function of the distortion signal of the main amplifier. As a result, the total gain of the distortion components will be 0 dB, see Fig.4.7. This technique uses constant Predistortion factors, so the main amplifier transfer function must be thoroughly characterized. Alternatively, new dynamic adjustment methods have been proposed [46] avoiding the influence of aging and environmental effects.

Simple analogue Predistortion devices are used for correction of the third order inter-modulation products. To deal with several inter-modulation orders (5, 7…), more complex devices should be developed [47].

4.3.1.1 Simple Analogue Predistortion

The simple analogue Predistortion technique avoids only the third order inter-modulation products using linear components as Predistortion devices. Initially, different configurations were used only with diodes and resistances, but in the course of the years new improvements have appeared based on field effect transistors [48].

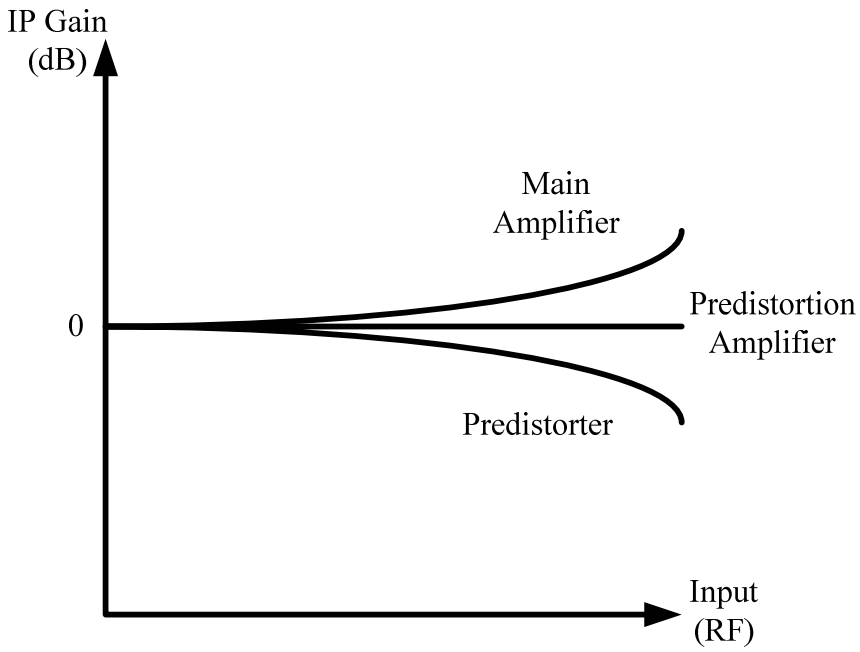

Figure 4.7 Gain factor of the inter-modulation product after predistortion

One nonlinear device is shown in Fig 4.8. A nonlinear transfer function with the odd distortion components is given by:

$$V_{nl} = a_1 v_{in} + a_3 v_{in}^3 + a_5 v_{in}^5 + ... \quad (4.2)$$

The transfer function of the Predistortion device must have only the nonlinear terms of the power amplifier transfer function. One of the architectures used in the subtraction of the linear term a_1 should be eliminated.

$$V_{ref} = -a_1 v_{in} \quad (4.3)$$

$$V_{out} = a_3 v_{in}^3 + a_5 v_{in}^5 + ... \quad (4.4)$$

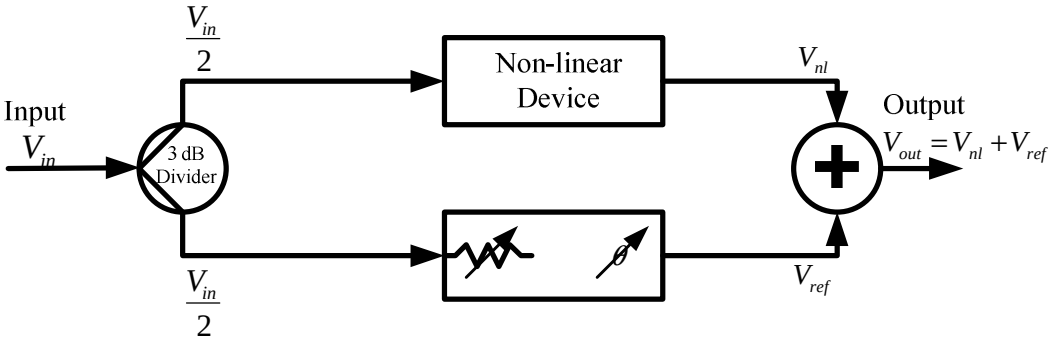

Figure 4.8 Linear component subtraction from a nonlinear device

Figure 4.9 shows a solution proposed by [49] that completely cancels the third order distortion generated by the main amplifier.

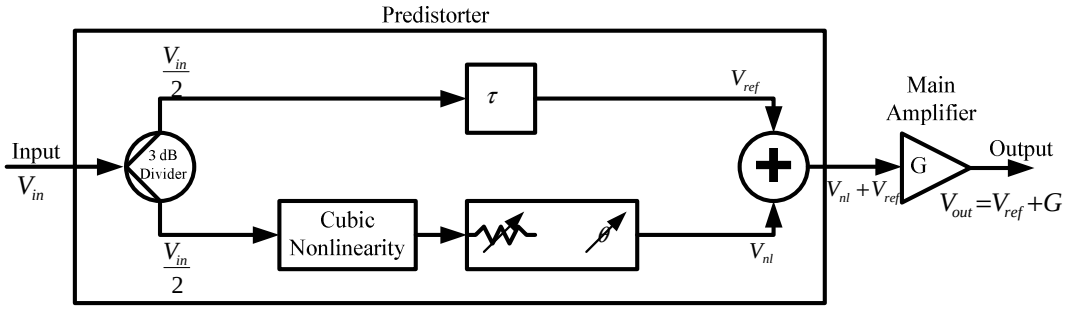

Figure 4.9 Simple analogue predistortion architecture

Despite the low production costs, this technique has three important disadvantages, [50]: the AM-PM conversion is worsened, the input power must be constant and the frequency response is narrowband. These disadvantages have caused the irruption of the Compound Predistortion.

4.3.1.2 Compound Predistortion

The Compound Analogue Predistortion subtracts all the distortion compounds $(a_3, a_5, ...)$ separately [51]. Usually, feedback controllers are used to adjust phase and amplitude in order to reduce distortion components. The production costs and the implementation complexity are high, and furthermore, the frequency dependency prevents linearizing wideband signals.

4.3.2 Envelope Predistortion

The Envelope Predistortion technique consists of dynamically changing the input signal phase and amplitude parameters, by means of variable attenuators and phase shifters, in order to compensate for the distortion caused by the main amplifier (Fig.4.10 and Fig.4.11) [50].

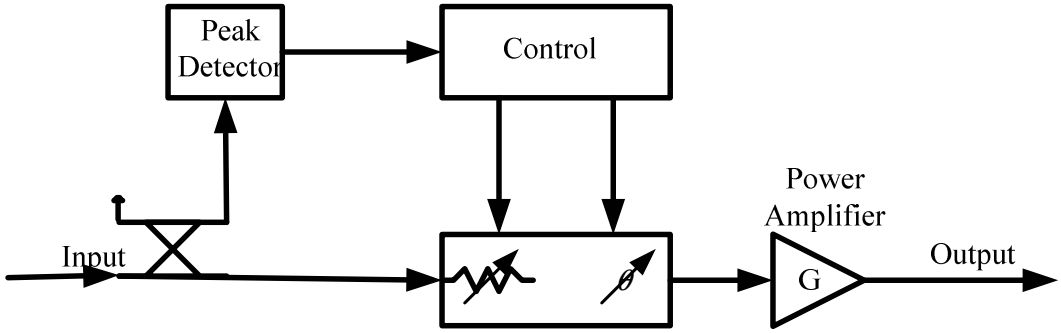

Figure 4.10 Envelope predistortion with analogue or DSP controller

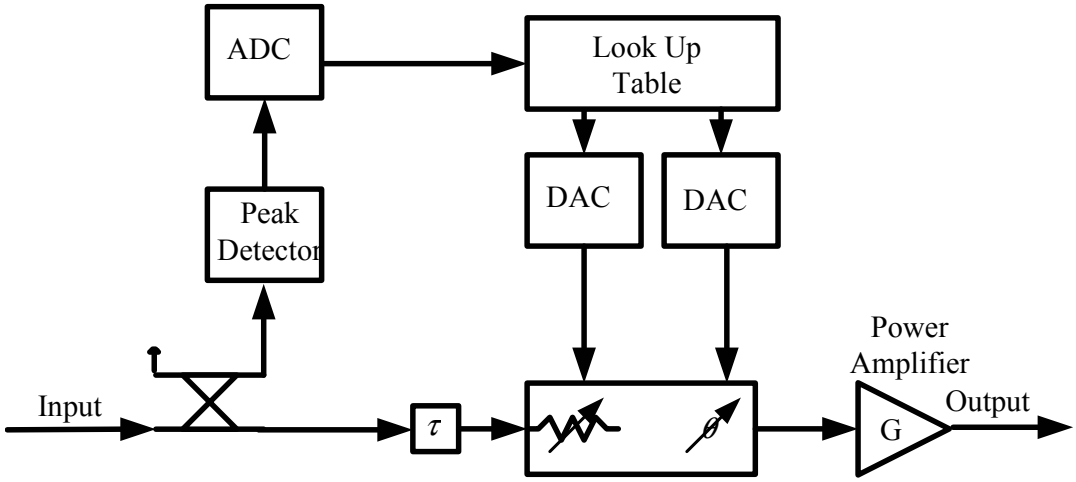

Figure 4.11 Envelope predistortion with a LUT controller

Analogue controllers, DSP and look up table (LUT) are used in this linearization technique [52]. The implementation complexity is low and the distortion is reduced by 5 to 15 dB. On the other hand, the system bandwidth is limited by the control frequency, necessarily 10 times greater than the modulator frequency [53].

4.3.3 Baseband Predistortion

The Baseband Predistortion techniques, as its name suggests, use the input baseband signals instead of the RF signals. Three Baseband Predistortion techniques are the

most developed: Mapping Predistortion, Complex Gain Predistortion and Analogue Predistortion [54-56]. The Mapping Predistortion techniques uses a large look up table (LUT) in order to distort the original I/Q signals and a DSP to consider the memory effects of the main amplifier [56]. Despite the inherent advantages of this technique, its adaptability directly depends on the memory required for dynamic control [56, 57].

Open loop and adaptive architectures having 25 dB cancellation levels have been achieved in some cases; see Fig.4.12 and Fig.4.13 [58]. The digital signal processor contains the signal separation and the complex weighting functions. These may be constructed in many ways, depending upon the amplifier model chosen (e.g., AM-AM, AM-PM, with or without memory, or combinations of these), but are typically formed from look-up tables of complex weighting coefficients at various amplitude levels (for each of the quadrature channels). The look-up tables are accessed by an algorithm which receives as its input the fed-back down converted RF output from the power amplifier. The coefficients in the look-up tables may then updated in the difference between this down converted signal and the input signal.

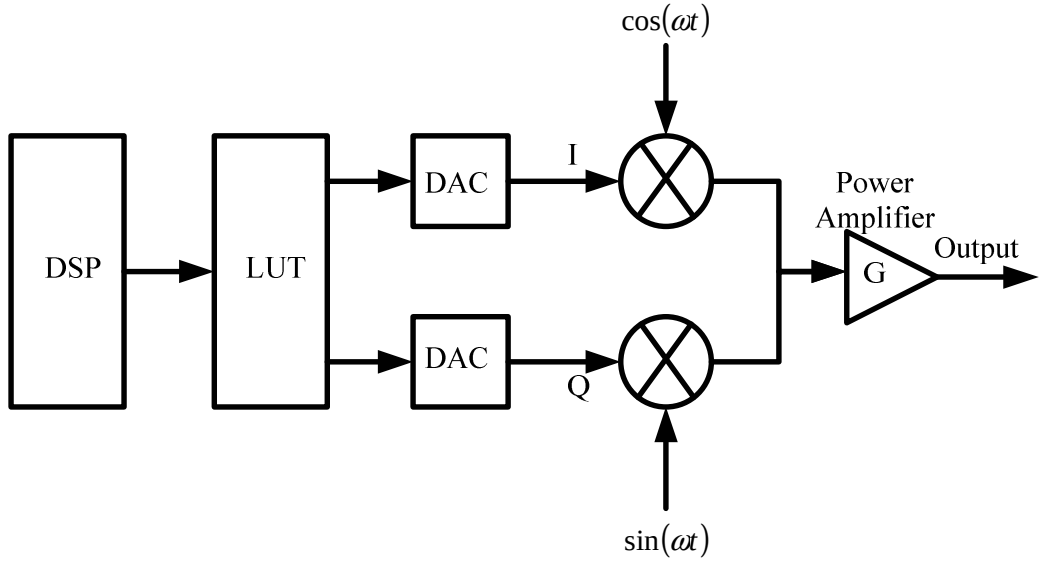

Figure 4.12 Open loop digital baseband predistortion architecture

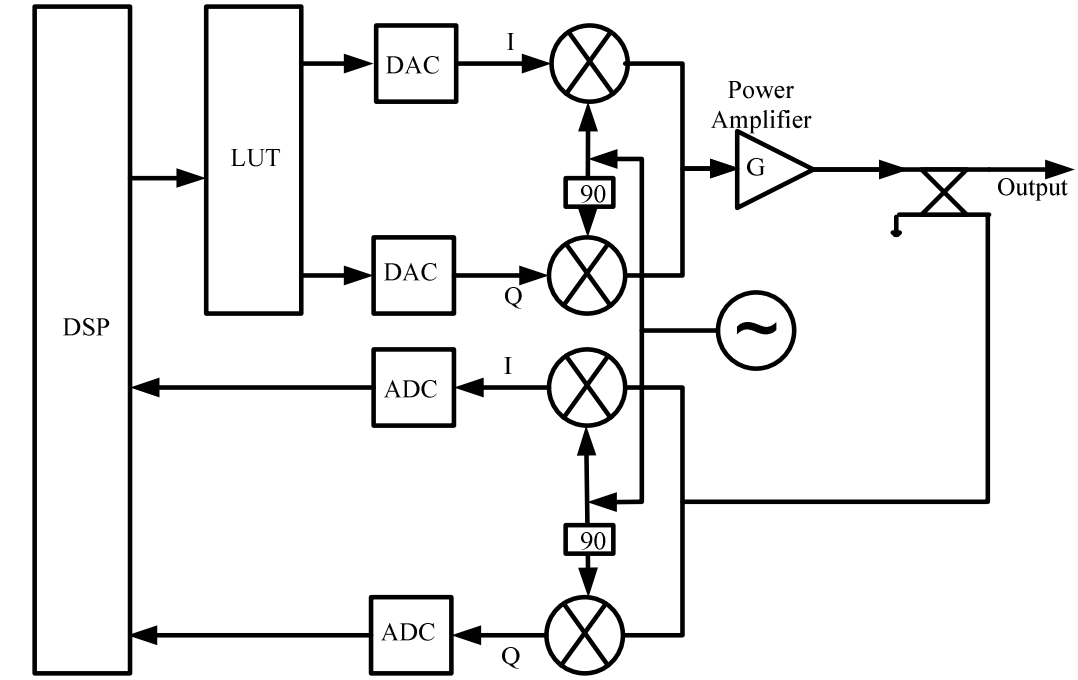

Figure 4.13 Adaptive digital baseband predistortion architecture

The Complex Gain Predistortion technique is derived from the mapping Predistortion technique with reduced requirement for memory used at the control stage. In this case only the amplitude of the input signal is used instead of the I/Q signals, reducing the memory requirement and increasing the computational cost [55].

On the other hand, the Analogue Baseband Technique uses analogue circuitry, sometimes controlled by DSP in the Predistortion stage. The theoretical bandwidth of this architecture could be considered a wideband in comparison to all other Predistortion techniques, limited by the DSP frequencies. The Baseband Predistortion techniques are easily implementable, low cost, and can be used in some wideband applications [59], but the I/Q signals must be available and the cancellation levels do not adequate.

4.4 Feedforward Linearization

This technique was developed by H. S. Black in 1928 [60], also developed by him in 1937. The Feedback technique in not unconditionally stable and the distortion cancellation is limited. The Feedforward technique however is unconditionally stable and the distortion introduced by the main amplifier can be, theoretically, completely subtracted. On the other hand, the Feedforward technique requires precise phase and

gain adjustment, making the implementation really complicated. This was the reason the Feedforward technique disappeared into obscurity in favour of the well-known Feedback technique.

With the evolution of technology, the frequency and bandwidth requirements began increasing; highlighting the feedback limitations and generating renewed interest in the feedforward technique. Feedforward became the most developed linearization scheme and was used in audio systems, cable television and RF applications. The basic Feedforward architecture is shown in Fig.4.14. The scheme consists of two cancellation loops. The first loop samples the amplified signal from the main amplifier output and extracts those distortion components from the main signal [63]. This linearization technique is open loop and unconditionally stable, so theoretically suitable for any wideband application. High cancellation levels (33 dB) are reported of the third order inter-modulation products with the two tone procedure [64], depending on bandwidth and frequency parameters.

The input signal is split to form two identical paths, although the ratio used in the splitting process need not be equal. The signal in the top path is amplified by the main power amplifier and the non-linearities in this amplifier result in inter-modulation and harmonic distortions being added to the original signal. Noise is also added by the main amplifier, although this is generally neglected in most applications. The directional coupler, C1, takes a sample of the main amplifier signal and feeds it to the subtracter (C3, 180 degree) where a time delayed portion of the original signal, present in the lower path, is subtracted. The result of this subtraction process is an error signal containing substantially the distortion information from the main amplifier; ideally none of the original signal energy would remain. The error signal is then amplified linearly to the required level to cancel the distortion in the main path and fed to the output coupler. The main path signal through coupler, C1, is time delayed by an amount approximately equal to the delay through the error amplifier, A2, and fed to the output coupler in anti-phase to the amplified error signal. The error signal will then reduce the distortion information of the main path signal leaving substantially an amplified version of the original input signal

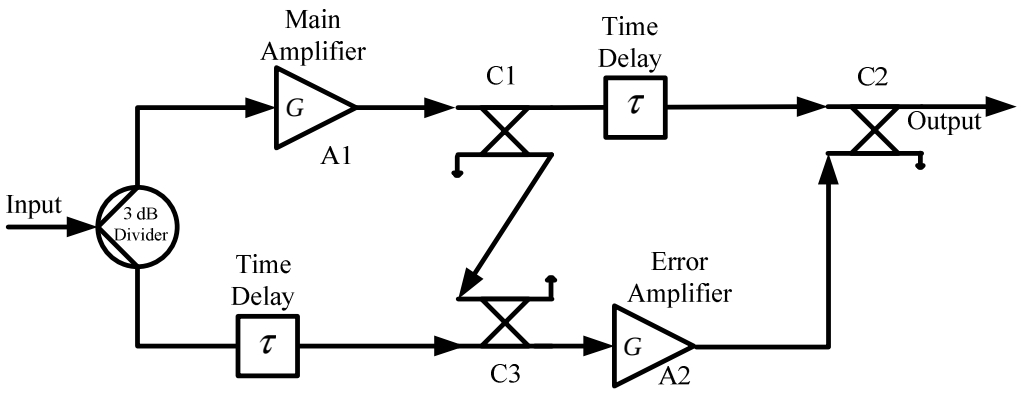

Figure 4.14 Basic feedforward architecture

4.5 Feedforward Linearization in Optical Domain

Today, modern communication systems use optical fibre. Hence, it is possible to transmit more data at higher data rates and preserve the quality of the signal without loss of information. In optical communication systems, various multiple access schemes such as time division multiple access (TDMA), code division multiple access (CDMA) and orthogonal frequency division multiple access (OFDM) have been used. However, the resulting output signal of main amplifier has a high envelope peak-to-average ratio (crest factor) and linear power amplifiers with high back-off are required in order not to degrade the quality of the signal. Linear power amplifiers that have high back-off power and high third order intercept point (IP3) give rise to the problem of power efficiency [65]. In order to improve system linearity, various linearization techniques such as pre-distortion, envelope elimination and restoration, Cartesian feedback, and feed-forward are used. Among these methods, feed-forward gives the best performance and provides a more wide-band stable operation since there is no feedback path, but at the cost of limitation of spectrum efficiency [66].

The operation of the feed-forward circuit is based on subtraction of two equal signals resulting in subsequent cancellation of the error signal in the amplifier output spectrum. It contains two cancellation loops. The first loop is the carrier cancellation

loop, which extracts the distortion products. The second loop is the error cancellation loop, which amplifies the distortion products and eliminates the distortion by cancelling the distorted main amplifier output. The amplifier used in this loop is called the error amplifier and must be sufficiently linear not to introduce additional distortion products. Amplitude, phase, and delay mis-matches are the main constraints on the linearization performance of the feed-forward, and its efficiency is limited by the IP3 of the main and error amplifiers, losses of the couplers and delay compensators [83]. For a complete feed-forward system where two power amplifiers and couplers participate, a similar closed-form expression which relates the linearity performance to the parameters of the whole linearizer and signal characteristics may be required. Using such a tool system parameters can be optimized for optimum efficiency and linearity improvement [65].

4.5.1 Feedforward Linearization Theory

To derive the output signal from feed-forward circuit, the results from [67-70] are used. The electric field input into the amplifier is given by:

$$e_{in}(t) = E_{in} Cos(\omega_k t) \tag{4.5}$$

where E_{in} is an amplitude optical field. The approximate field output from the amplifier e_A is given by:

$$e_A(t) = E_{in} A_1 \left\{1 - \frac{\beta}{\alpha} Cos(\Delta\omega t - \phi)\right\} \times Cos\{\omega_k t - \beta Cos(\Delta\omega t - \phi)\} \tag{4.6}$$

Where:

$$\beta = \frac{\alpha}{\sqrt{1+(\Delta\omega\tau)^2}} \frac{P_{ch}}{P_s} \times \frac{G_0^2 \log_e(G_0^2)}{\left\{\log_e(G_0^2) + 2G_0^2(\log_e(G_0^2) - 1)\frac{2P_{ch}}{P_s}\right\}} \tag{4.7}$$

$$\phi = \tan^{-1}(\Delta\omega\tau) \tag{4.8}$$

P_s is the saturation power, α the line-width enhancement factor, τ the effective spontaneous carrier lifetime, ϕ the unsaturated device phase delay, and G_0 the unsaturated field gain is given by:

$$G_0 = \exp\left(\Gamma g_0 L \big/ 2\right) \tag{4.9}$$

Γ Is the radiation confinement factor, g_0 is the unsaturated gain coefficient, L is cavity length, P_{ch} is the single channel input power and ω_1 and ω_2 are the two channel frequencies. $\Delta\omega = \omega_2 - \omega_1$ and, A is the field gain at quiescent point on the static characteristic. From Eq (4.6) it is clear that carrier density modulation imparts both amplitude and phase modulation on the output fields and that the modulation depths are β/α and, β respectively.

It is assumed that the input splitter is an ideal 3 dB hybrid divider. The output of the optical main amplifier for a system input optical signal $e_{in}(t)$, therefore $e_{A1}(t)$:

$$e_{A1} = \frac{E_{in}A_1}{2}\left\{1 - \frac{\beta}{\alpha}Cos(\Delta\omega t - \phi)\right\} \times Cos\{\omega_k t - \beta Cos(\Delta\omega t - \phi)\} \tag{4.10}$$

If $\Delta\omega t = \phi$

$$e_{A1} = \frac{E_{in}A_1}{2}\left(1 - \frac{\beta}{\alpha}\right) \times Cos(\omega_k t - \beta) \tag{4.11}$$

If $\beta << 1rad$

$$e_{A1} = \frac{E_{in}A_1}{2}\{Cos(\omega_k t) + \frac{\beta^2}{\alpha}Sin(\omega_k t) - \frac{\beta}{\alpha}Cos(\omega_k t) - \beta Sin(\omega_k t)\} \tag{4.12}$$

If we suppose:

$$e_d = \frac{E_{in}A_1}{2}\left\{\frac{\beta^2}{\alpha}Sin(\omega_k t) - \frac{\beta}{\alpha}Cos(\omega_k t) - \beta Sin(\omega_k t)\right\} \tag{4.13}$$

Substituting Eq (4.13) into Eq (4.12) yields:

$$e_{A1} = \frac{E_{in} A_1}{2} Cos(\omega_k t) + e_d \tag{4.14}$$

The proportion of this signal which reaches the subtracter will pass through a coupler with the coupling factor of C_1 and reaching to one of the subtracter ports which is $e_{sub1}(t)$ and from the lower path the delayed optical signal reaching to the other input port and called $e_{sub2}(t)$.

$$e_{sub1} = \frac{E_{in} A_1 Cos(\omega_k t)}{2C_1} + \frac{e_d}{C_1} \tag{4.15}$$

$$e_{sub2} = \frac{E_{in} Cos(\omega_k t)}{2} \tag{4.16}$$

Therefore the output of the subtracter is:

$$e_{error} = e_{sub1} - e_{sub2} \tag{4.17}$$

$$e_{error} = \frac{E_{in} A_1 Cos(\omega_k t)}{2C_1} + \frac{e_d}{C_1} - \frac{E_{in} Cos(\omega_k t)}{2} \tag{4.18}$$

It can be seen from Eq (4.18) that for the original optical input signal to be completely removed from this error signal, the following condition must be satisfied: $A_1 = C_1$

Thus the error signal is:

$$e_{error} = \frac{e_d}{C_1} \tag{4.19}$$

A similar process take place in the second part of the loop in which the error signal components are removed from the main amplifier output signal to leave substantially an amplified version of the original input signal. The output of the main amplifier passed through delay module is given by:

$$e_{coup1} = \frac{E_{in} A_1}{2} Cos(\omega_k t) e^{-j\omega_k \tau_2} + e_d e^{-j\omega_k \tau_2} \tag{4.20}$$

Where τ_2 is the time delay in the top path delay element and this element is assumed lossless. This signal is the main signal for the output coupler C_2.

The optical signal to be injected into the coupled port of this coupler from error signal, $e_{error}(t)$, is amplified by the error amplifier e_{A_2}. This signal will pass through a coupler with the coupling factor of C_2 (e_{coup2}):

$$e_{A_2} = \frac{A_2 e_d}{C_1} e^{-j\omega_k \tau_{A2}} \tag{4.21}$$

$$e_{coup2} = \frac{A_2 e_d}{C_1 C_2} e^{-j\omega_k \tau_{A2}} \tag{4.22}$$

The final output signal is:

$$e_{out} = e_{coup1} - e_{coup2} \tag{4.23}$$

$$e_{out} = \frac{E_{in} A_1}{2} Cos(\omega_k t) e^{-j\omega_k \tau_2} + e_d e^{-j\omega_k \tau_2} - \frac{A_2 e_d}{C_1 C_2} e^{-j\omega_k \tau_{A2}} \tag{4.24}$$

If $A_2 = C_1 C_2$ and $\tau_2 = \tau_{A2}$

$$e_{out} = \frac{E_{in} A_1}{2} Cos(\omega_k t) e^{-j\omega_k \tau_2} \tag{4.25}$$

Thus the output signal is an amplified and time-delayed replica of the input signal with the distortion from the main amplifier being removed.

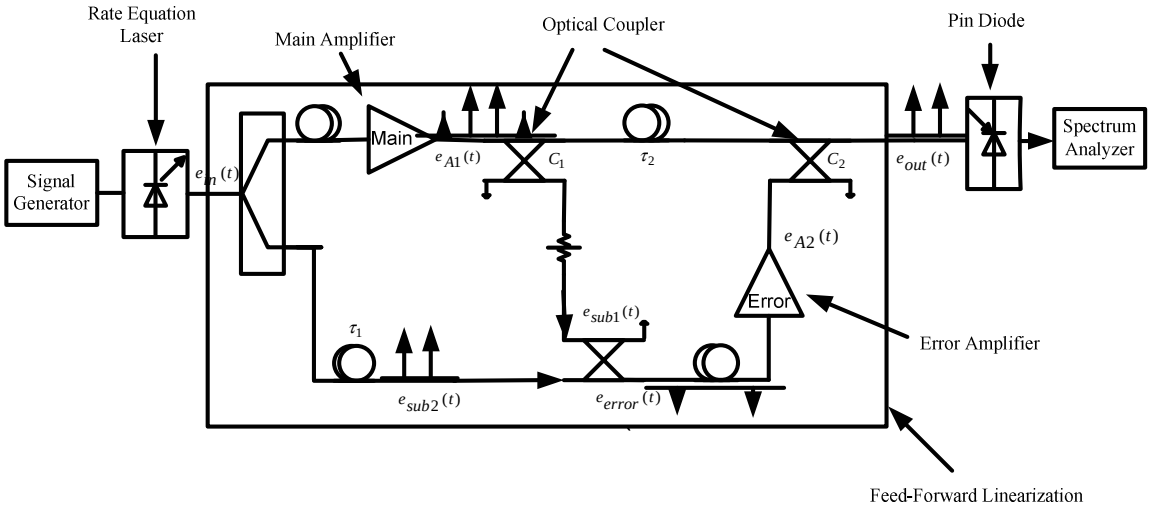

Figure 4.15 General diagram for feed-forward linearization

This part shows the effect of time delay on the cancellation, for full detail see [71].

Assume that the input $e_{in}(t)$ is a single CW tone of amplitude A, thus:

$$e_{in}(t) = A\cos(\omega t + \theta) \tag{4.26}$$

Therefore the output from C_2, is given by:

$$e_{out}(t) = A\cos\{\omega(t+\tau_1)+\theta\} - A\cos\{\omega(t+\tau_2)+\theta\} \tag{4.27}$$

Assuming that the error path delay is longer than the main path delay by $\Delta\tau$, the error path delay is given by:

$$\tau_2 = \tau_1 + \Delta\tau \tag{4.28}$$

Therefore, by substitution of Eqn. 27 into Eqn. 26, then expanding and simplifying, the above expression yields:

$$R^2 = (A - A\cos\omega\Delta\tau)^2 + (A\sin\omega\Delta\tau)^2 \tag{4.29}$$

Thus, the amplitude of the output signal R after normalisation (i.e. setting A=1) is given by:

$$R = 2\sin\left(\frac{\omega.\Delta\tau}{2}\right) \tag{4.30}$$

$$R_{dB} = 20\log_{10}\left\{2\sin\left(\frac{\omega.\Delta\tau}{2}\right)\right\} \tag{4.31}$$

To find the phase difference $\Delta\phi$, between the input tone and the output tone, the output phase is referenced to the input phase by setting $\theta = 0$, thus:

$$\Delta\phi = \tan^{-1}\left[\frac{\sin\omega\Delta\tau}{1-\cos\omega\Delta\tau}\right] \tag{4.32}$$

4.5.2 Feedforward Approach

In this research two applications have been used to simulate the output of the SOA using feed-forward approach to reduce the noise and linearize the output. The aim is to cancel out the noise and four wave mixing. Table.4.1 shows the parameters that have been used at 1550 nm for the theoretical analysis for SOA, and table. 4.2 represents the pin diode parameters base on the Sumitomo Electric Device Innovation Inc. devices.

Table 4.1

Parameters	Value	Unit
Refractive index	3.4	
optical confinement factor	0.3	
differential gain	2.78×10^{-20}	m^2
carrier density at transparency	1.4×10^{24}	m^3
Volume	$0.0005\times(3\times10^{-6})\times(8\times10^{-8})$	m^3
line width enhancement factor	5	
recombination coefficients A	143000000	$1/s$
recombination coefficients B	1×10^{-16}	m^3/s
recombination coefficients C	3×10^{-41}	m^6/s
insertion loss	3	dB
cavity loss	3	dB
facet reflection	10	

Table 4.2

Parameters	Value	Unit
Responsivity	0.8	A/W
dark current	5	nA
forward current	5	mA
reverse photo current	3	mA
Capacitance	0.3	pF
coupling ratio	10%	

Two applications are shown below:

4.5.2.1 Application A

Figure 4.16 shows a complete model of the radio-over-fibre transmission system with Feedforward linearization to linearize the output of SOA. Simulated optical spectra at two points in the system are also shown in Fig. 4.18 (a) and (b). The Feedforward system was constructed using a low cost WDM filter for routing different signals. In this system, there are two signal generators with an electrical carrier signal at 2.5 GHz and 1mW output power. These signals are indirectly modulated with two CW laser via Mach-Zehnder modulators. CW Laser 1, operating at 1551 nm wavelength λ_1, and CW Laser 2, operating at 1552 nm wavelength λ_2 are multiplexed and transported to the fibre. According to the characteristics of the FWM, the two wavelengths should satisfy: $\lambda_{FWM1} = 2\lambda_1 - \lambda_2$ and $\lambda_{FWM2} = 2\lambda_2 - \lambda_1$. To compensate for the SOA nonlinear distortion, feed-forward linearization is used.

The simulation software used is the Opti-System 5.0. Both CW lasers, output power is 5 mW. The signal in the top paths is amplified by the main power amplifier and the non-linearities in this amplifier result in inter-modulation and harmonic distortions

which are added to the original signal. Noise is also added by the main amplifier, which is discussed in the next application.

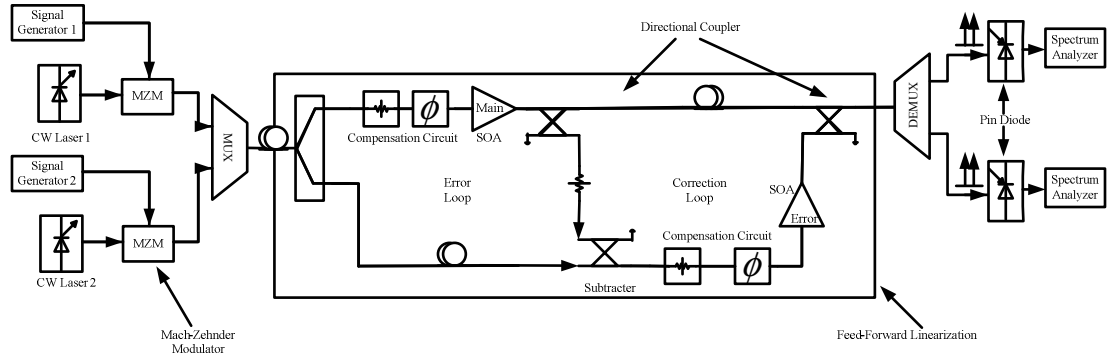

Figure 4.16 Feed-forward linearization for application A

A function of the main amplifier output subtracts from the time delayed original signal, in the lower path. The resulting output of error signal is then amplified to cancel the distortion in the main path and is combined with the signal in the upper path via a coupler. The main path signal is delayed by an amount approximately equal to the delay in the lower path (i.e. compensation circuit and amplifier), and is out of phase with the amplified error signal. The error signal cancel the distortion information on the main path and what emerges at the output of the feed forward linearization is the amplified version of the original input signal.

The simulator adjusts the amplitude, phase and delay line parameters belonging to the compensation circuits until the fundamental frequencies (λ_1 and λ_2) are cancelled, or at least minimized in the first loop. And the adjustment method consists in variations of amplitude, phase and delay line parameters belonging to the compensation circuit in correction loop. This adjustment continues until the third order inter-modulation products of the output signal are minimal or until the inter-modulation distance reach

the maximum value. The gain and phase adjustment components (compensation circuits) are shown in Fig. 4.16.

Since the gain and phase-matching characteristics of feed-forward amplifiers are critical to their performance, it is necessary to ensure that these can be maintained throughout the practical design of the amplifier. There is a compromise between the additional complexity of additional circuitry to monitor loop performance and correct for errors, or additional loops.

The idea of allowing the system to monitor its own performance and then perform the necessary correction implies some form of feedback system around the feed-forward loop. This feedback system in a practical world is required to control the gain and phase matching of the two loops, named as the error loop. Thus it is evident that two separate feedback systems are required. The first to correct for the gain and phase mismatches in the error loop. This method minimises the input signal component of the error signal. The second to correct for the gain and phase mismatches in the correction loop. This minimises the amount of distortion present in the final output signal.

Other consideration is error amplifier selection, which represents one of the highest restrictions in the feed-forward technique and must be competitive with a non-linearized amplifier. This means that production costs and above all efficiency rates must be taken into account. On the other hand linearity performance of the error amplifier should be dealt with. If highly linear error amplifiers are used, then the feed-forward technique turns become less efficient. Moreover, the distortion introduced by the error amplifier has a direct effect on the distortion component of the output signal. In other words, a trade-off is needed among the gain, linearity, cost and efficiency rates.

To simulate the model with feed-forward linearization, an input CW Laser with the following parameters was applied to the circuit shown in Fig. 4.16: line-width of 100 MHz and 5 mW. In order to obtain deep SOA saturation, the SOA (Fig. 4.16), were set to small-signal gains of 18.5 dB.

This configuration is appropriate for multiplexing access schemes such as WCDMA, Wireless LAN (OFDM) and GSM (TDMA) and higher data rates transmission systems.

4.5.2.2 Application B

An alternative application has shown in Fig. 4.17 the complete model of the radio-over-fibre transmission system with feed-forward linearization to linearize ASE noise of the output of the SOA. Simulated optical spectra at various points in the system are also shown in Fig. 4.19 (a) and (b). As mentioned in the previous application optical feed-forward linearization is a benefit to noise reduction in optical amplifiers.

Figure 4.17 illustrates the principle of operation. The electrical carrier (2.5 GHz, 1 mW) was generated by an external signal generator. A laser rate equation (1550 nm, 5 mW) converts the electrical input signal into an optical signal by means of direct modulation. This signal is sent to the divider and split to form two identical paths, and the rest of the processing is the same as previous application. But there is a consideration that has to be taken care of which has an important effect on the system. Maintaining a balance at the noise cancellation node is more complicated, since the result is not signal cancellation and integration is not directly applicable. A solution for effective automatic balance exists, which follows similar control guideline as the carrier cancellation loop. In any case, added circuit complexity is required and delay matching must be such that signals remain strictly in a single quadrant. Also the other important parameter is the noise figure of the main amplifier which should be better

than the error amplifier. The error amplifier ideally needs only to process the main amplifier distortion information and hence can be of a much lower power than the main amplifier. Thus, it is likely that a more linear and low noise error amplifier can be constructed. This in turn will result in lower overall system noise figure.

To test the circuit with feed-forward linearization, an input rate equation laser with the following parameters was applied to the circuit shown in Fig. 4.17: quantum efficiency of 0.4, group velocity of $8.5\times10^{10}\,cm\,/s$, spontaneous emission factor of 3×10^{-5}, power of 5 mW, and gain compression coefficient of $1\times10^{-17}\,cm^3$. In order to obtain deep SOA saturation, the SOAs in (Fig. 4.17), must be set to small-signal gains of 18.5 dB. The complex attenuator provided for adjusting the output signal from SOA via 10dB optical coupler to have the equal gain as the delayed line. The simulated output after the SOA is shown in Fig. 4.19 a. The complete optical performance by feed-forward linearization is shown by Fig. 4.19 b.

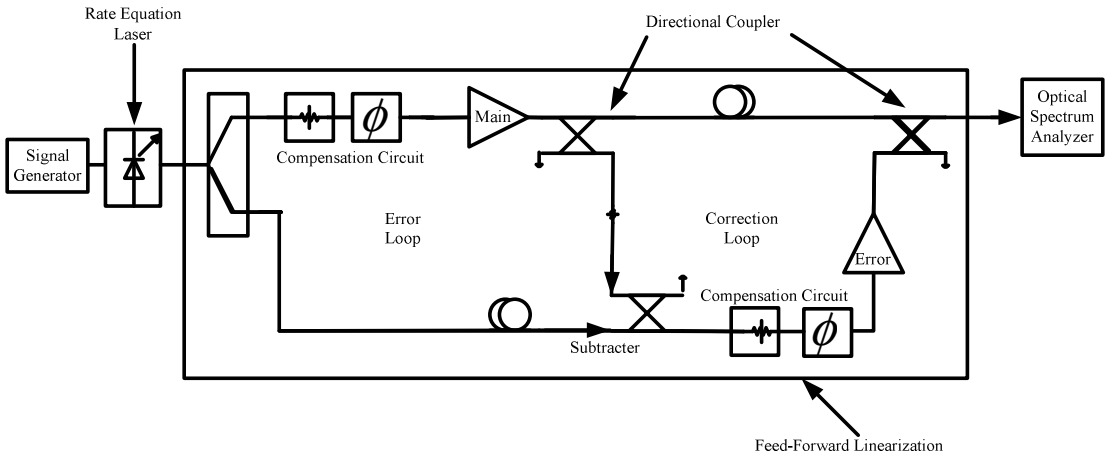

Figure 4.17 Feed-forward linearization for application B

4.5.3 Results

The input powers of both Channel 1 and Channel 2 were set equal at 0 dBm and the simulated RF spectra are shown in Fig. 4.18 for application A. It can be seen that

without the feed-forward linearization there was four waves mixing caused by the two high power input signals modulating Laser 1 and Laser 2. With feed-forward linearization, the four waves mixing were improved by more than 20 dB.

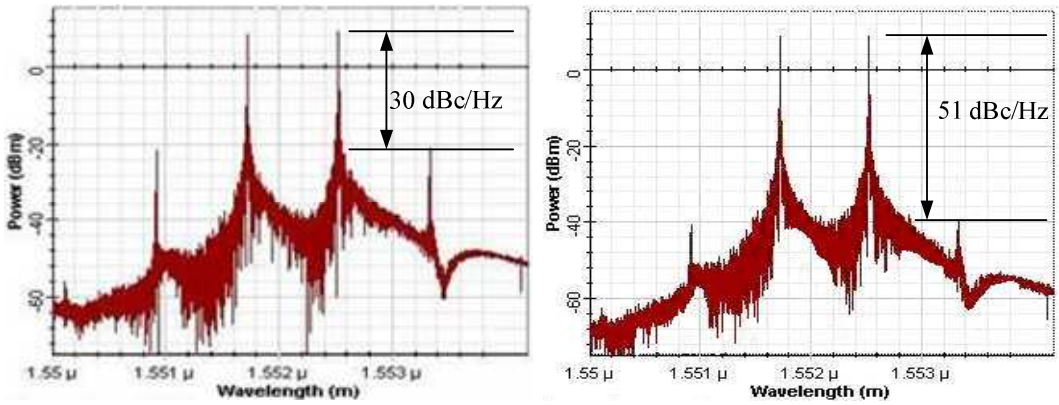

(a) **(b)**

Figure 4.18 (a): Signal spectrum before linearization for application A (b): signal spectrum after linearization for application A

The simulated spectra of the two tone CW RF signal indirectly modulated signal with and without the linearizer are shown in Fig 4.18.

In Figs. 4.18 (a) and (b), the carrier power is the same in both spectrum (11 dBm), and the IMD is -30 dBc/Hz without the linearizer and -51 dBc/Hz with the linearizer, respectively. As the IMD improvement by the linearizer is 21 dB. A comparison between Fig. 4.18 (a) and (b) shows that there is no power penalty for transmission.

Another very important characteristic of SOAs is noise since it largely determines the maximum number of devices which can be cascaded as linear repeaters within an optical fibre communication system [34]. The overall noise generated by an SOA comprises signal spontaneous beat noise, spontaneous-spontaneous beat noise, spontaneous emission shot noise and amplified signal shot noise [34].

Results of single tone simulations (application B) are shown in Fig. 4.19. The SOA output has a noise added to the signal which is shown in Fig. 4.19 (a). After the feed-

forward linearization as shown in Fig. 4.19 (b), that the noise spectrum is improved more than 8 dB, and also it is visualized that especially the asymmetry shape of spectrum because of the ASE noise has reduced more than 6 dB.

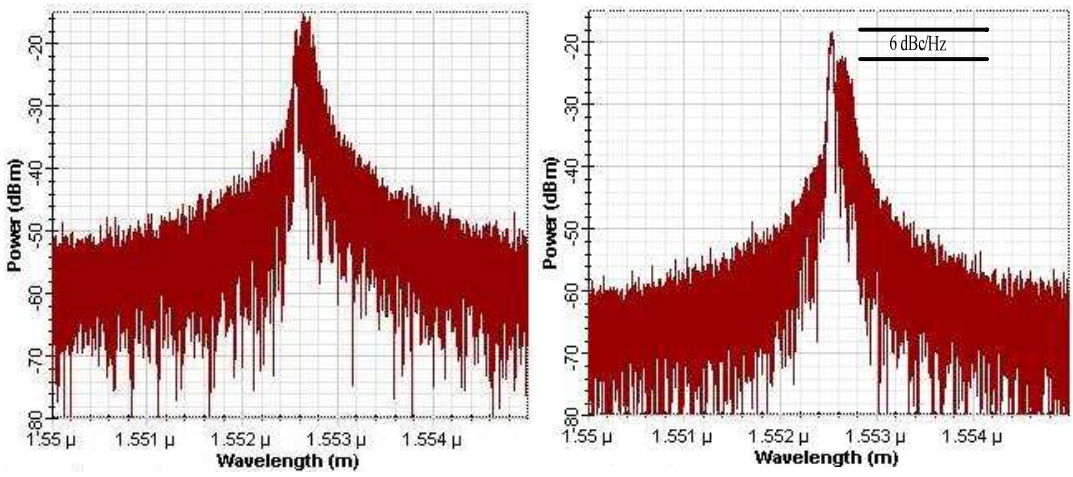

(a) **(b)**

Figure 4.19 (a): Signal spectrum before linearization for application B (b): signal spectrum after linearization for application B

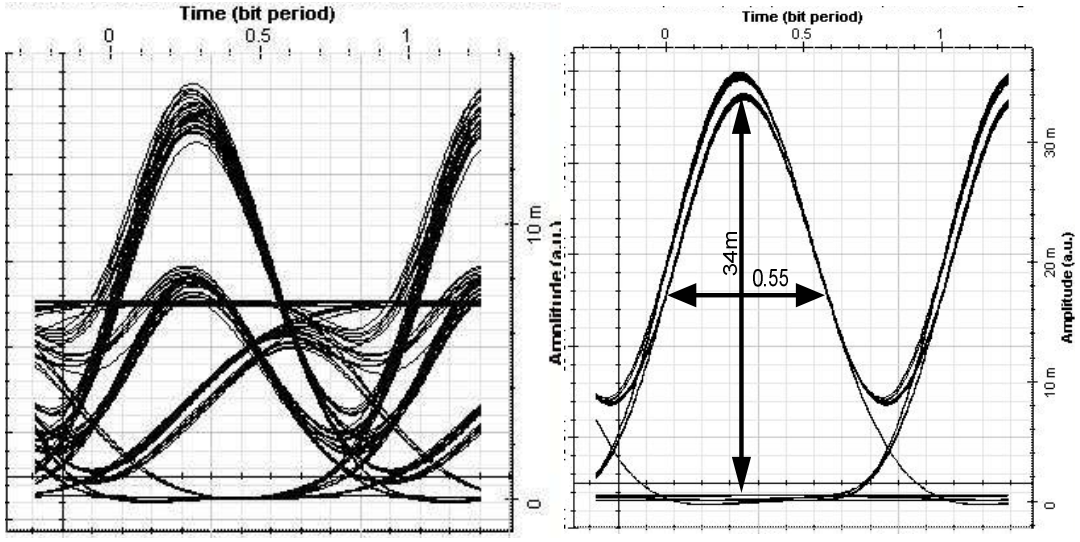

(a) **(b)**

Figure 4.20 (a): Eye diagram before linearization (b): eye diagram after linearization

Eye diagrams simulated for back-to-back operation for application A, at an optical power of 0 dBm are shown in Fig. 4.20. Without the feed-forward system, the eye

opening shown in Fig. 4.20 (a) is small and the excess noise inherent in the transmitted “ones” is clearly visible. Fig. 4.20 (b) shows that with the feed-forward system, the eye has a much wider opening and reduced noise on the “ones”. Figure 4.21 shows the quality factor which for a higher input the Q will be higher, which the quality factor increases with respect to power. As it is shown in Fig. 4.21 for the laser with 4 dBm output power the quality factor become more than 5 but as the power decreases the quality factor will decrease as well.

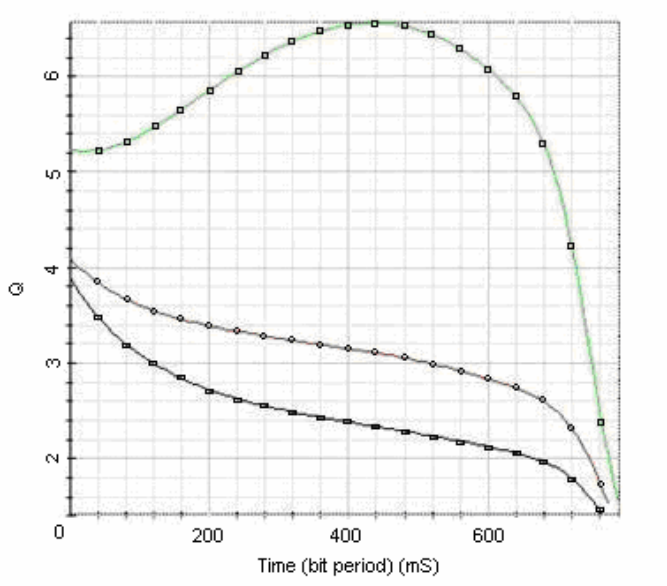

Figure 4.21 Quality factor after linearization with respect to input signal

4.6 Feed-Forward Linearization for Impulse Radio Ultra Wideband over Fibre

Ultra wideband (UWB) systems are highly useful for next generation short-distance, low-power-consumption, and high bit rates wireless indoor communications. The UWB radio typically has a short range in outdoor and indoor environments since the power level is regulated to -41 dBm/MHz across most part of the 3.1 to 10.6 *GHz* spectrum [73].

Current interests in UWB are fuelled by their intrinsic properties: immunity to multipath fading, extremely short time duration, carrier free, low duty cycle, wide occupied bandwidth, and low power spectral density [74]-[75]. A particularly attractive impulse technology is the carrier free modulation method, which does not adopt the complicated frequency mixers, intermediate frequency circuits, and electric filters, and thus significantly reduces its cost. Moreover, this method has good performance due to the UWB transmission, and is therefore, more suitable for indoor wireless communications. Moreover, the Gaussian pulse shaper (i.e., a special band-pass filter) must be utilized to generate Gaussian pulses or differential Gaussian monocycle pulses in the electronic impulse radio system.

High-speed wireless communications are gaining popularity to satisfy increasing demands for a broadband access. IEEE 802.15a proposes that data rates of UWB signals for the emerging standards should be around 100 Mbps to 480 Mbps for a distance of up to 10 meters [76],[77]. Attenuation and bandwidth limitations of copper cables will reduce transmission range and quality even more significantly for UWB signals.

The transmission distance of UWB radio systems, however, is limited up to ten meters due to the extremely low regulated power spectrum density by the Federal Communications Commission (FCC). Radio over Fibre (RoF) is a promising technology to extend the transmission distance by distributing such UWB signals over an optical link. Through the optical link, a number of stand-alone UWB applications in a building, for example, can be networked with each other, which leads the system to overcome the distance limitation. On the other hand, it is always desirable that the optical link has capacity to transmit the UWB signal with full spectrum released by the regulator such as FCC's. RoF technology is a cost effective way to distribute

UWB signals over extended distances, allows centralized operations and reduce infrastructure and operational costs [78].

UWB pulse signal over optical fibre is proposed for short distance by Yao [73] and Yee [77]. They investigate the transmission characteristic of UWB radio through a single mode RoF system for different lengths up to 3 km with different pulse shape. But in this research, the distance has been extended up to 50 Km.

This section investigates impulse radio ultra wideband (IR-UWB) over Fibre system based on a feedforward linearizer to suppress the FWM cancellation by the use of the SOA. The RF signal of UWB is transmitted over 50 Km single mode fibre (SMF) using external Mach Zehnder modulator (MZM), amplified, linearized and detect by a photo detector receiver. For improving the linearity and suppressing the FWM of SOA, the amplifier uses the feed forward technique. The simulation setup investigates the effects of optical link with the amplification on the transmission characteristics of the UWB signal, including the effects of dispersion of optical fibre and optical nonlinearity of the photonic devices, which are important to realize a high quality communication system. In addition this section presents a simulation model for investigation of a RoF transmission. The UWB pulse is generated by using a novel UWB band pass filter (BPF) with a high performance filter. The simulation includes the external optical modulation, fibre-optic transmission, SOA amplification, feed-forward linearization and photo detection of the full UWB signals. This simulation results show that RoF technology can be used to reliably distribute UWB signals and enhance the coverage.

4.6.1 RoF Structure

The simulation model configuration shown in Fig. 4.22 demonstrates an electrical to optical (E/O) module that uses laser diode technology to indirectly modulate the IR-

UWB radio signal via MZM into optical frequencies at a 1550 nm wavelength. It is simulated to transmit two UWB RF signals from a UWB transmitter to the fibre via indirect modulation (Fig. 4.22). The data source is derived from a Pseudo-Random Binary Sequence (PRBS) generator which can produce arbitrary data stream to create pseudo random data stream. The electrical IR-UWB signal is generated by pico-second impulse forming. On the optical side, the optical signal has passed through 50 km fibre and then amplified by the SOA amplifier. The feed-forward linearization technique is used to compensate the nonlinearity, caused by the fibre and SOA. The optical signal is converted back to electrical signal by using a photo detector at the receiver end. A variable attenuator between the UWB transmitter and E/O converter acts as an automatic gain control (AGC), thus preventing link saturation. BER analyzer calculates BER by analyzing the demodulated binary data with the reference binary data stream.

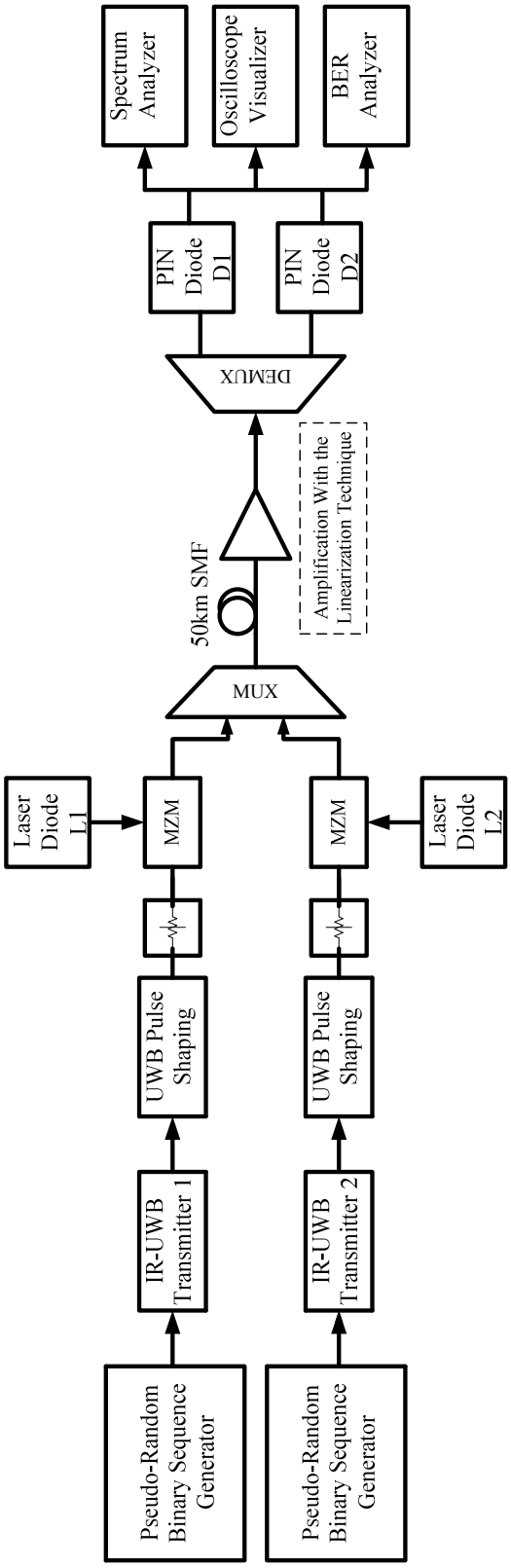

Figure 4.22 Radio-over fibre structure

A general UWB transmitter block diagram is shown in Fig. 4.23. First, data are generated by applications that are quite separate from the physical layer transmitter known as 'back end'. This binary information stream is then passed to the 'front end', which is the part of the transmitter which we are concerned about. If higher modulation schemes are to be used the binary information should be mapped from bits to symbols, with each symbol representing multiple bits. These symbols are then mapped to an analogue pulse shape generator. Precise time synchronisation is essential to ensure system operation. In PPM based systems both slot and frame synchronisation is required. Pulses can then be optically amplified before being passed to the transmitter. In general though, to meet power spectral requirements, a large gain is typically not needed and may be omitted. Although this is an extremely simplistic transmitter model, which omits any forward error correcting scheme, it serves the purpose to show that UWB transmitters can be quite simple [79].

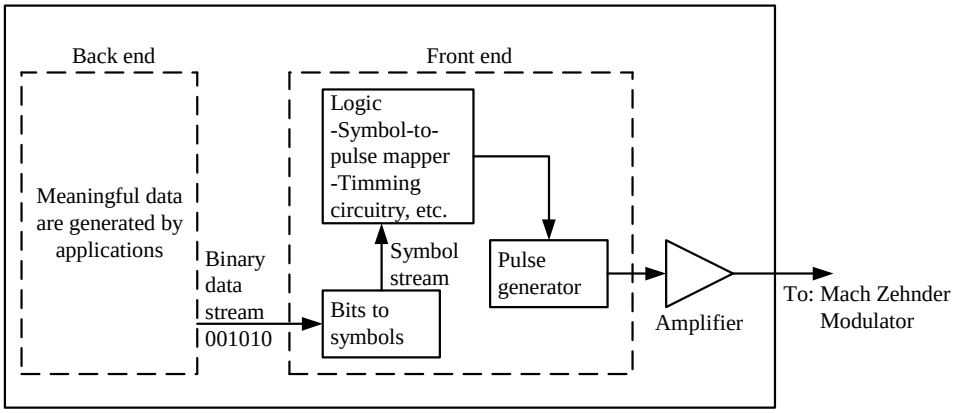

Figure 4.23 A general UWB transmitter block diagram

The normalized optical field being phase-modulated by the Gaussian pulse train can be expressed in the form of [79]:

$$E(t) = \exp\left[j\omega_c t + \beta . s(t)\right] \tag{4.33}$$

where ω_c is the angular frequency of the optical carrier, β is the phase modulation index, and $s(t)$ is the pulse train represented by:

$$s(t) = \sum_{n=-\infty}^{+\infty} p(t - nT) \tag{4.34}$$

where T is the pulse repetition interval, and $p(t)$ represents an ideal Gaussian pulse waveform. It is known that the energy spectral density of $p(t)$ is large at dc and low-frequency region, and due to the high wavelength makes wireless transmission of such a signal, impractical [80], [81]. The Gaussian function is described by [79]:

$$p(t) = \frac{1}{\sqrt{2\pi\sigma^2}} e^{-(t-\mu)^2/(2\sigma^2)} \tag{4.35}$$

where σ the standard deviation and μ the mean of the Gaussian distribution. For $\mu = 0$, the Gaussian function is given by [79]:

$$p(t) = \frac{1}{\sqrt{2\pi\sigma^2}} e^{-t^2/(2\sigma^2)} \tag{4.36}$$

More waveforms can be created by high-pass filtering of Gaussian pulse. Filtering acts in a manner similar to the Eq. (4.36). The first derivative of a Gaussian pulse is a Gaussian monocycle which has the form of [79]:

$$p(t) = \left(\frac{32k^6}{\pi} \right) t e^{-(kt)^2} \tag{4.37}$$

A Gaussian monocycle has a single zero crossing. Further derivatives yield additional zero crossing. The input signal to the fibre should be the 2nd derivative of the Gaussian function. The Gaussian doublet is given in time domain as:

$$p(t) = \left(\frac{32k^2}{9\pi} \right)^{\frac{1}{4}} \left(1 - 2(kt)^2\right) e^{-(kt)^2} \tag{4.38}$$

The approach proposed in this section is to convert the doublet Gaussian pulses into UWB pulses in the optical domain, which can be employed as UWB pulse source in a

UWB-over-fibre network. In addition, in the proposed approach since the SOA produce the nonlinearity, the feed-forward linearization technique can be applied to improve the operational capabilities of the UWB impulse systems.

4.6.2 Results

In this section, we have only focused on the BPSK UWB signal. A typical doublet Gaussian waveform is shown in Fig. 4.24(a) which used to drive a laser diode, whereas the output of the optical receiver is shown in Fig. 4.24(b). The full width at half maximum (FWHM) of the UWB radio signal before laser is 36.74 picoseconds according to Fig. 4.24(a) and the spectrum of the modulated Gaussian pulse for positive frequencies is illustrated in Fig. 4.25(a).

After 50 km fibre and the linearization the UWB waveform has spread to 70.14 picoseconds and the delay of 92.42 picoseconds at the photo receiver output with respect to the signal before laser as shown in Fig. 4.24 b. Also its spectrum is shown in 4.25 b which shows the impact of pseudo random noise (PN) time offsets on energy distribution in the frequency domain. If the original UWB signal needs to be preserved, additional pulse compression or high pass filtering may be applied at the optical receiver output to compress the UWB pulses.

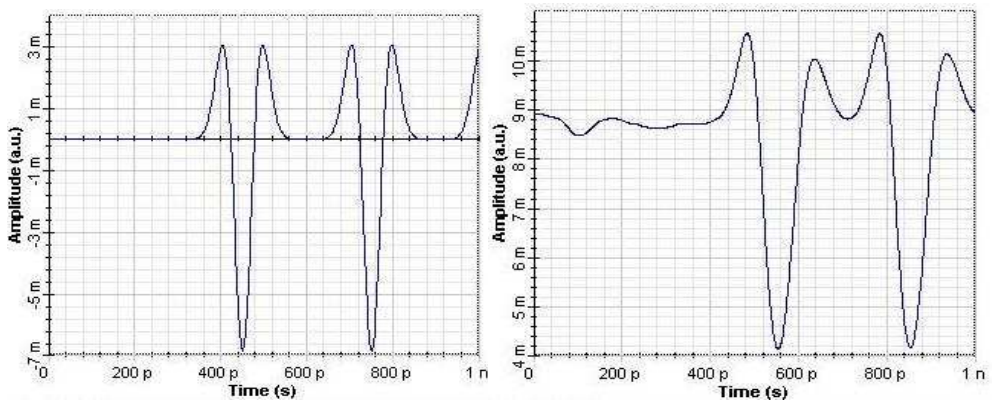

(a) **(b)**

Figure 4.24 (a): The input signal to the laser diode, and (b): the optical receiver output signal

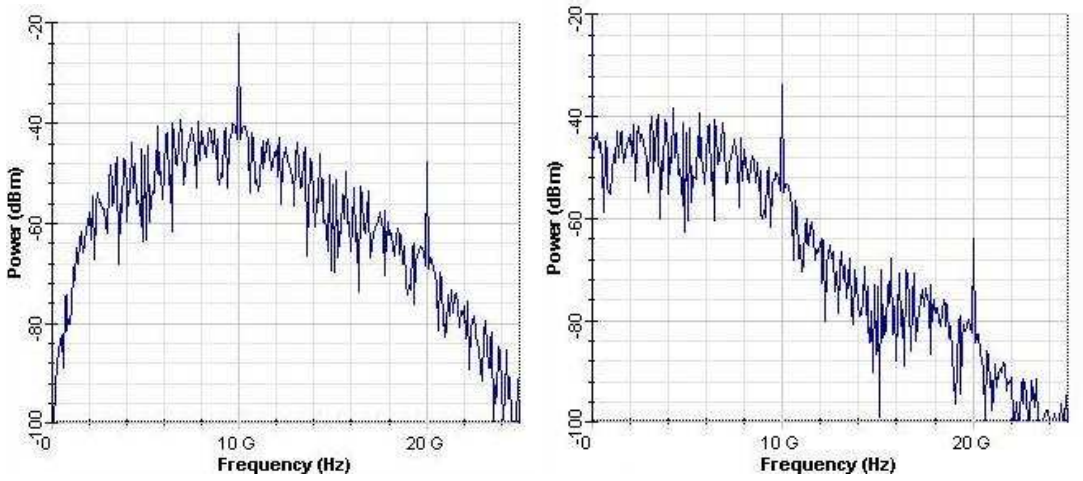

(a) **(b)**

Figure 4.25 (a): Signal spectrum before linearization, and (b): signal spectrum after linearization

The input power of both Channel 1 and Channel 2 were set equal at -41 dBm/MHz and the simulated RF spectra at different points are shown in Fig. 4.26. It can be seen that without the feed-forward linearization there is FWM caused by the laser sources and the SOA. With feed-forward linearization, FWM is reduced by more than 25 dB see Fig. 4.26(d).

Figure 4.26(a) shows the optical signal spectrum at the output of the multiplexer with a carrier power of 4.4 dBm. Figure 4.26(b) shows the optical spectrum of the UWB signals having passed through a 50 km SMF. Note that the carrier signal power is reduced by 5.6 dB. Figures.4.26(c) illustrates the signal spectrum at the output of the SOA showing increases the carrier power of 12.2 dBm and the IMD of -39.7 dBc/Hz. Following linearization, the carrier power has remained the same as input (i.e. 12.2 dBm), and the IMD is suppressed to -67.3 dBc/Hz see Fig. 4.26(d), an IMD improvement of 27.6 dB. A comparison between Fig.4.26(c) and (d) show that there is no power penalty.

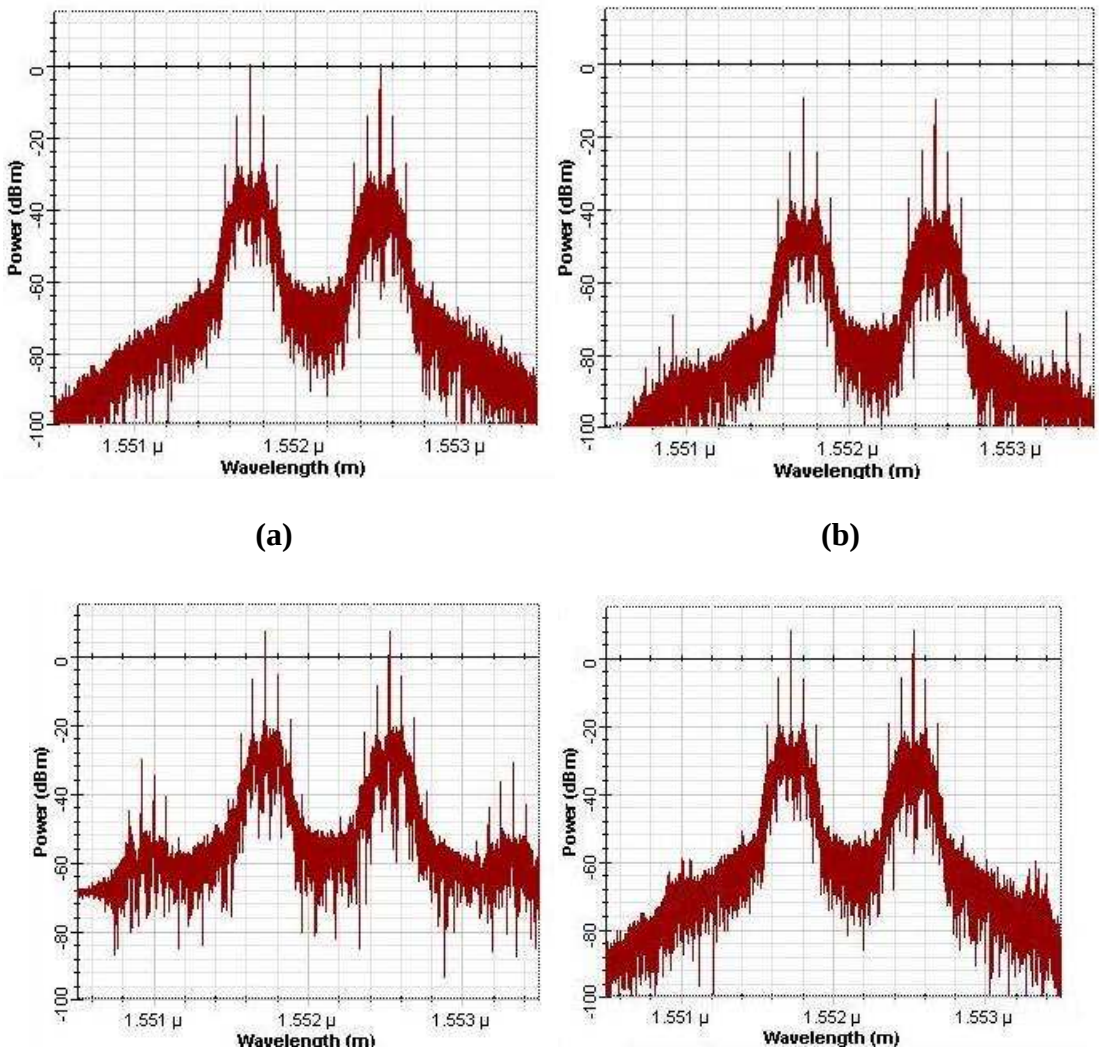

Figure 4.26 (a): Signal spectrum after multiplexer (b): signal spectrum after 50km SMF (c): signal spectrum after SOA, and (d): signal spectrum after linearization

Eye diagrams simulated for back-to-back operation are shown in Fig.4.27, for an optical power of 0 dBm. Without the feed-forward system, the eye opening shown in Fig. 4.27(a) is small and the excess noise inherent in the transmitted bits “1” is clearly visible. Fig. 4.27(b) shows that with the feed-forward system, the eye has a much wider opening and reduced noise level on the binary bits “1”.

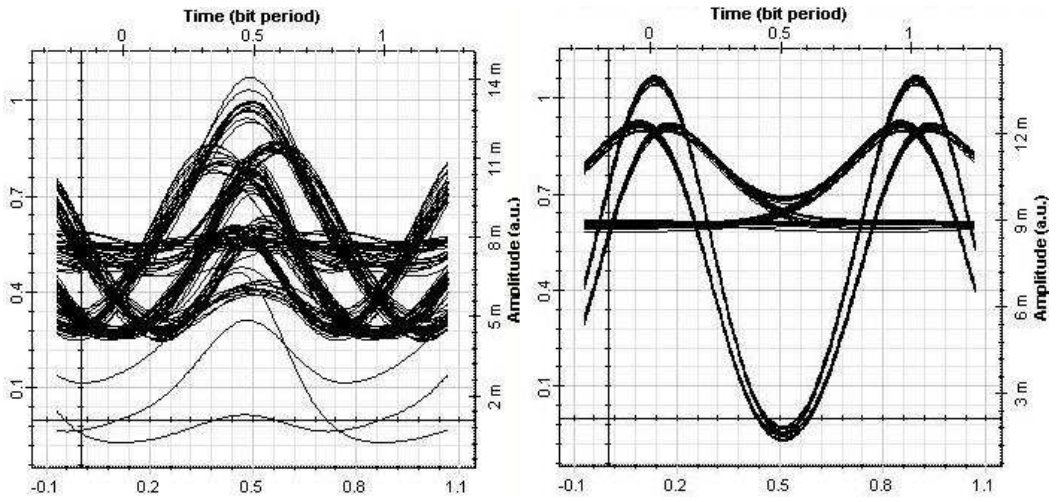

(a) **(b)**

Figure 4.27 (a): Eye diagram before linearization, and (b): eye diagram after linearization

4.7 Predistortion Feedback Linearization for IR-UWB over Fibre

Predistortion feedback techniques have been widely investigated for RF amplifier linearization. IMD suppression has been achieved along with a reduction in linear amplifier gain equal to the loop gain of the feedback amplifier. It has small and simple circuitry which is the most important advantage [82]. For the first time the application of optical predistortion feedback (OPDFB) is proposed to linearize the overall optical amplifier response so that spectral re-growth of the amplified optical modulated signal can be avoided. There is a strong demand for a linearizer that has a simple optical circuit configuration, a minimal control circuit, and a large improvement in IM3 components. This research investigates a simple and a low cost method using OPDFB linearization to suppress the FWM and reduce the ASE noise due to the SOA used in RoF systems.

A promising technique to remove the drawbacks of the RF linearization technique is, Predistortion (PD). The PD based on the error feedback correction is a powerful linearization technique because the error correction is insensitive to amplifier

variations, such as temperature, supply voltage, and device variations, as well as nonlinear characteristics of the PA. Among the PD linearization techniques, the lookup table (LUT)-based PD has been widely used because it is relatively simple and easily implemented to build the inverse function of PAs. In the PD algorithms that provide as the inverse function of the amplitude and phase distortions (AM/AM and AM/PM) generated by the PAs, the basic and most important issue is that the estimation error, the difference between the desired and the estimated values, should reach the minimum value for a given input signal.

4.7.1 RoF Architecture

The OFBPD linearization method can accurately extract the PD signal and enhance the tolerance of the IM distortion cancellation by the feedback linearization. In the linearizer, the main signal, as well as the error, is fed back, suppressing the open loop gain. We believe that this is the first reported optical PA linearization technique using PD and feedback techniques in the optical domain, which eliminates the problems of the optical feedback circuit. As a result, the distortion correction of the PD is carried out by the PD and further enhanced by the feedback linearization. Compared to conventional PD, the IMD cancellation tolerance is enhanced by a factor of the gain compression of the feedback circuit, and the error extraction algorithm is very simple.

The input signal is split to form two identical paths, although the ratio used in the splitting process need not be equal. The signal in the top path is amplified by the main power amplifier and the non-linearities in this amplifier result in inter-modulation and harmonic distortions being added to the original signal. The directional coupler, C2, takes a sample of the main amplifier signal and feeds it to the subtracter (C3, 180 degree) where a time delayed portion of the original signal, present in the lower path, is subtracted. The result of this subtraction process is an error signal containing substantially the distortion information from the main amplifier; ideally none of the original signal energy would remain. The error signal is then amplified linearly to the

required level to cancel the distortion in the main path and fed to the output coupler. The main path signal is time delayed, and fed to the coupler C1 in anti-phase to the amplified error signal. The error signal will then reduce the distortion information of the main path signal and after passing the main amplifier leaving substantially an amplified version of the original input signal.

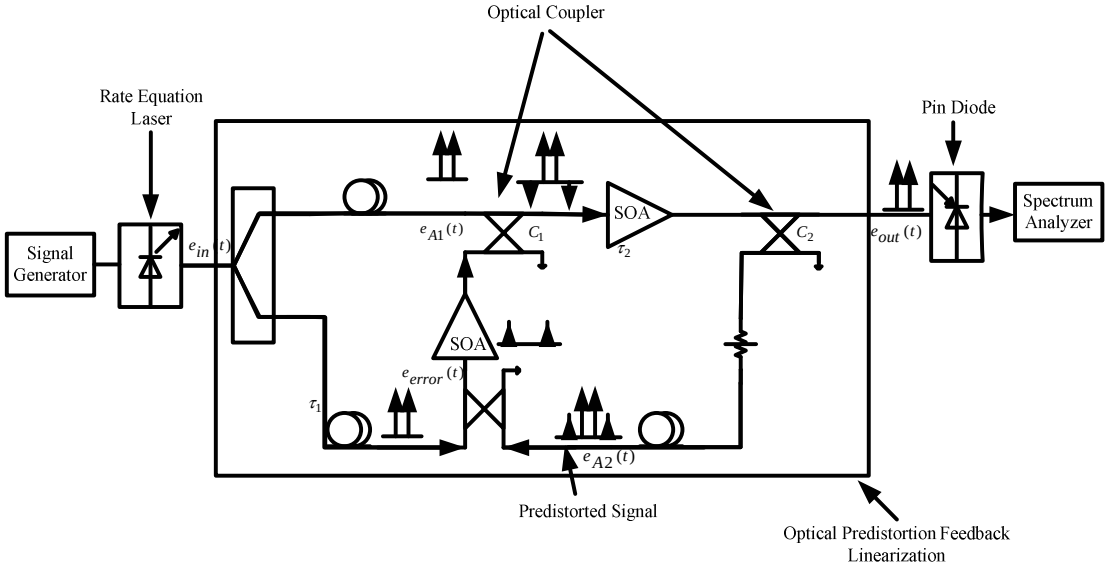

Figure 4.28 General diagram for predistortion feedback linearization

4.7.2 Predistortion Feedback Approach

In this section CW and IR-UWB signals have been used to simulate the output of the SOA using optical Predistortion feedback approach to reduce the noise and linearize the output. The aim is to cancel out the noise and four wave mixing. Table 4.3 shows the parameters that have been used at 1550 nm for the theoretical analysis for SOA, and table 4.4 represents the pin diode parameters.

Table 4.3

Parameters	Value	Unit
Refractive index	3.4	
optical confinement factor	0.3	
differential gain	2.78×10^{-20}	m^2
carrier density at transparency	1.4×10^{24}	m^3
Volume	$0.0005\times(3\times10^{-6})\times(8\times10^{-8})$	m^3
line width enhancement factor	5	
recombination coefficients A	143000000	$1/s$
recombination coefficients B	1×10^{-16}	m^3/s
recombination coefficients C	3×10^{-41}	m^6/s
Insertion loss	3	dB
cavity loss	3	dB
facet reflection	10	

Table 4.4

Parameters	Value	Unit
Responsivity	0.8	A/W
dark current	5	nA
forward current	5	mA
reverse photo current	3	mA
capacitance	0.3	pF
Coupling ratio	10%	

This section, demonstrate the first illustration of the transmission of multi-channel IR-UWB signals which are in the range 3.1-10.6 GHz in fibre distribution architecture with OPDFB linearization employed to improve system performance. Signals are generated and distributed using a WDM and 50 km fibre ring architecture. The wavelength spacing for the channels is based on a 1 nm. Changing the phase and amplitude of the optical signal in the proposed linearization scheme, carrier to IMD ratio is improved to more than 20 dB with optimal conditions.

Figure 4.28 contains elements of both feedback and feed-forward, although it is essentially a feedback technique in terms of its distortion cancellation methodology.

Its detailed operation is illustrated by various spectra (amplitude versus frequency plots) shown at a number of points within the figure. In this system, there are two signal generators with the electrical carrier of 2.5 GHz and 1mW output power. These signals are indirectly modulated with two CW laser via a MZM. CW Laser 1, operating at 1551 nm wavelength (λ_1), and CW Laser 2 1552 nm wavelength (λ_2) are multiplexed and transported to the fibre. According to the characteristics of the FWM, the two wavelengths should satisfy: $\lambda_{FWM1} = 2\lambda_1 - \lambda_2$ and $\lambda_{FWM2} = 2\lambda_2 - \lambda_1$. To compensate for the SOA nonlinear distortion, feed-forward linearization scheme is used.

Two CW lasers, one with 1551 nm wave length and the other with 1552 nm wavelength were both generating optical signals with 5mW output power. This signal is sent to the multiplexer and then to the divider and split to form two identical paths.

This feedback system in a practical world is required to control the gain and phase matching of the two loops. Thus it is evident that two separate feedback systems are required. The first to correct for the gain and phase mismatches in the error loop. This correction minimizes the input signal component of the error signal. The second to correct for the gain and phase mismatches in the correction loop. This minimizes the amount of distortion present in the final output signal. The signal in the top paths is amplified by the main power amplifier and the non-linearities in this amplifier result in inter-modulation and harmonic distortions being added to the original signal. Noise is also added by the main amplifier. The directional coupler C2 takes a sample of the main amplifier output signal and feeds it to the subtracter where a time delayed portion of the original signal, present in the lower path, is subtracted. The result of

this subtraction process is an error signal containing substantially the distortion information from the main amplifier.

The purpose of the error signal is to act as a predistorting signal for the coupler C1, with feedback mechanism operating continuously in real-time (unlike that of, say, conventional Predistortion). The error signal V_e used to modify the amplifier's characteristics to minimize distortion, is defined as.

$$V_e = DV_{out} - DV_{in} \tag{4.60}$$

where DV_{out} and DV_{in} are, respectively, the detected output and input signals. Error signal V_e can be used to control the gain of the amplifier by means of a variable attenuator. Superior linearity can be obtained by correcting both amplitude and phase. The magnitude and phase error signals can be determined. The resulting voltages are used to control an attenuator and a phase shifter to minimize signal error.

The resulting optical error signal should be comparable with the optical input signal (although containing unwanted distortion). Finally, a copy of the input signal is subtracted from the optical error signal, with an appropriate gain and phase weighting to ensure near-ideal vector subtraction. The resulting error signal resembles those typically seen in a feed-forward system. It is then gain and phase weighted and amplified. Next it is added to the original input signal, to form the optical input to the output, as described earlier.

The degree of gain and phase matching required in the main-signal cancellation process, to achieve good performance, is reported to be quite high. A match of 0.1dB and 0.1 degree was used to generate the results. To achieve and maintain these levels of matching in a practical solution would require an automatic control system, in very much the same way as that of the error-generating loop in a feed-forward system. The

main advantage of the technique lies in its potentially high linearity improvement capability. The technique is capable of some 20-25dB of IMD improvement for two-tone test carrier [70]. This represents a useful improvement in receiver intercept point. This linearity improvement was achieved with a minimal degradation in overall noise figure. This is a clear advantage over both feed-forward and Predistortion techniques.

The main disadvantages of the technique lie in its relative complexity, particularly when a control scheme is included to maintain the performance of the vector cancellation part of the system.

There has been considerable work on the use of feedback for the linearization of RF and microwave amplifiers. Feedback techniques can be divided into several distinct branches. The use of linear networks for feedback is well documented but has seen little use at microwave frequencies. The reason for this reluctance is probably due to concerns with amplifier stability and the difficulty in making networks with non-ideal components function over wide frequency bands.

The simulator adjusts the amplitude, phase and delay line parameters belong to the compensation circuits until the fundamental frequencies (λ_1 and λ_2) are cancelled, or at least minimized in the first loop. The adjustment method consists in variations of amplitude, phase and delay line parameters belonging to the compensation circuit in the correction loop until the third order inter-modulation products of the output signal are minimal or until the inter-modulation distance reach the maximum value. The gain and phase adjustment components (compensation circuits) are shown in Fig.4.29. Since the gain and phase-matching characteristics of feed-forward amplifiers are critical to their performance, it is necessary to ensure that these can be maintained throughout the practical design of the amplifier. There is a compromise between the

additional complexity of additional circuitry to monitor loop performance and correct for errors, or additional loops.

To simulate the model with feed-forward linearization, an input CW Laser with the following parameters was applied to the circuit shown in Fig.4.29: line-width of 100 MHz and 5 mW. In order to obtain deep SOA saturation, the SOA (Fig.4.29), were set to small-signal gains of 18.5 dB. The simulated output after the SOA is shown in Fig.4.31(a). The complete optical performance by the feed-forward linearization has shown by Fig.4.31(b).

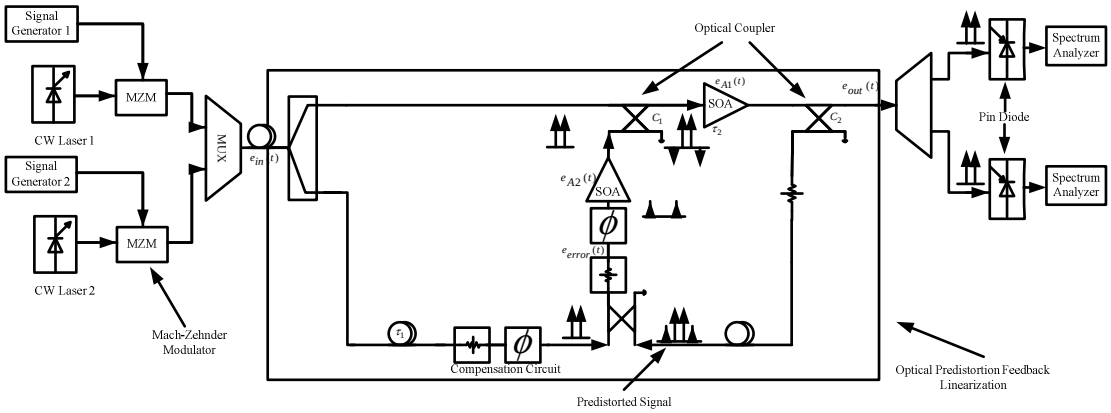

Figure 4.29 OPDFB linearization with CW input

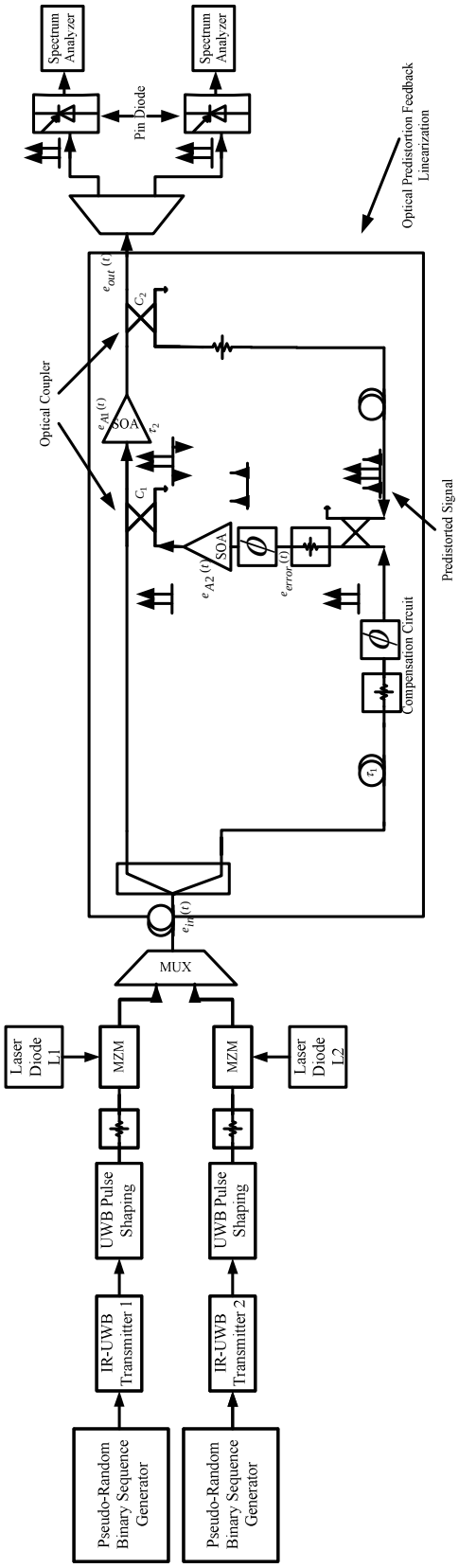

Figure 4.30 OPDFB linearization with IR-UWB input

4.7.3 Results

The input powers of both Channel 1 and Channel 2 were set equal at 0 dBm and the simulated RF spectra are shown in Fig.4.31 for application A. It can be seen that without the OPDFB linearization there is FWM caused by the two high power input signals modulating Laser 1 and Laser 2. With OPDFB linearization, FWM is reduced by more than 20 dB.

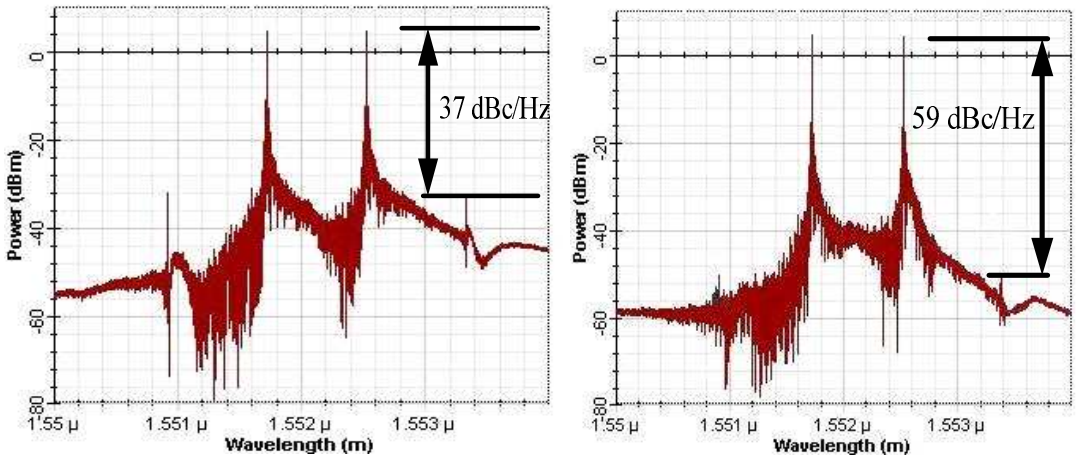

(a) **(b)**

Figure 4.31 (a): Signal spectrum before linearization, and (b): signal spectrum after linearization

The simulated spectra of the two tone CW RF signal indirectly modulated signal with and without the linearizer are shown in Fig.4.31.

In Figs.4.31 (a) and (b), the carrier average power is the same in both spectrum (8 dBm), and the IMD is -37 dBc/Hz without the linearizer and -59 dBc/Hz with the linearizer, respectively. A comparison between Fig.4.31 (a) and (b) show that there is no power penalty for transmission, an IMD improvement of 22 dB.

The simulated spectra of the two IR-UWB signals indirectly modulated signal via MZM (application B) with and without the linearizer are shown in Fig.4.32. Figures 4.32 (a) illustrate the signal spectrum after SOA to compensate for the transmission

loss over 50km SMF showing a carrier power of 18.1dBm and IMD of -24.7 dBc/Hz. After linearization, the carrier power is the same as before linearization (18 dBm), but IMD is reduced to -45.3 dBc/Hz which is shown in Fig.4.32(b), as the IMD improvement by the linearizer is 20.6 dB. A comparison between Fig.4.32 (a) and (b) show that there is no power penalty for transmission.

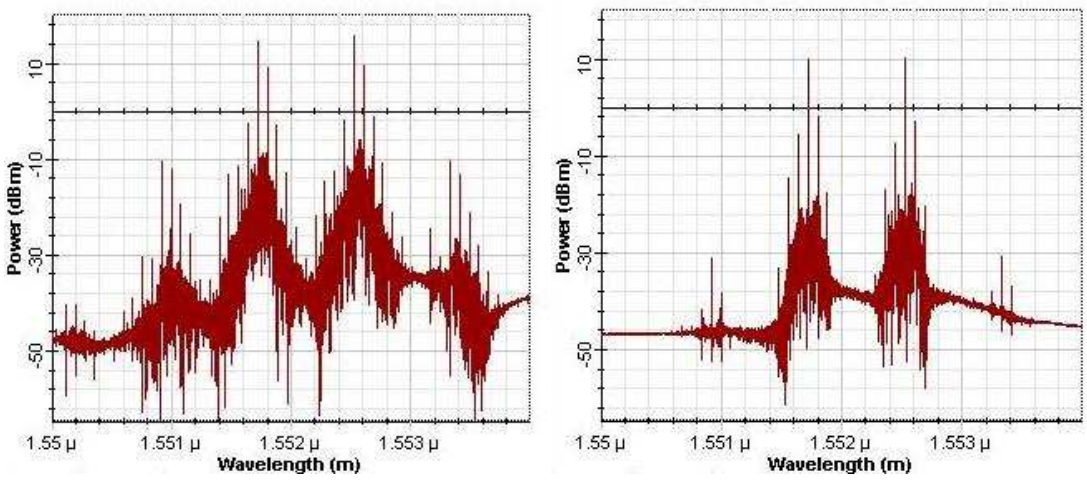

(a) **(b)**

Figure 4.32 (a): Signal spectrum before linearization for application B, and (b): signal spectrum after linearization for application B

In this part, is only focused on the BPSK UWB signal. A typical doublet Gaussian waveform is shown in Fig.4.33(a). The input signal to the laser diode is given in Fig.4.33(a) and the photo receiver output signal is shown in Fig.4.33(b). The pulse width measured at 50 % of the maximum amplitude of the UWB radio signal before laser is 36.74 picoseconds according to Fig.4.34(a) and its spectrum measured is shown in Fig 4.34(a).

After 50 km fibre and the linearization the UWB waveform has spread to 70.14 picoseconds and this is a delay of 92.42 picoseconds at the optical receiver output UWB spectrum is shown in Fig.4.34(b). If the original UWB signal needs to be preserved, additional pulse compression or high pass filtering may be applied at the

photo detector output to compress the UWB pulse. Alternatively, the UWB antenna can also be used to shape the signal to meet the emission spectrum mask at the downlink.

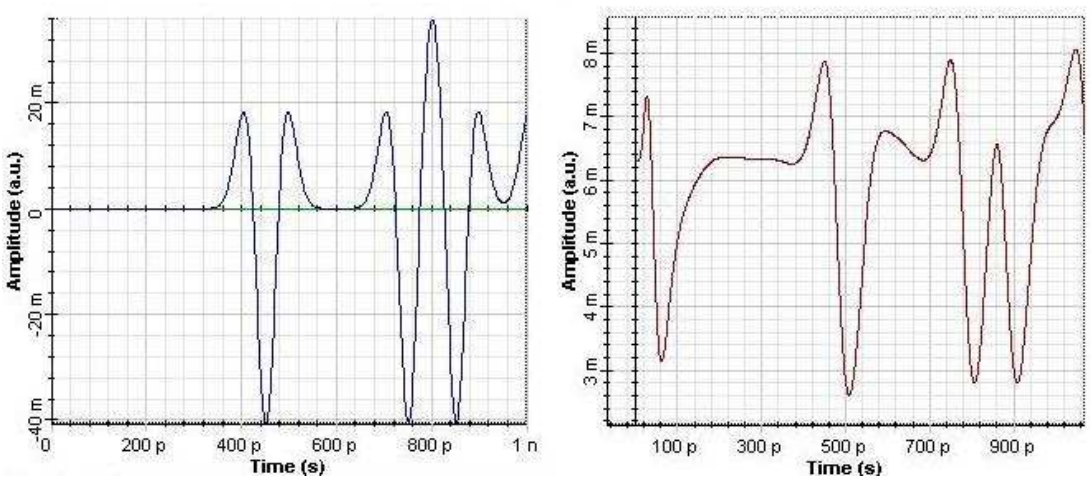

(a) **(b)**

Figure 4.33 (a): The input signal to the laser diode, and (b): the photo receiver output signal

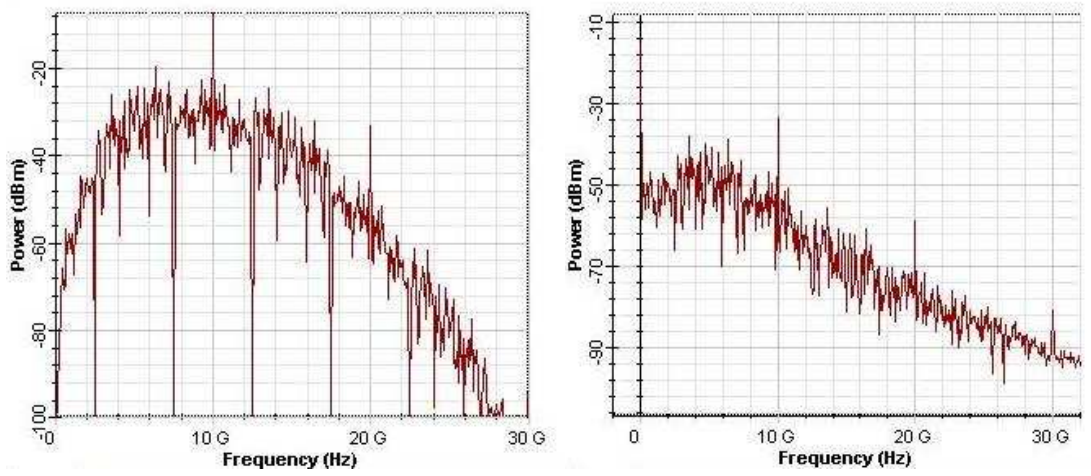

(a) **(b)**

Figure 4.34 (a): Signal spectrum of the input signal, and (b): Signal spectrum after linearization

Figure 4.35 illustrate the obtained BER of the signal with linearization with respect to the optical signal to noise ratio (OSNR). Increasing the OSNR improves the BER as one would expect. Also it is shown with the back-to-back signal it has obtained the $\mathrm{BER} = 10^{-9}$ at 76.2 dB OSNR.

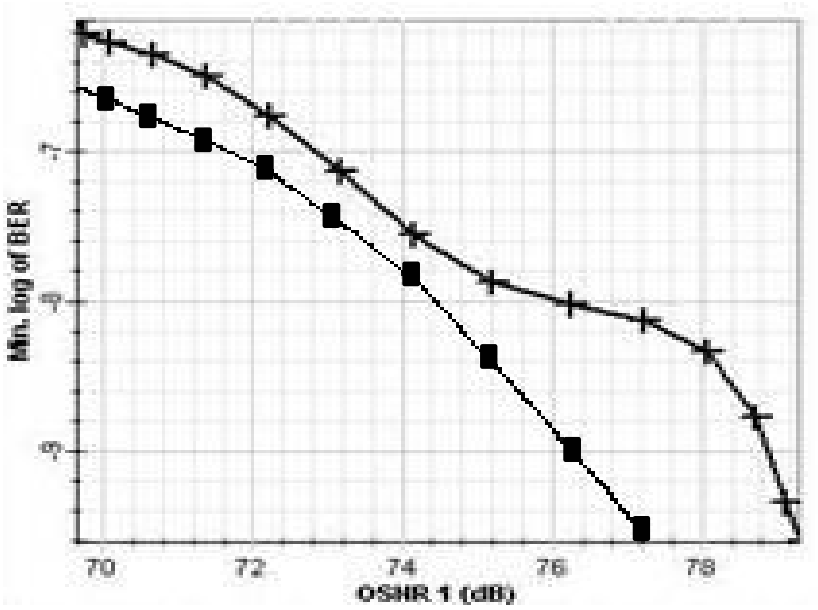

Figure 4.35 Bit error rate graph for the predistortion feedback linearization using UWB signal for source "square mark–back to back signal" and "cross mark- BER of the signal with linearization

Eye diagrams simulated for back-to-back operation for application A, at an optical power of 0 dBm are shown in Fig.4.36 Without the feed-forward system, the eye opening shown in Fig.4.36 (a) is small and the excess noise inherent in the transmitted "ones" is clearly visible. Fig.4.36 (b) shows that with the feed-forward system, the eye has a much wider opening and reduced noise on the "ones".

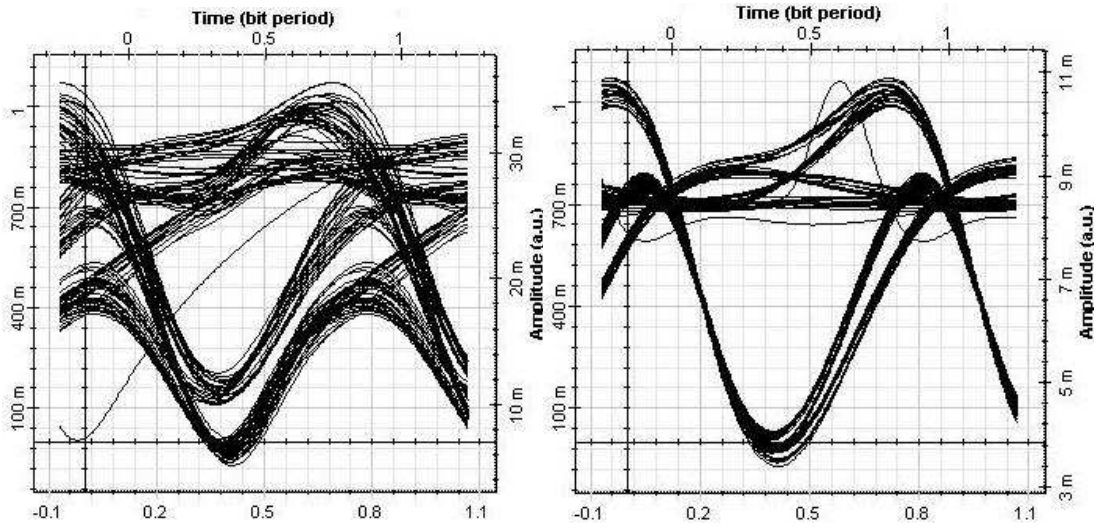

(a) **(b)**

Figure 4.36 (a): Eye diagram before linearization, and (b): eye diagram after linearization

In order to estimate the performance of this system, the optical signal to noise ratio (OSNR) is varied at the input of the device. Figure 4.37 shows the regenerator performance as a function of the OSNR in back-to-back for the two channels for an OSNR of 78 dB. Figure 4.37 shows the quality factor which for a higher OSNR the Q will be higher. As it is shown in Fig. 4.37 for the laser with 78.4 dB OSNR the quality factor become more than 6.

Regeneration may also be used for a single channel input. In this case, the regenerator improvement increases due to the reduction of XPM.

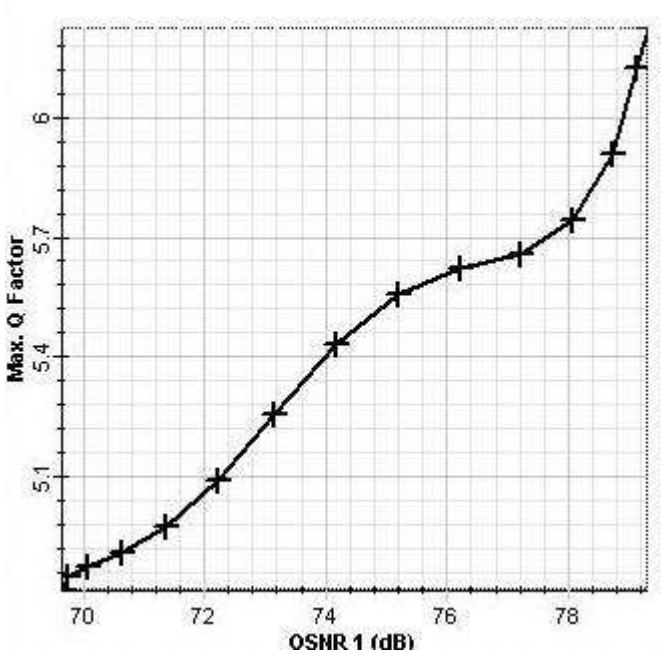

Figure 4.37 Quality factor after linearization with respect to input signal

4.8 Optimization Method for Compensation Circuitry

OptiSystem provides a powerful multi-parameter multi-target optimization tool. The optimization is performed by simulating the optical system or sub-system. In general, the optimization tool adjusts one or more signal or component parameters before each run, based on previous results obtained using the optimization algorithm. It can also force several user-defined constraints on selected parameters. This is especially important when for example a selected parameter or several parameters is must be kept between certain values.

The optimization tool also allows setting up multiple multi-parameter optimizations and running them in sequence. If proper parameters are selected optimization procedure can find the optimum parameters after reasonable number of iterations. Number of iterations depends on number of parameters selected, number of target values, degree of sensitivity, starting values of parameters, complexity of the system,

etc. For example optimizing length to maximize the Q factor may take a couple of iterations, while adjusting the gain and phase in feedforward linearization for cancelation are more than 300 iterations. However, as all optimization procedures, the selected procedure may give a local minima or maxima instead of a global one. In that respect, it could give two different results depending on initial parameter values. Since the parameter range is well known, this is not a problem most of the times.

A flowchart of compensation circuitry for the error loop is shown in Fig. 4.38. The first step is to read the power and phase value of the sampled signal at the coupling port of the C1, and reference unamplified signal respectively. Then it compares the power and phase between these two arms. If power P1 of the sampled signal is greater than power P2 of the unamplified, the variable attenuator increases by 0.1 dB, and if it is smaller than P2 the attenuator decreases by 0.1 dB, until they become equal. Next step is to compare the phases, it increases the phase shifter by 1 degree on the unamplified reference signal arm until the $e_{error}(t)$ become minimum.

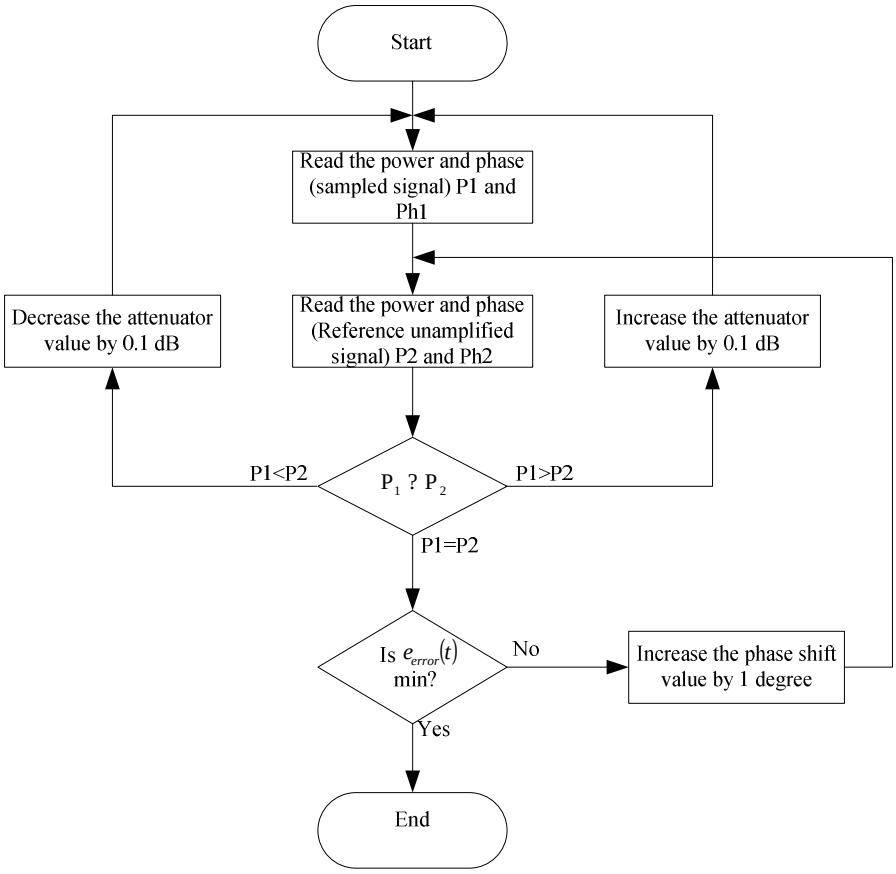

Figure 4. 38 Optimization flowchart for error loop

A flowchart of compensation circuitry for the correction loop is shown in Fig. 4.39. The first step is to read the power and phase value of the error amplified signal, and distorted amplified signal respectively. Then it compares the power and phase between these two arms. If power P1 of the error amplified signal is greater than power P2 of the distorted amplified signal, the variable attenuator increases by 0.1 dB, and if it is smaller than P2 the attenuator decreases by 0.1 dB, until they become equal. Next step is to compare the phases, it increases the phase shifter by 1 degree on the error amplified signal arm until the harmonics at the $e_{out}(t)$ become minimum.

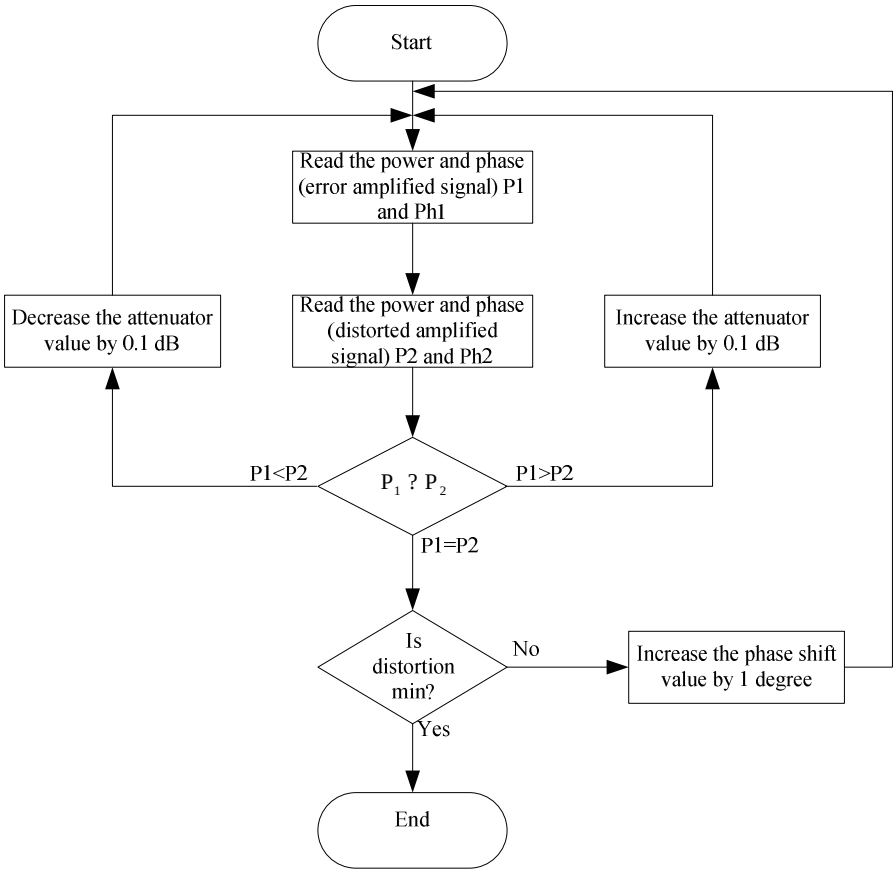

Figure 4.39 Optimization flowchart for correction loop

4.9 Summary

Different linearization techniques were summarized in this chapter, each one with different advantages and disadvantages which make them suitable for specific applications such as feedback, predistortion, and feedforward linearization. Optical feedforward and predistortion feedback linearization have been discussed in detail, and improved the harmonic distortion more than 20 dB for both techniques for two CW tone signals, and more than 6 dB for single tone to suppress the ASE noise. Those techniques also applied for IR-UWB over fibre and provided the same performance, and the results are provided in time and frequency domain. Finally the optimization procedure is described for the error and correction loop.

CHAPTER 5

WDM for Radio over Fibre Applications

5.1 Introduction

In principle, single-mode fibres used for optical communication systems have enormous capacity and can transport information at bit rates exceeding 10 Tb/s. In practice, however, the bit rate was limited to 10 Gb/s or less until 1995 by the speed of electronic components and by the limitations imposed by the dispersive and non-linear effects occurring inside optical fibres. Since then, transmission of multiple optical channels over the same fibre through wavelength-division multiplexing (WDM) has extended the system capacity to beyond 1 Tb/s.

5.2 WDM Lightwave Systems

Wavelength Division Multiplex corresponds to the scheme in which multiple optical carriers at different wave length are modulated by using independent electrical bit streams (which may themselves use TDM and FDM techniques in the electrical domain) and are then transmitted over the same fibre. The optical signal at the receiver is demultiplexed into separate channels by using an optical technique. WDM has the potential for exploiting the large bandwidth offered by optical fibres. For example, hundreds of 10-Gb/s channels can be transmitted over the same fibre when channel spacing is reduced to below 100GHz [39].

The low-loss transmission windows of optical fibres centred near are 1.3 and 1.55 μm. If the OH peak can be eliminated using “dry” fibres, the total capacity a WDM system can ultimately exceed 30-Tb/s [39]. The concept of WDM has been pursued since the first commercial lightwave system became available in 1980. In its simplest form,

WDM was used to transmit two channels in different transmission widows of an optical fibre. For example, an existing $1.3\,\mu m$ lightwave system can be upgraded in capacity by adding another channel near $1.55\,\mu m$, resulting in a channel spacing of $250\,nm$. Considerable attention was directed during the 1980s toward the reducing channel spacing, and multichannel systems with a channel spacing of less than $0.1\,nm$ had been demonstrated by 1990 [84]–[87]. However, it was during the decade of the 1990s that WDM systems were developed most aggressively. Commercial WDM systems first appeared around 1995, and their total capacity exceeded 1.6-Tb/s by the year 2000. Several laboratory experiments demonstrated in 2001 a system capacity of more than 10-Tb/s although the transmission distance was limited to below 200km [42]. Clearly, the advance of WDM has led to a virtual revolution in design in lightwave systems.

5.2.1 High-Capacity Point-to-Point Links

The ultimate capacity of WDM fibre links depends on how closely channels can be packed in the wavelength domain. The minimum channel spacing is limited by inter-channel crosstalk. Typically channel spacing Δv_{ch} should exceed $2B$ at the bit rate B. This requirement wastes considerable bandwidth. It is common to introduce a measure of the spectral efficiency of a WDM system as $\eta_s = B/\Delta v_{ch}$. Attempts are made to make η_s as large as possible.

The channel frequencies (or wavelengths) of WDM systems have been standardized by the International Telecommunication Union (ITU) on a 100 GHz grid in the frequency range 186-196 THz (covering the C and L bands in the wave length range 1530-1612 nm). For this reason, channel spacing for most commercial WDM systems is 100 GHz (0.8 nm at 1552 nm). This value leads to only 10% spectral efficiency at

the spacing bit rate of 10 Gb/s. More recently ITU has specified WDM channels with a frequency spacing of 50 GHz. The use of this channel spacing in combination with the bit rate of 40 Gb/s has the potential of increasing the spectral efficiency to 80%. WDM systems were moving in that direction in 2001.

The low-loss region of the state-of-the-art “dry fibres” (e.g. fibres with reduced OH-absorption near 1.4 um) extends over 300 nm in the wavelength region 1.3-1.6 um. The minimum channel spacing can be as small as 50 GHz or 0.4 nm for 40 Gb/s channels. Since 750 channels can be accommodated over 300 nm bandwidth, the resulting effective bit rate can be as large as 30 Tb/s. If we assume that the WDM signal can be transmitted over 1000 Km by using optical amplifiers with dispersion management, the effective BL product may exceed 30,000 (Tb/s)-Km with the use of WDM technology. This should be contrasted with the third-generation commercial lightwave systems, which transmitted a single channel over 80 Km or so at a bit rate of up to 2.5 Gb/s, resulting in BL values of at most 0.2 (Tb/s)-Km. Clearly, the use of WDM has the potential of improving of the performance of modern lightwave systems by factor of more than 100,000.

In practice many factors limit the use of the entire low-loss window. Most optical amplifiers have a finite bandwidth the number of channels is often limited by the bandwidth over which amplifiers can provide nearly uniform gain. The bandwidth of Erbium-doped fibre amplifiers is limited to 40 nm even with the use of gain-flattening techniques. The use of Raman amplification has extended the bandwidth to near 100 nm. Among other factors that limit the number of channels are (i) stability and tunability of distributed feedback (DFB) semiconductor lasers, (ii) signal degradation during transmission because of various non-linear effects, and (iii) inter-channel cross talk during demultiplexing. High-capacity WDM fibre links require many high-

performance components, such as transmitters integrating multiples DFB lasers, channels multiplexers and demultiplexers with add drop capability, and large-bandwidth constant-gain amplifiers.

Experimental results reported on WDM systems can be divided into two groups based on whether the transmission distance is ≈ 100 Km or exceeds 1,000 Km. Since the 1985 experiment in which ten 2 Gb/s channels where transmitted over 68 Km [3], both the numbers of channels and the bit rate of individual channels have increased considerably. A capacity of 340 Gb/s was demonstrated in 1995 by transmitting 17 channels, each operating at 20 Gb/s, over 150 Km [89]. This was followed within a year by several experiments that realized a capacity of 1 Tb/s. By 2001 the capacity of WDM systems exceeded 10 Tb/s in several laboratory experiments. In one experiment, 273 channels, spaced 0.4 nm apart and each operating at 40 Gb/s, were transmitted over 117 Km using three in-line amplifiers, resulting in a total bit rate of 11 Tb/s and BL product of 1300 (Tb/s)-Km [90]. Table 5.1 lists several WDM transmission experiments in which the system capacity exceeded 2 Tb/s.

Table 5.1 High capacity WDM transmission experiments

Channels N	Bit Rate B (Gb/s)	Capacity NB (Tb/s)	Distance L (km)	NBL Product [(Pb/s)-km]
120	**20**	**2.40**	**6200**	**14.88**
132	**20**	**2.64**	**120**	**0.317**
160	**20**	**3.20**	**1500**	**4.80**
82	**40**	**3.28**	**300**	**0.984**
256	**40**	**10.24**	**100**	**1.024**
273	**40**	**10.92**	**117**	**1.278**

The second group of WDM experiments is concerned with transmission distance for more than 5,000Km for submarine applications. In a 1996 experiment, 100-Gb/s transmission (20 channels at 5-Gb/s) over 9,100Km was realized using the polarization-scrambling and forward-error-correction techniques [91]. The number of

channels was later increased to 32, resulting in a160-Gb/s transmission over 9,300Km [92]. In a 2001 experiment, a 2.4-Tb/s WDM signal (120 channels, each operating at 20Gb/s) was transmitted over 6,200Km, resulting in a NBL product of almost 15 (Pb/s)-Km (see table 5.1). This should be compared with first fibre-optic cable laid across the Atlantic Ocean (TAT-8); it operated at 0.27-Gb/s with NBL ≈ 1.5 (Tb/s)-Km The use of WDM had improved the capacity of undersea systems by a factor of 10,000 by 2001.

On the commercial side, WDM systems with a capacity of 40-Gb/s (16 channels at 2.5-Gb/s or 4 channels at 10-Gb/s) were available in 1996. The 16 channels system covered a wavelength range of about 12nm in the 1.55-um region with a channel spacing of 0.8nm. WDM fibre links operating at 160-Gb/s (16 channels at 10-Gb/s) appeared in 1998. By 2001, WDM systems with a capacity of 1.6-Tb/s (realized by multiplexing 160 channels, each operating at 10-Gb/s) were available. Moreover, systems with a 6.4Tb/s capacity were in the development stage (160 channels at 40-Gb/s). This should be contrasted with the 10-Gb/s capacity of the third-generation systems available before the advent of the WDM technique. The use of WDM had improved the capacity of commercial terrestrial systems by a factor of more than 6,000 by 2001.

5.2.2 Wide-Area and Metro-Area networks

Optical networks are used to connect a large group of users spread over a geographical area. They can be classified as a local-area network (LAN), metropolitan-area network (MAN), or a wide area network (WAN) depending on the area they cover [93]-[98]. All three types of networks can benefits from the WDM technology. They can be designed using the hub, ring, or star topology. A ring topology is most practical for MANs, while the star topology is commonly used for

LANs. At the LAN level, a broadcast star is used to combine multiple channels. At the next level, several LANs are connected to a MAN by using passive wavelength routing. At the highest level, several MANs connect to a WAN whose nodes are interconnected in a mesh topology. At the WAN level, the network makes extensive use of switches and wavelength-shifting devices so that it is dynamically configurable. Consider first a WAN covering a wide area (e.g. a country). Historically, telecommunication and computer networks (such as the internet) occupying the entire US geographical region have used a hub topology. Such networks are often called mesh networks [99]. Hubs or nodes located in large metropolitan areas house electronic switches, which connect any two nodes either by creating a "virtual circuit" between them or by using packet switching through protocols such as TCP-IP (transmission control protocol-Internet protocol) and asynchronous transfer mode (ATM). With the advent of WDM during the 1990's the nodes were connected through point to point WDM links, but the switching was being done electronically even in 2001. Such transport networks are turned "opaque" networks because they require optical electronic conversion. As a result neither the bit rate nor the modulation format can be changed without changing the switching equipment.

An all-optical network in which the WDM network can pass through multiple nodes (possibly modified by adding or dropping certain channels) is called optically "transparent." Transparent WDM network are desirable as they do not require demultiplexing and optical-to-electronic conversion of all WDM channels. As a result, they are not limited by the electronic-speed bottleneck and may help in reducing the cost of installing and maintaining the network. The nodes in a

transparent WDM network switch channels using optical cross-connects. Such services were still in their infancy in 2001.

An alternative topology implements a regional WDM network in the form of several interconnected rings. Figure 5.1 shows such a scheme [100]. The feeder ring is connected to the backbone of the network through an egress node. This ring employs four fibres to ensure robustness. Two of the fibres are used to route the data in the clockwise and counter clockwise directions. The other two fibres are called protection fibres and are used in case a point to point link fails (self-healing). The feeder ring supplies data to several other rings through access nodes. An add-drop multiplexer can be used at all nodes to drop and to add individual WDM channels. Dropped channels can be distributed to users using bus, tree or ring networks. Notice those nodes are not always directly connected and require data transfer at multiple hubs. Such networks are called multi hubs networks.

Metro networks or MANs connect several central offices within metropolitan area. The ring topology is also used for such networks the main difference from the ring shown in Fig 5.1 stems from the scaling and cost consideration. The traffic flow in a metro ring at a modest bit rate compared with a WAN ring forming the backbone of a nationwide network. Typically each channel operates at 2.5 Gb/s. To reduce the cost, a coarse WDM technique is used (in place of dense WDM common in the backbone rings) by using channel spacing in the 2 to 10 nm range. Moreover, often just two fibres are used inside the ring, one for carrying the data and the other for protecting against a failure. Most metro networks were using electrical switching in 2001 although optical switching is the ultimate goal.

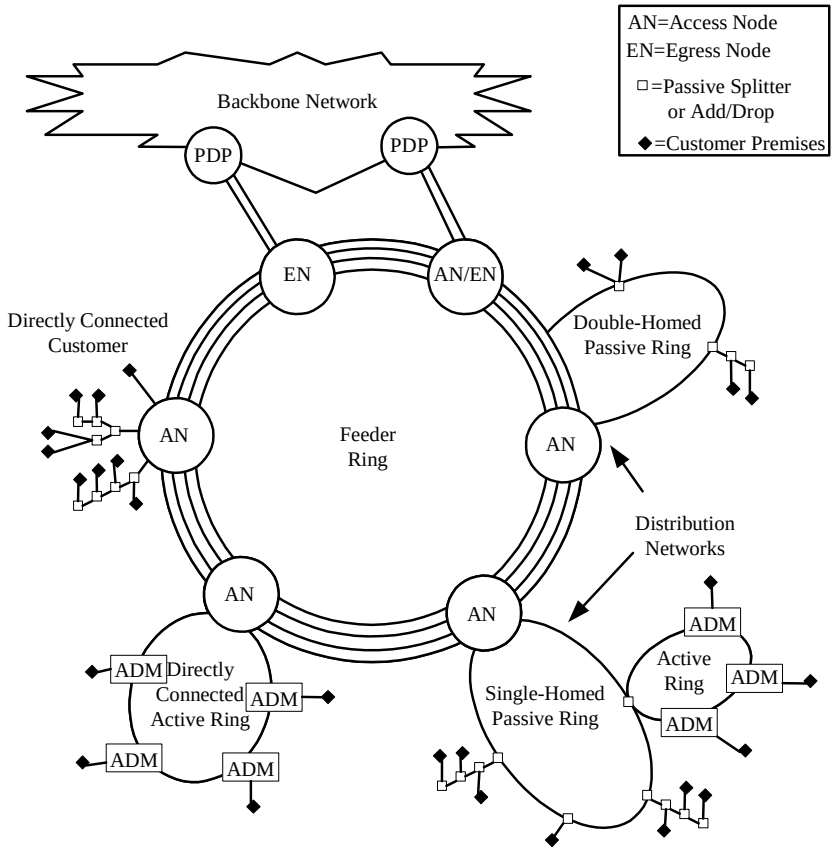

Figure 5.1 A WDM network with a feeder ring connected to several local distribution networks

In a test-bed implantation of an optically switched metro network, called the multi-wavelength optical network (MONET), several sites within the Washington, DC, area of the United State were connected using a set of eight standard wavelengths in the 1.55 um region with a channel spacing of 200 GHz [101]. MONET incorporated diverse switching technologies [synchronous digital hierarchy (SDH), asynchronous transfer mode (ATM), etc.] into an all optical ring network using cross connect switches based on the LiNbO3 technology.

5.2.3 Multi-Access WDM Networks

Multi access networks offer a random bidirectional access to each subscriber. Each user can receive and transmit information to any other user of the network at all times.

Telephone networks provide one example; they are known as subscriber loop, local loop, or access networks. Another example is provided by Internet used for connecting multiple computers. In 2001, both the local-loop and computer networks were using electrical techniques to provide bidirectional access through circuit or packet switching. The main limitation of such techniques is that each node on the network must be capable of processing the entire network traffic. Since it is difficult to achieve electronic processing speeds in excess of 10-Gb/s, such networks are inherently limited by the electronics.

The use of WDM permits a novel approach in which the channel wavelength itself can be used for switching, routing, or distributing each channel to its destination, resulting in an all-optical network. Since wavelength is used for multiple access, such a WDM approach is referred to as wavelength division multiple access (WDMA). A considerable amount of research and development work was done during the 1990s for considerable amount of research and development work was done during the 1990s for developing WDMA networks [102]-[106]. Broadly speaking, WDMA networks can be classified into two categories, called single-hop and multi-hop all-optical networks [93].Every node is directly connected to all other nodes in a single-hop network, resulting in a fully connected network. In contrast, multi-hop networks are only partially connected such that an optical signal sent by one node may require several hops through intermediate nodes before reaching its destination. In each category, transmitters and receivers can have their operating frequencies either fixed or tuneable.

Several architectures can be used for all optical multi-hop networks [93]-[98]. Hypercube architecture provides one example it has been used for interconnecting multiple processors in a supercomputer [107]. The hypercube configuration can be

easily visualized in three dimensions such that eight nodes are located at eight corners of a simple cube. In general, the number of nodes N must be of the form 2^m, where m is the dimensionality of the hypercube. Each node is connected to m different nodes. The maximum number of hops is limited to m, while the average number of hops is about m/2 for large N. Each node requires m receivers. The number of receivers can be reduced by using a variant, known as the deBruijn network, but it requires more than m/2 hops on average. Another example of a multi-hop WDM network is provided by the shuffle network or its bidirectional equivalent the Banyan network.

Figure 5.2 shows an example of the single hop WDM network based on the use of a broadcast star. This network, called the Lambdanet [108], is an example of the broadcast and select network. The new feature of the Lambdanet is that each node is equipped with one transmitter emitting at unique wavelength and N receivers operating at N wavelengths, where N is the number of node. The output of all transmitters is combined in a passive star and distributed to all receivers equally. Each node receives the entire traffic flowing across the network. A tuneable optical filter can be used to select the desired channel. In the case Lambdanet, each node uses a bank of receivers in palace of a tuneable filter this feature creates a non blocking network whose capacity and connectivity can be reconfigured electronically depending on the application. The network is also transparent to the bit rate or the modulation format. Different users can transmit data at different bit rates with different modulation formats. The flexibility of the Lambdanet makes it suitable for many applications. The main drawback of the Lambdanet is that the number of users is limited by the number of available wavelengths. Moreover, each node requires many receivers (equal to the number of nodes), resulting in considerable investment in hardware costs.

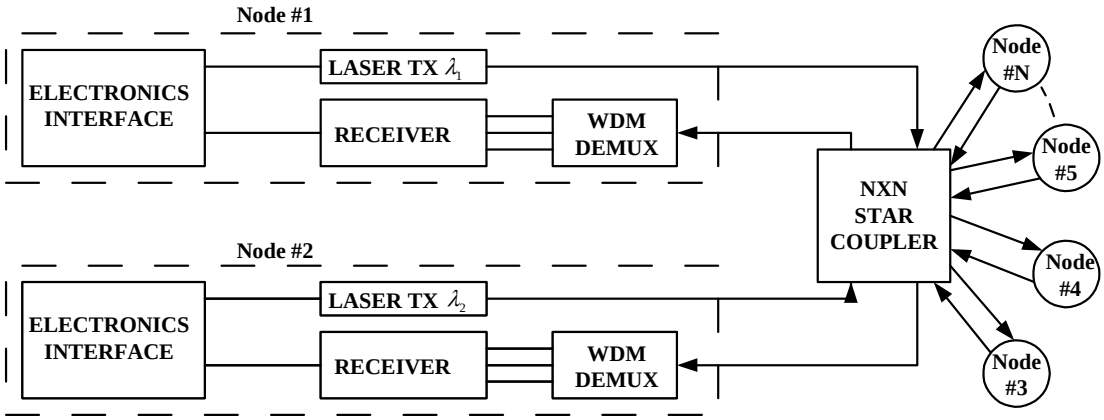

Figure 5.2 Schematic of the Lambdanet with N nodes, each node consists of one transmitter and N receivers

A tuneable receiver can reduce the cost and complexity of the Lambdanet. This is the approach adopted for the rainbow network [109]. This network can support up to 32 nodes, each of which can transmit 1 Gb/s over 10-20 Km. It makes use of a central passive star (see Fig.5.2) together with high-performance parallel interface for connection multiple computers. A tuneable optical filter is used to select the unique wavelength associated with each node the main shortcoming of the rainbow network is that tuning of receivers is a relatively slow process, making a difficult to use packet switching. An example of the WDM network that uses packet switching is provided by Starnet. It can transmit data at bit rates of up to 1.25 Gb/s per node over 10 km diameter while maintaining a signal-to-noise ratio (SNR) close to 24 dB [110].

WDM networks making use of a passive star coupler are often called passive optical networks (PONs) because they avoid active switching. PONs has the potential for bringing optical fibres to the home (or at least to the curve). In one scheme, called passive photonic loop [111], multiple wavelengths are used for routing signals in the local loop. Fig.5.3 shows a block diagram of such a network. The central office

contains N transmitters any thing at wavelengths $\lambda_1, \lambda_2, ..., \lambda_N$ and N receivers operating at wavelengths $\lambda_{N+1}, ..., \lambda_{2N}$ for network of N subscribers. The signals to each subscriber are carried on separate wavelengths in each direction. A remote node multiplexes signals from the subscribers to send the combined signal to the central office. It also demultiplexes the signals for individual subscribers. The remote node is passive requires little maintenance if passive WDM component are used. A switch at the central office routes signals depending on the wavelengths.

The design of access networks for telecommunication application was still a evolving in 2001 [106]. The goal is to provide broadband access to each user and to deliver audio, video, and data channels on demand, while keeping the cost down. Indeed, low-cost WDM components are being developed for this purpose [113].

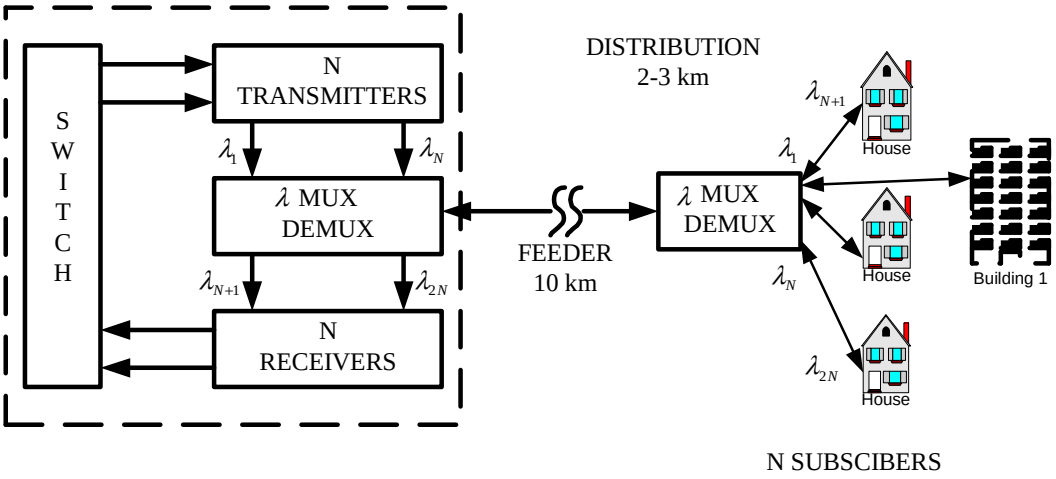

Figure 5.3 Passive photonic loop for local-loop applications [28]

5.3 System Performance Issues

The most important issue in the design of WDM lightwave systems is the inter-channel crosstalk. The system performance degrades whenever crosstalk leads to transfer of power from one channel to another. Such a transfer can occur because of the nonlinear effects in optical fibres, a phenomenon referred to as nonlinear crosstalk as it depends on the nonlinear nature of the communication channel. However, some

crosstalk occurs even in a perfectly linear channel because of the imperfect nature of various WDM components such as optical filters, demultiplexers, and switches. In this section both the linear and nonlinear crosstalk mechanisms is discussed and also is considered other performance issues relevant for WDM systems.

5.3.1 Hetero Wavelength Linear Crosstalk

Linear crosstalk can be classified into two categories depending on its origin [112]. Optical filters and demultiplexers often let leak a fraction of the signal power from neighbouring channels that interferes with the detection process. Such crosstalk is called hetero-wavelength or out-of-band crosstalk and is less of a problem because of its incoherent nature than the homo-wavelength or in-band crosstalk that occurs during routing of the WDM signal from multiple nodes. Subsection focuses on the hetero-wavelength crosstalk.

Consider the case in which a tuneable optical filter is used to select a single channel among the N channels incident on it. If the optical filter is set to pass the mth channel, the optical power reaching the photo-detector can be written as $P = P_m + \sum_{n \neq m}^{N} T_{mn} P_n$ where P_m is the power in the mth channel and T_{mn} is the filter transmittivity for channel n when channel m is selected. Crosstalk occurs if $T_{mn} \neq 0$ for $n \neq m$. It is called out-of-band crosstalk because it belongs to the channels lying outside the spectral band occupied by the channel detected. Its incoherent nature is also apparent from the fact that it depends only on the power of the neighbouring channels.

To evaluate the impact of such crosstalk on system performance, one should consider the power penalty, defined as the additional power required at the receiver to

counteract the effect of crosstalk. The photocurrent generated in response to the incident optical power is given by

$$I = R_m P_m + \sum_{n \neq m}^{N} R_n T_{mn} P_n \equiv I_{ch} + I_X \qquad (5.2)$$

where $R_m = \eta_m q / h\nu_m$ is the photo-detector responsivity for channel m at the optical frequency ν_m and η_m is the quantum efficiency. The second term I_X in Eq. (5.2) denotes the crosstalk contribution to the receiver current I. Its value depends on the bit pattern and becomes maximum when all interfering channels carry 1 bit simultaneously (the worst case).

A simple approach to calculating the crosstalk power penalty is based on the eye closure occurring as a result of the crosstalk [112]. The eye closes most in the worst case for which I_X is maximum. In practice, I_{ch} is increased to maintain the system performance. If I_{ch} needs to be increased be a factor of δ_X, the peak current corresponding to the top of the eye is $I_1 = \delta_X I_{ch} + I_X$. The decision threshold is set at $I_D = I_1/2$. The eye opening from I_D to the top level would be maintained at its original value $I_{ch}/2$ if:

$$(\delta_X I_{ch} + I_X) - I_X - \frac{1}{2}(\delta_X I_{ch} + I_X) = \frac{1}{2} I_{ch} \qquad (5.3)$$

or when $\delta_X = 1 + I_X / I_{ch}$. The quantity δ_X is just the power penalty for the mth channel. By using I_X and I_{ch} from Eq. (5.2), δ_X can be written (in dB) as:

$$\delta_X = 10 \log_{10} \left(1 - \frac{\sum_{n \neq m}^{N} R_n T_{mn} P_n}{R_m P_m} \right) \qquad (5.4)$$

where the powers correspond to their on-state values. If the peak power is assumed to be the same for all channels, the crosstalk penalty becomes power independent.

Further, if the photo-detector responsivity is nearly the same for all channels $(R_m \approx R_n)$, δ_X is well approximated by:

$$\delta_X \approx 10\log_{10}(1+X) \tag{5.5}$$

where $X = \sum_{n\neq m}^{N} T_{mn}$ is a measure of the out-of-band crosstalk; it represents the fraction of total power leaked into a specific channel from all other channels. The numerical value of X depends on the transmission characteristics of the specific optical filter. For a FP filter, X can be obtained in a closed form [114].

The preceding analysis of crosstalk penalty is based on the eye closure rather than the BER. One can obtain an expression for the BER if I_X is treated as a random variable in Eq. (5.2). The BER is given by Eq. (5.6) with the on and off state currents given by $I_1 = I_{ch} + I_X$ and $I_0 = I_X$ if we assume that $I_{ch} = 0$ in the off state [113].

$$BER = \frac{1}{4}\left[erfc\left(\frac{I_1 - I_D}{\sigma_1\sqrt{2}}\right) + erfc\left(\frac{I_D - I_0}{\sigma_0\sqrt{2}}\right)\right] \tag{5.6}$$

The decision threshold is set at $I_D = I_{ch}(1+X)/2$, which corresponds to the worst-case situation in which all neighbouring channels are in the on state. The final BER is obtained by averaging over the distribution of the random variable I_X. The distribution of I_X has been calculated for a FP filter and is generally far from being Gaussian. The crosstalk power penalty δ_X can be calculated by finding the increase in I_{ch} needed to maintain a certain value of BER.

5.3.2 Homo-wavelength Linear Crosstalk

Homo-wavelength or in-band crosstalk results from WDM components used for routing and switching along an optical network and has been of concern since the advent of WDM systems [115]-[117]. Its origin can be understood by considering a

static wavelength router such as a WGR Fig. 5.4. For an $N \times N$ router, there exist N^2 combinations through which N -wavelength WDM signals can be split. Consider the output at one wavelength, say λ_m. Among the $N^2 - 1$ interfering signals that can accompany the desired signal, $N-1$ signals have the carrier wavelength λ_m, while the remaining $N(N-1)$ belong different carrier wavelengths and likely to be eliminated as they pass through other WDM components.

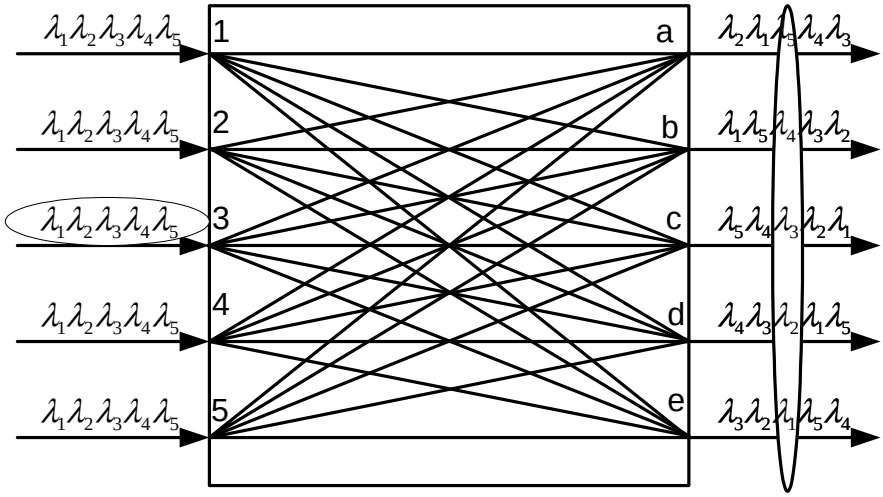

Figure 5.4 Schematic illustration of a wavelength router

The $N-1$ crosstalk signals at the same wavelength (in-band crosstalk) originate from incomplete filtering through a waveguide-grating router (WGR) because of its partially overlapping transmission peaks [35]. The total optical field, including only the in-band crosstalk, can be written as [117]:

$$E_m(t) = \left(E_m + \sum_{n \neq m}^{N} E_n\right) \exp(-i\omega_m t), \qquad (5.7)$$

where E_m is the desired signal and $\omega_m = 2\pi c/\lambda_m$. The coherent nature of the in-band crosstalk is obvious from Eq. (5.7).

To see the impact of in-band crosstalk on system performance, the power penalty should be again considered. The receiver current $I = R|E_m(t)|^2$ in this case contains interference or beat terms similar to the case of optical amplifier. One can indentify two types of beat terms; signal-crosstalk beating with terms like $E_m E_n$ and crosstalk-crosstalk beating with terms like $E_k E_n$, where $k \neq n$ and $m \neq n$. The latter terms are negligible in practice and can be ignored. The receiver current is then given approximately as [118]:

$$I(t) \approx RP_m(t) + 2\sum_{n \neq m}^{N} \sqrt{P_m(t)P_n(t)} \cos[\phi_m(t) - \phi_n(t)] \qquad (5.8)$$

where $P_n = |E_n|^2$ is the power and $\phi_n(t)$ is the phase. In practice $P_n \langle\langle P_m$ for $m \neq n$ because a WGR is built to reduce the crosstalk. Since phases are likely to fluctuate randomly, we can write Eq. (5.8) as $I(t) = R(P_m + \Delta P)$.

The calculation of crosstalk penalty in the case of dynamic wavelength routing through optical cross-connects becomes quite complicated because of a large number of crosstalk elements that a signal can pass through in such WDM networks [119]. The worst case analysis predicts a large power penalty (>3dB) when the number of crosstalk elements becomes more than 25 even if the crosstalk level of each component is only -40dB [120]. Clearly, the linear crosstalk is of primary concern in the design of WDM networks and should be controllable. A simple technique consists of modulating or scrambling the laser phase at the transmitter at a frequency much larger than the laser line-width [120].

5.3.3 Cross Phase Modulation

The SPM and XPM both affect the performance of WDM systems. The effects SPM applied to the individual channels of a WDM system. The phenomenon of XPM is an

important mechanism of nonlinear crosstalk in WDM lightwave systems. XPM originates from the intensity dependence of the refractive index, which produces as intensitive-dependent phase shift as a signal propagates through the optical fibre. The phase shift for a specific channel depends not only on the power of that channel but also on the power of other channels [121]. The total phase shift for the jth channel is given by:

$$\phi_j^{NL} = \frac{\gamma}{\alpha}\left(P_j + 2\sum_{m\neq j}^{N} P_m\right) \qquad (5.9)$$

where the first term is due SPM and L_{eff} has been replaced with $1/\alpha$ assuming $\alpha L \rangle\rangle 1$. The parameter γ is in the range $1-10W^{-1}km^{-1}$ depending on the type fibre used, larger values occurring for dispersion compensating fibres. The nonlinear phase shift depends on the bit pattern of various channels and varies from zero to its maximum value $\phi_{\max} = (\gamma/\alpha)(2N-1)P_j$ for N channels, if we assume equal channel powers.

Strictly speaking, the XPM induced phase shifts not affect system performance if the GVD effects were negligible. However, any dispersion in fibre converts pattern dependent phase shifts to power fluctuations, reducing the SNR at the receiver. This conversion can be understood by noting that time-dependant phase changes lead to frequency chirping that affects dispersion induced broadening of the signal. The root mean square (RMS) value of fluctuations depends on the channel power and can be reduced by lowering it. As a rough estimate if we use the condition $\phi_{\max} \langle 1$, the channel power is restricted to:

$$P_{ch} \langle \alpha/[\gamma(2N-1)] \qquad (5.10)$$

For typical value of α and γ, P_{ch} should be below 10mW even for five channels and reduces to below 1mW fro more than 50 channels.

The preceding analysis provides only a rough estimate as it ignores the fact that pulses belonging to different channels travel at different speeds and walk through each other at a rate that depends on their wavelength difference. Since XPM can occur only when pulses overlap in the time domain, its impact is reduced considerably by the walk-off effects. As a faster-moving pulse belonging to one channel collides with and passes through a specific pulse in another channel, the XPM induced chirp shifts the pulse spectrum first toward red and then toward blue. In a lossless fibre, collisions of two pulses are perfectly symmetric, resulting in no net spectral shift at the end of the collision. In a loss managed system with optical amplifiers placed periodically along the link, power variations make collisions between pulses of different channels asymmetric, resulting in a net frequency shift that depends on the channel spacing. Such frequency shifts lead to timing jitter (the speed of a channel depends on its frequency because of GVD) since their magnitude depends on the bit pattern as well as on the channel wavelengths. The combination of XPM induced amplitude and timing jitter degrades the SNR at the receiver, especially for closely spaced channels, and leads to XPM induced power penalty that depends on channels spacing and the type of fibres used for the WDM link. The power penalty increases for fibres with large GVD and for WDM systems designed with small channel spacing and can exceed 5 dB even for 100 GHz spacing.

Clearly, the use of low GVD fibres will reduce this problem to some extend but is not practical because of the onset of FWM. In practice, dispersion management is employed in virtually all WDM systems such that the local dispersion is relatively large. Careful selection of the dispersion map parameters may help from the XPM standpoint but may not be optimum from the SPM point of view [122]. A simple approach to XPM suppression consists of introducing relative time delays among the

WDM channels after each map period such that the "1" bits in neighbouring channels are unlikely to overlap most of the time [123]. The use of RZ format is quite helpful in this context because all 1 bits occupy only a fraction of the bit slot.

5.3.4 Four Wave Mixing

The nonlinear phenomenon of FWM requires phase matching. It becomes a major source of nonlinear crosstalk whenever the channel spacing and fibre dispersion are small enough to satisfy the phase matching condition approximately [121]. This is the case when a WDM system operates close to the zero dispersion wavelength of dispersion shifted fibres. For this reason, several techniques have been developed for reducing the impact of FWM in WDM systems [124].

The physical origin of FWM induced crosstalk and the resulting system degradation can be understood by noting that FWM generates a new wave at the frequency $\omega_{ijk} = \omega_i + \omega_j - \omega_k$, whenever three waves at frequencies ω_i, ω_j, and ω_k co-propagate inside the fibre. For an N-channel system, i, j, and k can vary from 1 to N, resulting in a large combination of new frequencies generated by FWM. In the case of equally spaced channels, the new frequencies coincide with the existing frequencies, leading to coherent in-band crosstalk. When channels are not equally spaced, most FWM components fall in between the channels and lead to incoherent out-of-band crosstalk. In both cases, the system performance is degraded because of a loss in the channel power, but the coherent crosstalk degrades system performance much more severely.

The FWM process in optical fibres is governed by a set of four coupled equations whose general solution requires a numerical approach [121]. If we neglect the phase shifts induced by SPM and XPM, assume that the three channels participating in the

FWM process remain nearly undepleted, and include fibre losses, the amplitude A_F of the FWM component at the frequency ω_F is governed by:

$$\frac{dA_F}{dz} = -\frac{\alpha}{2} A_F + d_F \gamma A_i A_j A_k^* \exp(-i\Delta k z) \qquad (5.11)$$

where $A_m(z) = A_m(0)\exp(-\alpha z/2)$ for $m = i, j, k$ and $d_F = 2 - \delta_{ij}$ is the degeneracy factor defined such that its value is 1 when $i = j$ but doubles when $i \neq j$. This equation can be easily integrated to obtain $A_F(z)$. The power transferred to the FWM component in a fibre of length L is given by [125]:

$$P_F = |A_F(L)|^2 = \eta_F (d_F \gamma L)^2 P_i P_j P_k e^{-\alpha L} \qquad (5.12)$$

where $P_m = |A_m(0)|^2$ is the launched power in the mth channel and η_F is a measure of the FWM efficiency defined as:

$$\eta_F = \left| \frac{1 - \exp[-(\alpha + i\Delta k)L]}{(\alpha + i\Delta k)L} \right|^2 \qquad (5.13)$$

The FWM efficiency η_F depends on the channel spacing through the phase mismatch governed by:

$$\Delta k = \beta_F + \beta_k - \beta_i - \beta_j \approx \beta_2 (\omega_i - \omega_k)(\omega_j - \omega_k) \qquad (5.14)$$

where the propagation constants were expanded in a Taylor series around $\omega_c = (\omega_i + \omega_j)/2$ and β_2 is the GVD parameter at that frequency. If the GVD of the transmission fibre is relatively large, ($|\beta_2| \rangle 5\, ps^2/km$), η_F nearly vanishes for typical channel spacing of 50GHz or more. In contrast, $\eta_F \approx 1$ close to the zero dispersion wavelength of the fibre, resulting in considerable power in the FWM component, especially at high channel powers. In the case of equal channel powers, P_F increases as P_{ch}^3. This cubic dependence of the FWM component limits the channel powers to

below 1mW if FWM is nearly phase matched. Since the number of FWM components for an M -channel WDM system increases as $M^2(M-1)/2$, the total power in all FW components can be quite large.

A simple scheme for reducing the FWM induced degradation consists of designing WDM systems with unequal channel spacing [126]. The main impact of FWM in this case is to reduce the channel power. This power depletion results in a power penalty that is relatively small compared with the case of the advantage of unequal channel spacing. In a 1999 experiment, this technique was used to transmit 22 channels, each operating at 10 Gb/s, over 320 km of dispersion shifted fibre with 80km amplifier spacing. Channel spacing ranged from 125 to 275 GHz in the 1532 to 1562 nm wavelength region and were determined using a periodic allocation scheme [127]. The zero dispersion wavelength of the fibre was close to 1548nm, resulting in near phase matching of many FWM components. Nonetheless, the system performed quite well with less than 1.5 dB power penalty for all channels.

The use of non-uniform channel spacing is not always practical because many WDM components, such as optical filters and waveguide grating routers, require equal channel spacing. The use of dispersion management is common for suppressing FWM in WDM systems because of its practical simplicity. In fact, new kinds of fibres, called nonzero dispersion shifted fibres (NZDSFs), were designed and marketed after the advent of WDM systems. Typically, GVD is in the range of 4-8 ps/(km-nm) in such fibres to ensure that the FWM induced crosstalk is minimized [113].

5.4 Simulation Procedure

This section explains the simulation procedure of the WDM with four channels for four different modulation scheme, BPSK, QPSK, 16-QAM and 64-QAM which the

overall block diagram has been shown in Fig 5.5. The four RF modulated light signals are multiplexed with the 100 GHz spacing in 1550 nm range. The multiplexed signals after passing through 50 km SMF and amplifier with a gain of 20 dB is demultiplexed and then demodulated. Finally, the system quality is assessed by means of the BER and the constellation visualizer.

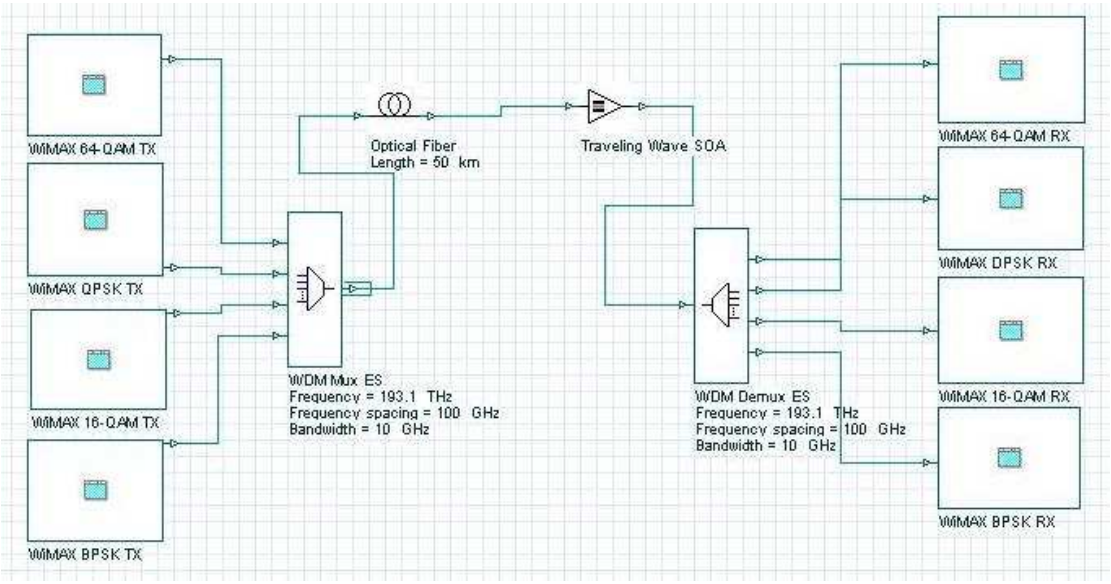

Figure 5.5 WDM block diagram with four different modulations

5.4.1 Transmission Block Diagrams

The BPSK and QPSK transmission block diagram are shown in Fig.5.6 and Fig.5.7 respectively.

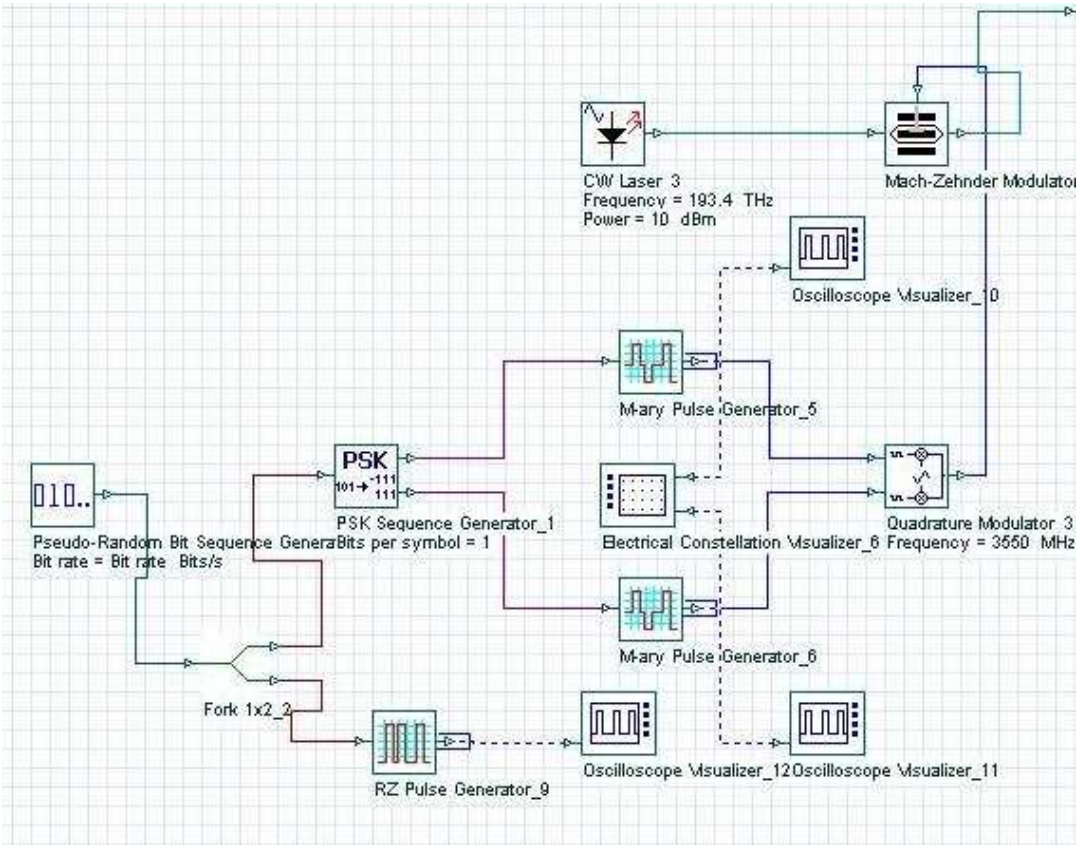

Figure 5.6 BPSK modulation transmission signal block diagram

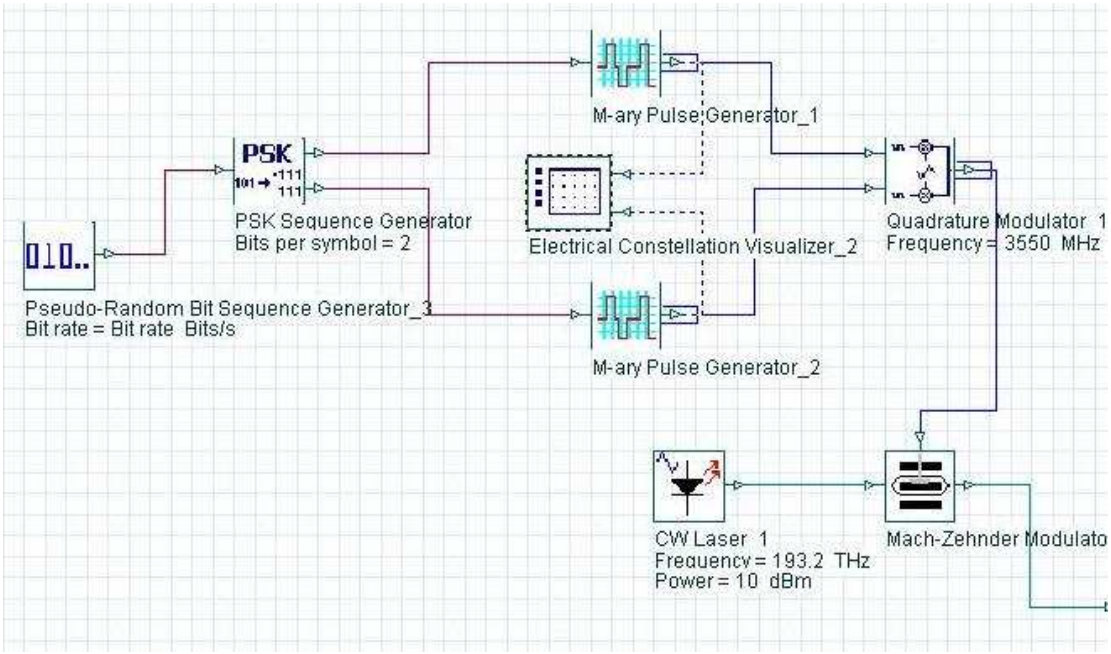

Figure 5.7 QPSK modulation transmission signal block diagram

Parameter for the bit rate, order, number of leading and trailing zeros used PRBS. The sequence length is defined by:

$$N = T_W B_r \tag{5.15}$$

T_W is the global parameter time window and B_r is the parameter bit rate.

The phase of the transmitting information signal can vary by PSK sequence generator according to the source symbols. The phase values are taken from the set of angles:

$$\varphi_i = \left(\frac{2\pi}{M}(i-1) + \phi \right), i = 1,2,...M \tag{5.16}$$

where $M = 2^h$ the number of is possible sequence of binary digits, and h is the number of bits per symbol, and ϕ is the phase offset. The in-phase and the quadrature-channel will have amplitudes according to:

$$I_i = \cos(\varphi_i), i = 1,2,...M \tag{5.17}$$

$$Q_i = \sin(\varphi_i), i = 1,2,...M \tag{5.18}$$

With using Gray code, the adjacent signal amplitudes that correspond to the binary sequences will differ by only one digit.

This model generates pulses according to:

$$I_{k-out}(t) = I_k, 0 \le t < T \tag{5.19}$$

$$Q_{k-out}(t) = Q_k, 0 \le t < T \tag{5.20}$$

where I_k and Q_k are the amplitudes of the output signals k and T is the bit period.

Assuming $\phi = 0$, if $h = 1$, $M = 2$, then the generated signal is BPSK (Fig.5.6) and if $h = 2$, $M = 4$, then the generated signal is QPSK (Fig.5.7). Then the M-ary pulse generator model generates pulses according to [39]:

$$v_{out}(t)=\begin{cases} b & 0 \le t < t_1 \\ av_{in}(t)+b & t_1 \le t < t_1 + t_c \\ b & t_1 + t_c \le t < T \end{cases} \quad (5.21)$$

where v_{in} is the input M-ary, a is the linear gain, and b is the parameter bias. t_c is the duty cycle, and t_1 is the pulse position.

The I and Q signals will pass through a quadrature modulator which implements a quadrature analogue amplitude modulator the output signal is modulated according to:

$$v_{out}(t)=G\left[I(t)\cos\left(2\pi f_c t+\phi_c\right)-Q(t)\sin\left(2\pi f_c t+\phi_c\right)\right]+b \quad (5.22)$$

where I and Q are the input electrical signals, G is the parameter gain, b is the bias, f_c is the carrier frequency, and ϕ_c is the phase of the carrier, which WiMAX system is considered in here as an example and the carrier frequency is 3.55 GHz .

Finally the modulated signal externally modulated by the CW laser using MZM, which is an intensity modulator based on an interferometric principle. It consists of two 3 dB couplers which are connected by two waveguides of equal length. By means of an electro-optic effect, an externally applied voltage can be used to vary the refractive indices in the waveguide branches. The different paths can lead to constructive and destructive interference at the output, depending on the applied voltage. Then the output intensity can be modulated according to the voltage.

The equations that describe the behaviour of the MZM are [141]:

$$E_{out}(t)=E_{in}(t).\cos\left(\Delta\theta(t)\right).\exp\left(j.\Delta\phi(t)\right) \quad (5.23)$$

where $\Delta\theta(t)$ is the phase difference between the two branches and is defined as:

$$\Delta\theta(t)=\frac{\pi}{2}.\left(0.5-ER.\left(Modulation(t)-0.5\right)\right) \quad (5.24)$$

$$ER=1-\frac{4}{\pi}.\arctan\left(\frac{1}{\sqrt{extrat}}\right) \quad (5.25)$$

and $\Delta\varphi$ is the signal phase change defined as:

$$\Delta\varphi(t) = SC.\Delta\theta(t).\frac{(1+SF)}{(1-SF)} \tag{5.26}$$

Where the parameter SC is -1 if negative signal chirp is true, or 1 if negative signal chirp is false. extract is the extinction ratio, SF is the symmetry factor, and modulation(t) is the electrical input signal. The electrical input signal is normalized between 0 and 1.

Fig.5.8 and Fig.5.9 are shown the QAM 16-QAM and 64-QAM transmission block diagram, respectively.

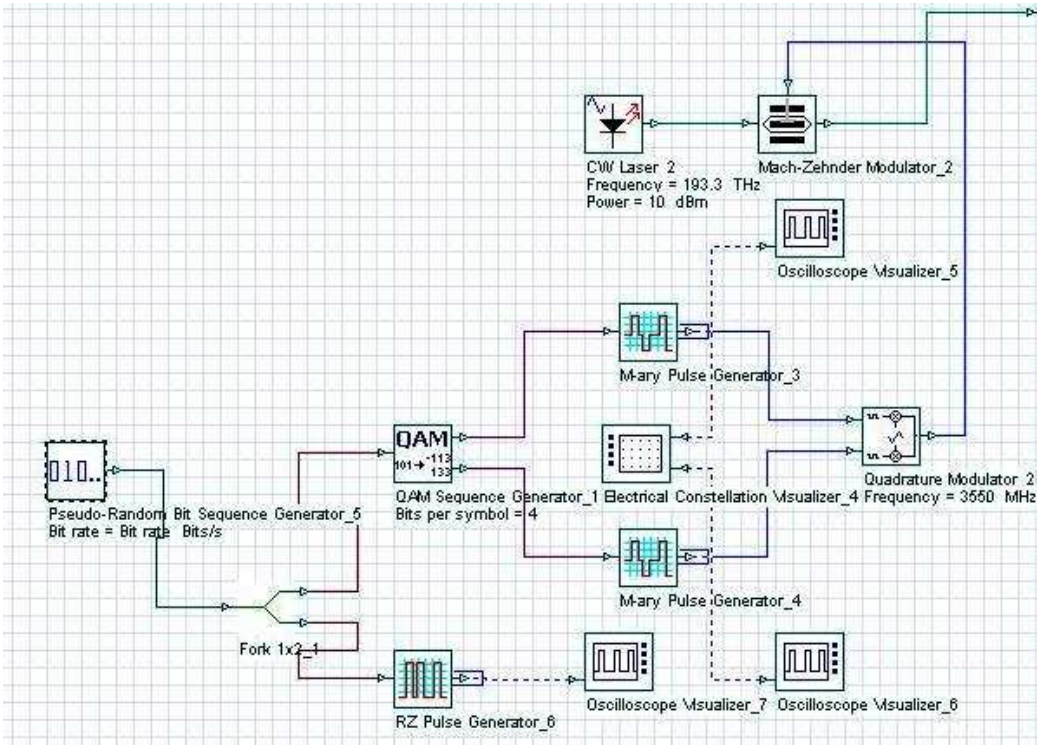

Figure 5.8 16-QAM modulation transmission signal block diagram

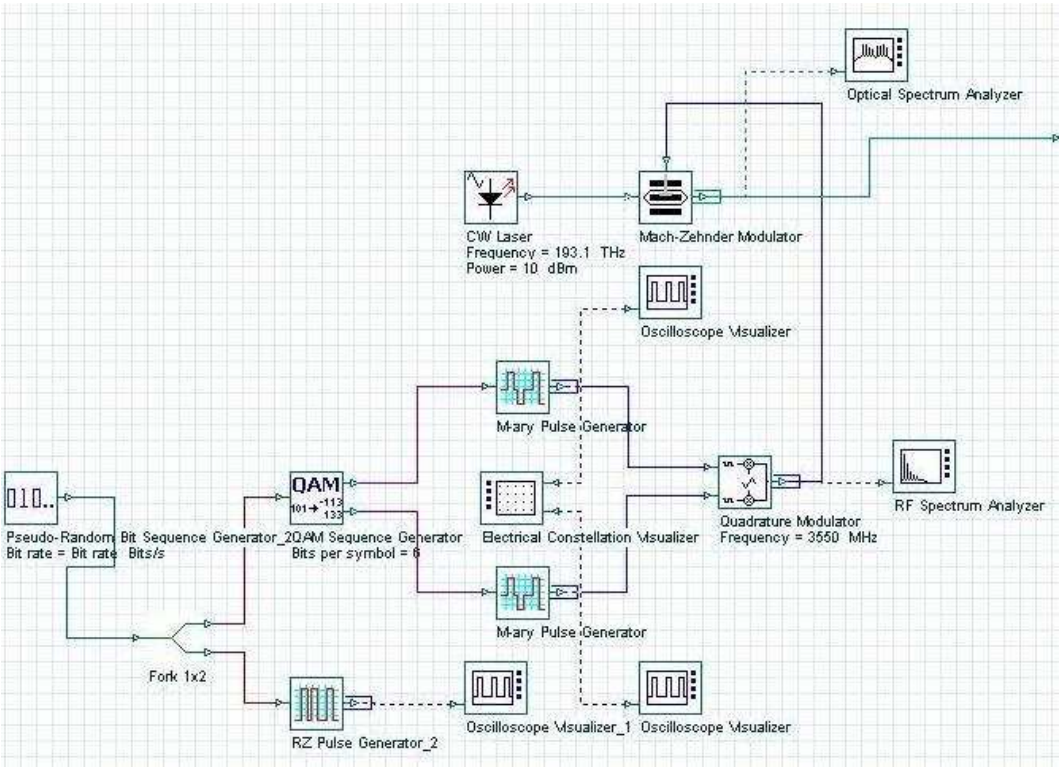

Figure 5.9 64-QAM modulation transmission signal block diagram

The procedure is the same as BPSK and QPSK except the QAM sequence generator, which the bit sequence is split into two parallel subsequence, each can be transmitted in two quadrature carriers when building a QAM modulator. This is achieved by using a serial to parallel converter. The amplitude of the transmitting information signal can vary by QAM sequence generator according to the source symbols. For each output port, the amplitude takes one of the values from the set of amplitudes:

$$a_1 = (2i - 1 - M), i = 1,2,...,M \qquad \text{where} \quad M = 2^{h/2} \tag{5.27}$$

The equivalent QAM set is given by the square of M . This means: If $h = 4$, $M = 4$, then we have a 16-QAM (Fig.5.8) , and if $h = 6, M = 8$, then we have a 64-QAM (Fig.5.9).

These signals are used to indirectly modulate four CW laser via a MZM to convert electrical signal to it optical version. CW Laser 1, operating at 193.1 THz wavelength

(λ_1), CW Laser 2, operating at 193.2 THz wavelength (λ_2), CW Laser 3, operating at 193.3 THz wavelength (λ_3), and CW Laser 4, operating at 193.4 THz wavelength (λ_4) are multiplexed and transported to the fibre. Four CW lasers were all generating optical signals with 10 mW output power.

5.4.2 Receiver Block Diagrams

Figures 5.10-13 show BPSK, QPSK, 16-QAM, and 64 QAM receiver block diagrams. The combined optical electric field is then converted to optical power. The electrical current at the output of photo detector is given by:

$$i(t) = i_s(t) + i_{th}(t) + i_d(t) + i_{sh}(t) \tag{5.28}$$

where $i_s(t)$ is the photo current and calculated from the responsivity r:

$$i_s(t) = rP_s(t) \tag{5.29}$$

where $i_{th}(t)$ is the thermal noise current calculated from the power spectral density defined by the parameter thermal noise, and i_d is the dark current.

The shot noise current $i_{sh}(t)$ is calculated according to the power spectral density:

$$\langle i_s(t) i_s(t+\tau) \rangle = \int_{-\infty}^{\infty} S_S(f) \exp(2\pi i f \tau) df \tag{5.30}$$

where angle brackets denote an ensemble average over fluctuations. The spectral density of shot noise $S_S(f)$ is constant.

After the PIN diode the 2nd order Bessel filter have the following transfer function:

$$H(s) = \alpha \frac{d_0}{B_N(s)} \tag{5.31}$$

where α is the parameter insertion loss, N is the parameter order, and

$$d_0 = \frac{(2N)!}{2^N N!} \tag{5.32}$$

Being a normalizing constant and $B_N(s)$ an nth-order Bessel polynomial of the form:

$$B_N(s) = \sum_{k=0}^{N} d_k s^k \tag{5.33}$$

where:

$$d_k = \frac{(2N-k)!}{2^{N-k}.k!(N-k)!} \tag{5.34}$$

and

$$s = j\left(\frac{f_{W_b}}{f_c}\right) \tag{5.35}$$

where f_c is the filter cut off frequency defined by the parameter frequency and is 3750 MHz and f_{W_b} denotes the normalized 3dB bandwidth and can be approximated by:

$$f_{W_b} \approx \sqrt{(2N-1).\ln 2} \tag{5.36}$$

To implement an analog demodulator a carrier generator is used to generate Q and I quadrature components. The output signal is demodulated according to:

$$v_I(t) = [Gv_{in}(t)\cos(2\pi f_c t + \phi_c)]^* h_{low}(t) \tag{5.37}$$

$$v_Q(t) = [-Gv_{in}(t)\sin(2\pi f_c t + \phi_c)]^* h_{low}(t) \tag{5.38}$$

where $v_{in}(t)$ is the input electrical signal, G is the parameter gain here is two. WiMAX system is considered in here as an example and f_c, carrier frequency is 3550 MHz. ϕ_c is the phase of the carrier, and h_{low} is the time response of the low pass filter.

M-ary threhold detector compares the electrical signal at a user-defined decision instant with a list of threshold levels. The comparison generates an index used to generate the output amplitude.

With PSK sequence decoder we can vary the phase of a signal according to the source symbols. The phase values are taken from the set of angles:

$$\varphi_i = \left(\frac{2\pi}{M}(i-1)+\phi\right), i = 1,2,...,M \qquad \text{where } M = 2^h \tag{5.39}$$

where h is the number of bits per symbol and is equal to 1 and 2 for BPSK (Fig.5.10) and for QPSK (Fig.5.11), respectively and ϕ is the phase offset. The in-phase and the quadrature channel will have amplitudes according to:

$$I_i = \cos(\varphi_i), i = 1,2,...,M \tag{5.40}$$

$$Q_i = \sin(\varphi_i), i = 1,2,...,M \tag{5.41}$$

The PSK detector will calculate the value of i for the phase of each signal input k :

$$\varphi_k - \arctan\left(\frac{Q_k}{I_k}\right) \tag{5.42}$$

$$i = \frac{(\varphi_k - \varphi)M}{2\pi} + 1 \tag{5.43}$$

and convert the values of i to the equivalent binary sequence.

In the QAM sequence decoder, the bit sequence is split into two parallel subsequences, each can be transmitted in two quadrature carriers when building a QAM modulator. This is achieved by using a serial to parallel converter. When transmitting information, the amplitude of a signal can be varied according to the source symbols. For each output port, the value of the amplitude takes value from the set of amplitudes:

$$a_1 = (2i-1-M), i = 1,2,...,M \qquad \text{where } M = 2^{h/2} \tag{5.44}$$

The equivalent QAM set is given by the square of M . This means; if $h = 4$, $M = 4$ then it provides 16-QAM (Fig.5.12), and if $h = 6$, $M = 8$ then we have 64-QAM (Fig.5.13).

The QAM decoder calculates the value of i for the amplitude of each signal input k is given by:

$$i-(a_k+1+M)/2 \qquad (5.45)$$

The SC values of i are then converted to at equivalent binary sequence.

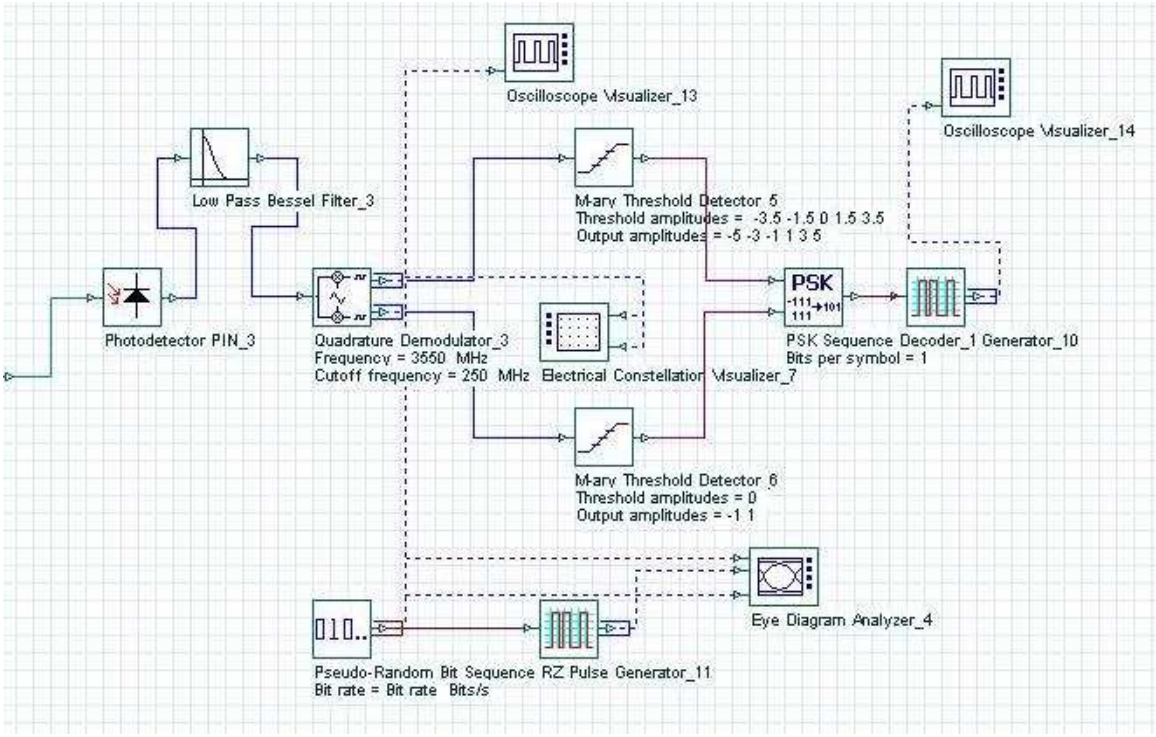

Figure 5.10 BPSK demodulator receiver signal block diagram

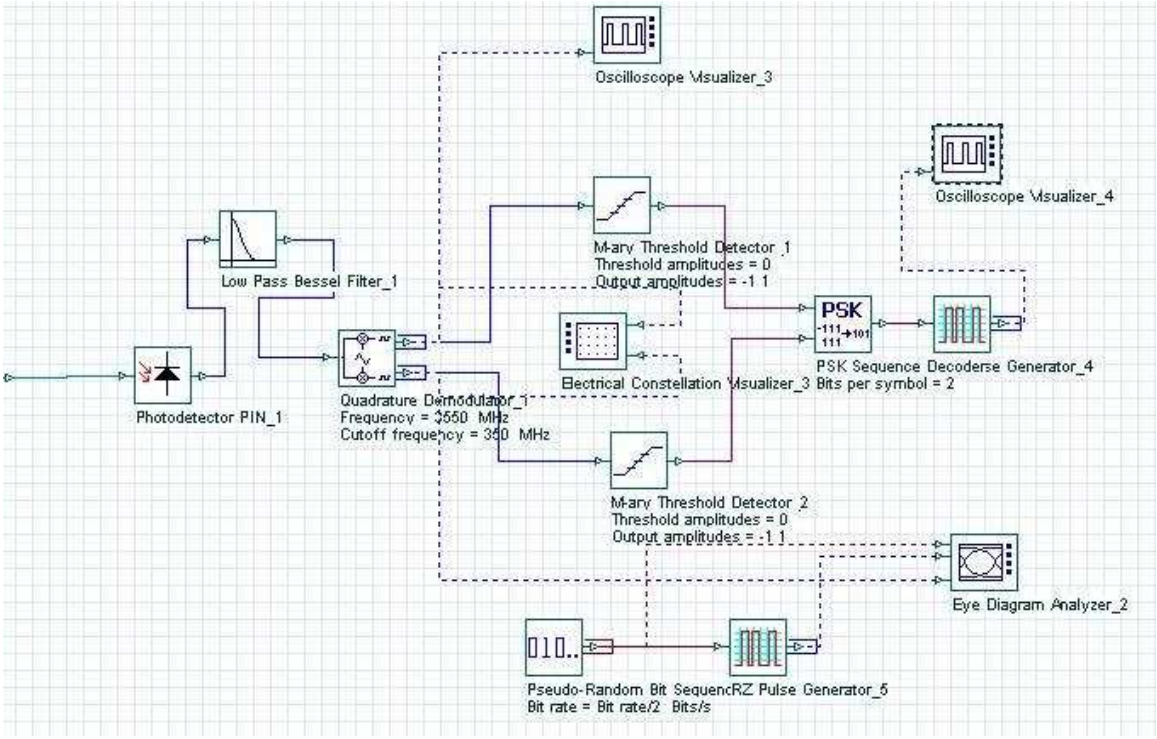

Figure 5.11 QPSK demodulator receiver signal block diagram

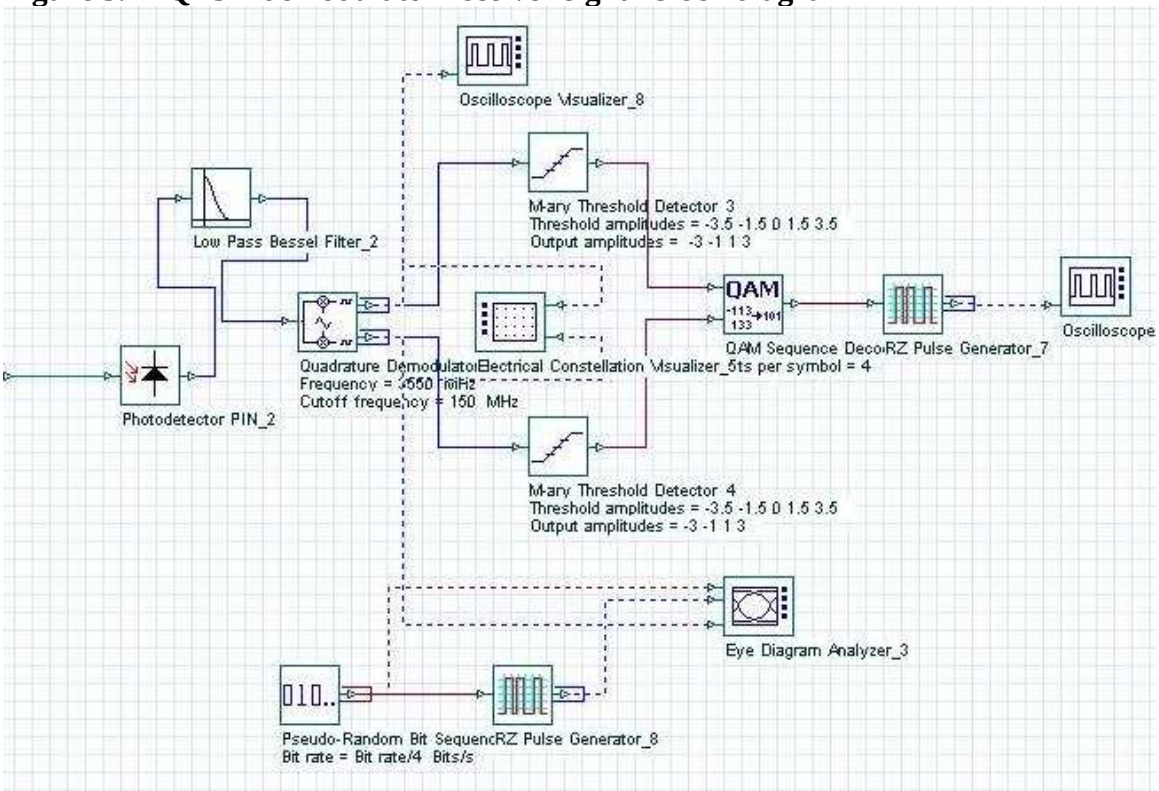

Figure 5.12 16-QAM demodulator receiver signal block diagram

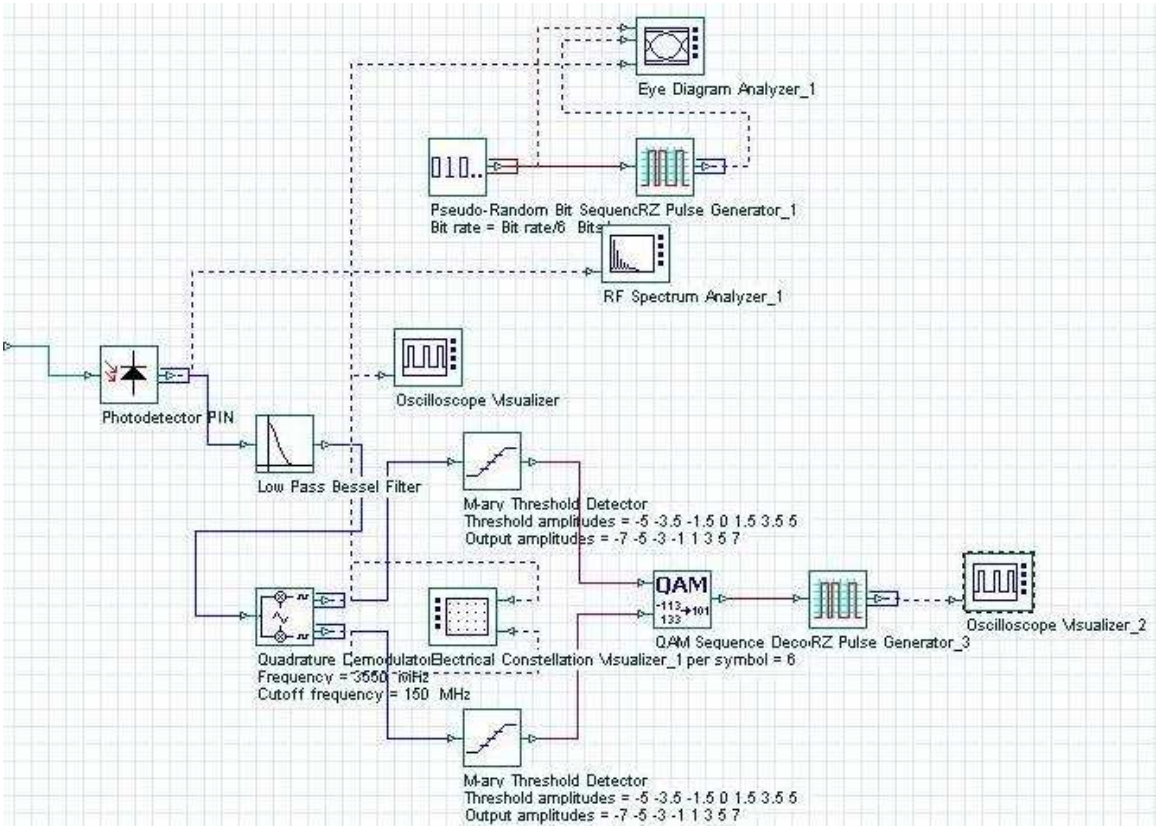

Figure 5.13 64-QAM demodulator receiver signal block diagram

5.5 Simulation Results

This section discusses the simulation results for the constellation and the eye diagrams for BPSK, QPSK, 16-QAM, and 64-QAM. Also discussed is the crosstalk between the channels. Figure 5.14 (a) and (b) show the constellation point and eye diagrams for BPSK demodulator, respectively, where the EVM is less than 3.5%.

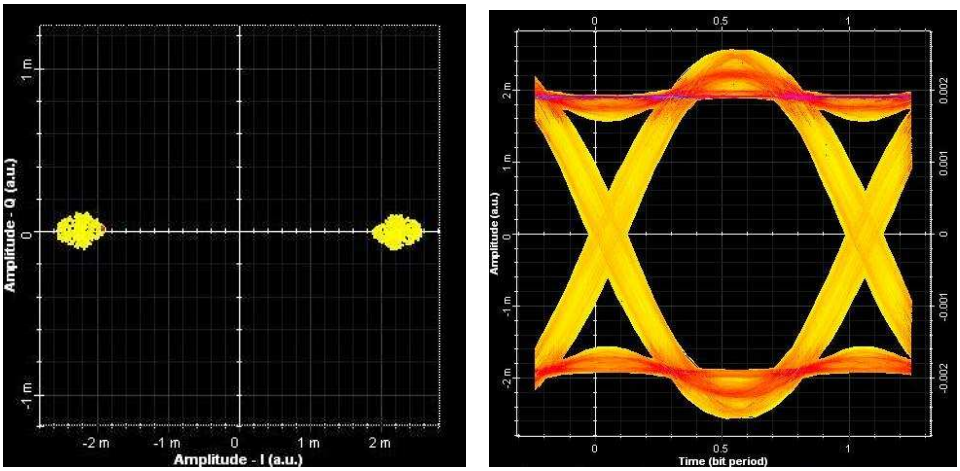

(a) **(b)**

Figure 5.14 (a) BPSK constellation point diagram Figure, and (b) BPSK eye diagram

Figure 5.15 (a) and (b) show the constellation point and eye diagrams for QPSK demodulator, respectively, where the EVM is less than 3.7%.

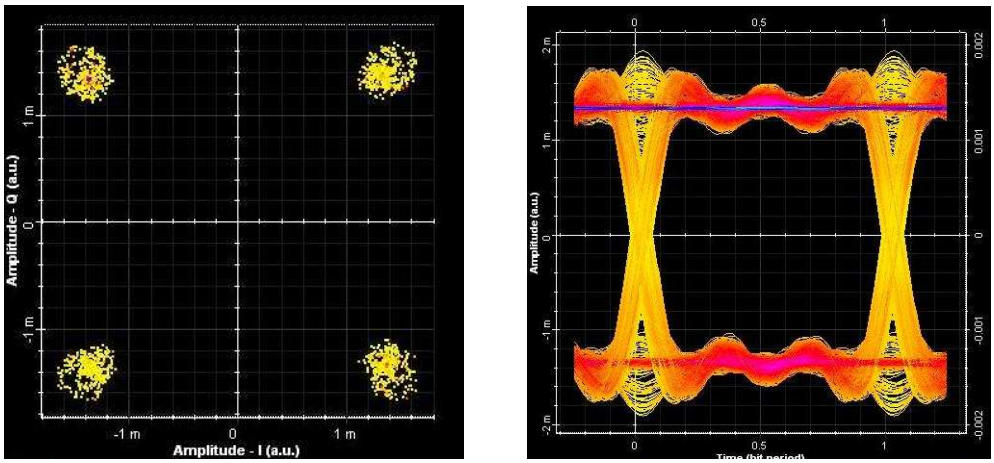

(a) **(b)**

Figure 5.15 (a) QPSK constellation point diagram, and (b) QPSK eye diagram

Figure 5.16 (a) and (b) show the constellation point and eye diagrams for 16-QAM demodulator, respectively, where the EVM is less than 4.2%.

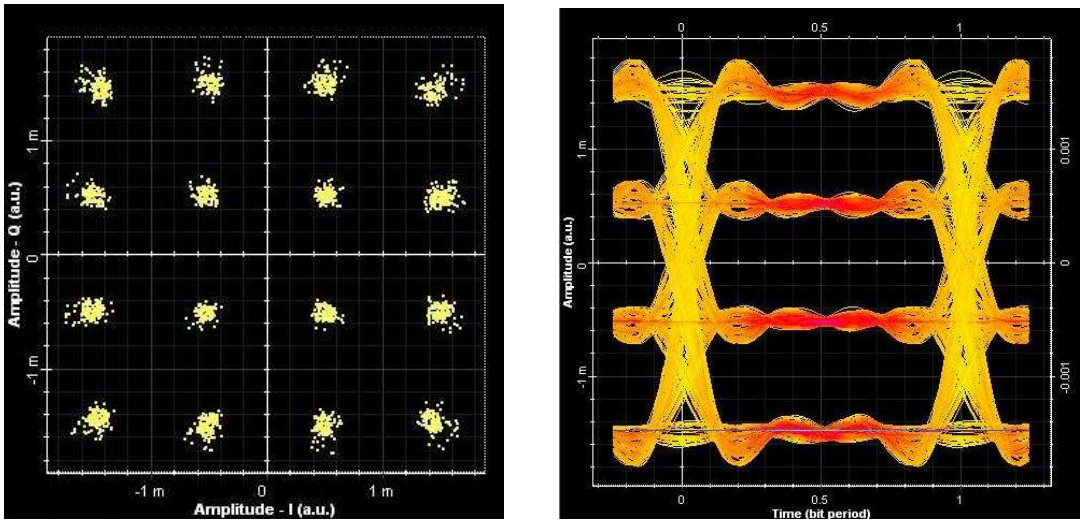

(a) **(b)**

Figure 5.16 (a) 16-QAM constellation point diagram, and (b) 16-QAM eye diagram

Figure 5.17 (a) and (b) show the constellation point and eye diagrams for 64-QAM demodulator, respectively, where the EVM is less than 4.5%.

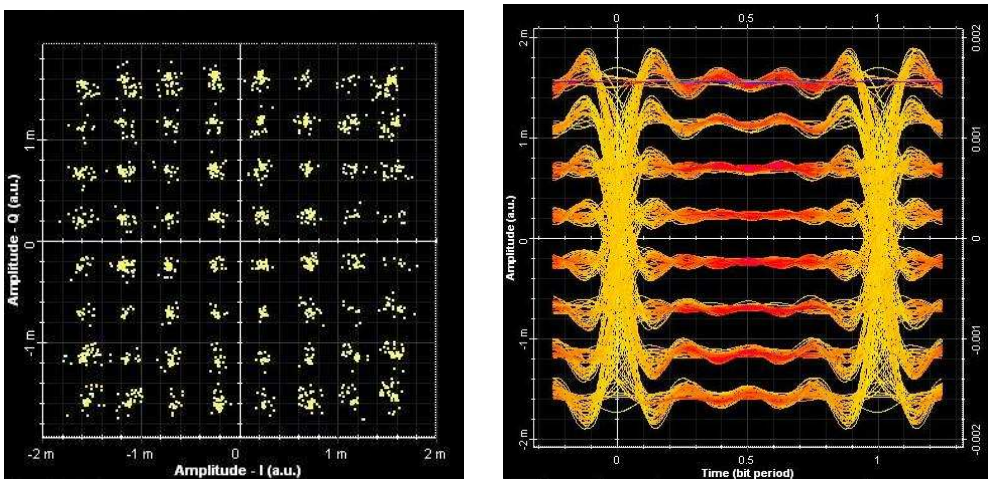

(a) **(b)**

Figure 5.17 (a) 64-QAM constellation point diagram, and (b) 64-QAM eye diagram

Table 5.2 shows the optical signal-to-noise ratio (OSNR) at each channel. Almost all the channels have the same OSNR at 50 dB.

Table 5.2 WDM OSNR

Frequency (THz)	Signal Power (dBm)	Noise Power (dBm)	OSNR (dB)
193.1	**16.84**	**-33.98**	**50.81**
193.2	**16.88**	**-33.97**	**50.85**
193.3	**17.46**	**-33.97**	**51.43**
193.4	**16.84**	**-33.97**	**50.81**

Figure 5.18 (a-e) illustrate the spectrum of the four channels before and after demultiplexer. Figure 5.18 (a) illustrates the four channel at 193.1, 193.2, 193.3, and 193.4 THz before demultiplexing. In Fig 5.18 (b) the isolation of channel 1 at 193.1 THz with respect to other channel is illustrated, where the isolation between the channel 1 and channel 2 is about 50 dB but this isolation is around 60 dB for channel

3 and 70 dB for channel 4. Figure 5.18 (c) illustrates the channel isolation between channel 2 and the others, where the isolation of channel 2 with the adjacent channels are close to 50 dB and with channel 4 is around 60 dB. The isolation for channel 3 and channel 4 are shown in Fig 5.18 (d) and (e) which are the same as Figs (c) and (b) respectively. The conclusion is that the isolation become higher as getting further away from the original signal

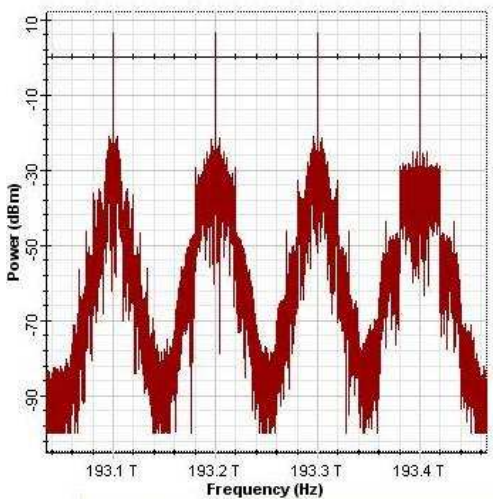

(a)

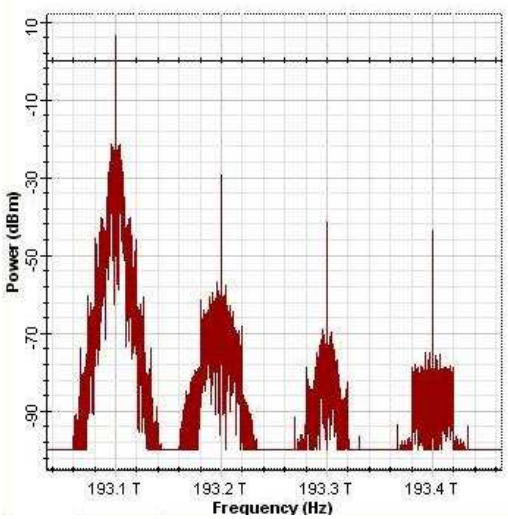

(b)

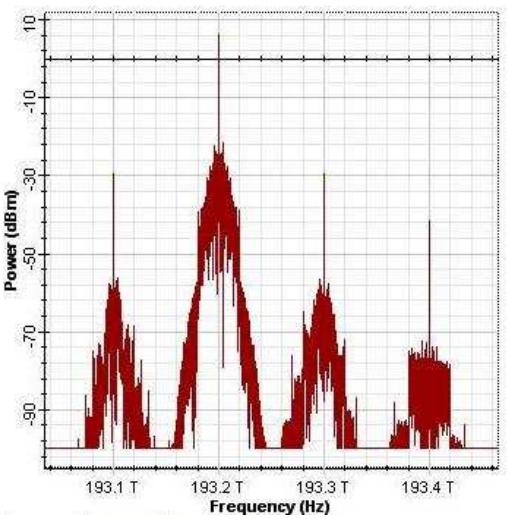

(c)

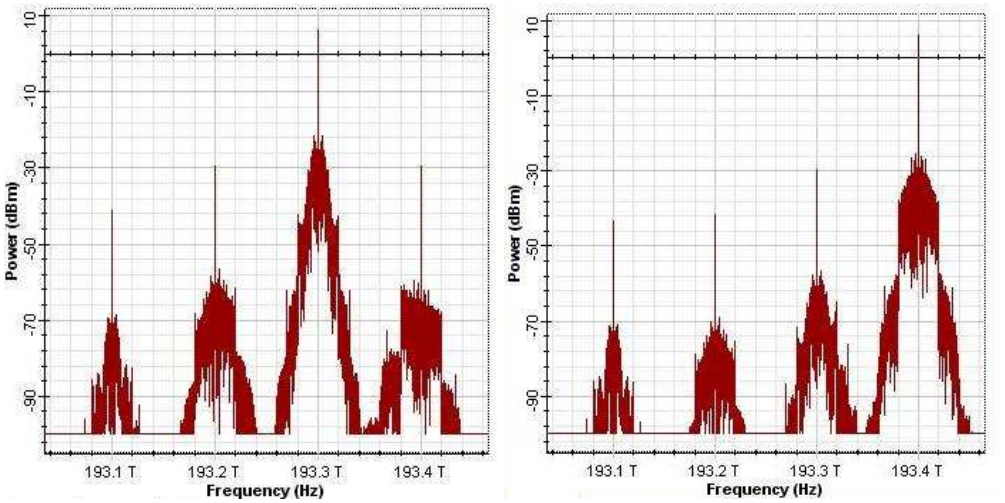

(d) **(e)**

Figure 5.18 (a) Four channels WDM before multiplexing (b) channel 1 at 193.1 THz after demultiplexing (c) channel 2 at 193.2 THz after demultiplexing (d) channel 3 at 193.3 THz after demultiplexing, and (e) channel 4 at 193.4 THz after demultiplexing

5.6 Linearization Performance in WDM System

This section explains the simulation procedure of the WDM with four channels for four different modulation scheme, BPSK, QPSK, 16-QAM and 64-QAM which the overall block diagram has been shown in Fig. 5.19. Feedforward linearization technique is implemented to the WDM system. The four RF modulated light signals are multiplexed with the 100 GHz spacing in 1550 nm range. The multiplexed signals after passing through 50 km SMF and amplifier with a gain of 20 dB is demultiplexed and then demodulated. Finally, the system quality is assessed by means of the BER and the constellation visualizer.

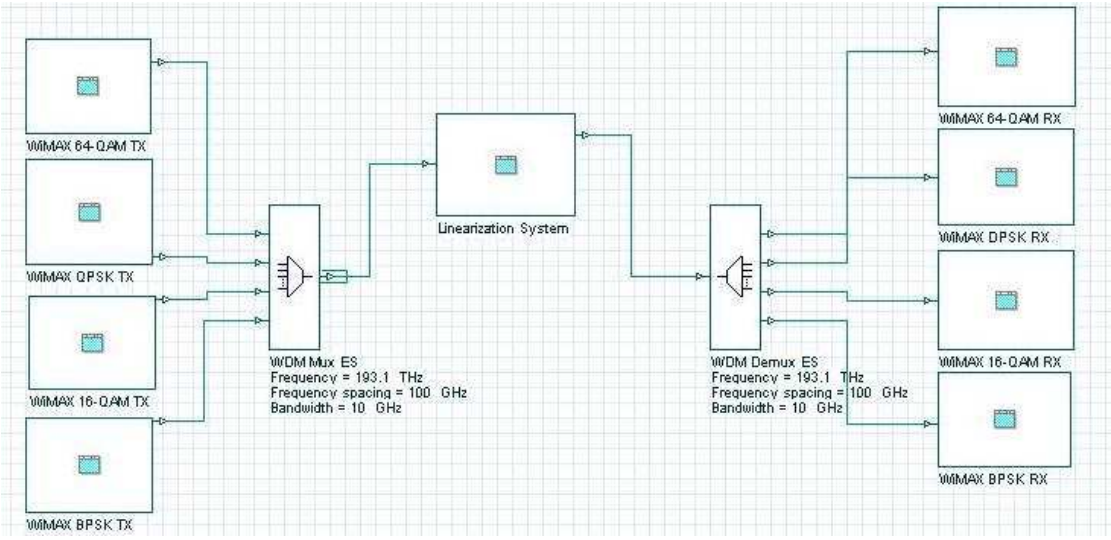

Figure 5.19 WDM block diagram with four different modulations and feedforward linearization

5.7 Simulation Results

It can be seen that without the feedforward linearization there is FWM caused by the two high power input signals modulating Laser 1 and Laser 2. With feedforward linearization, FWM is reduced by more than 29 dB.

The simulated spectra of the four modulated RF signal indirectly modulated signal with and without the linearizer are shown in Fig.5.20.

In Figs.5.20 (a) and (b), the carrier average power is the same in both spectrum (16 dBm), and the IMD is -11 dBc/Hz without the linearizer and -40 dBc/Hz with the linearizer, respectively. An IMD improvement of 29 dB is observed. A comparison between Fig.5.20 (a) and (b) show that there is no power penalty for transmission.

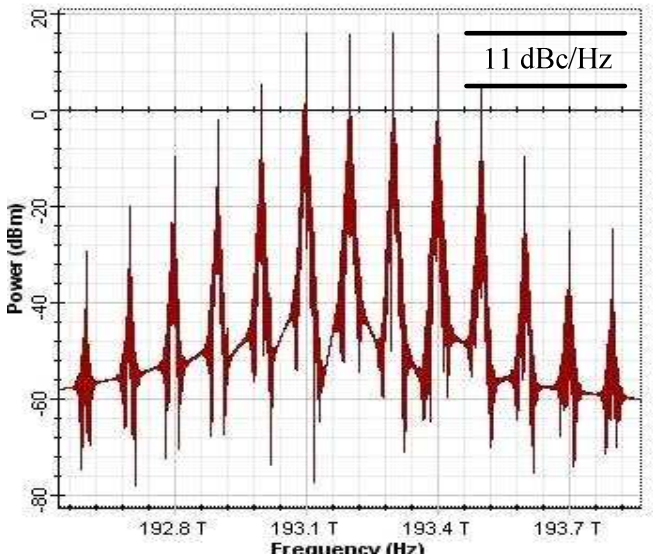

(a)

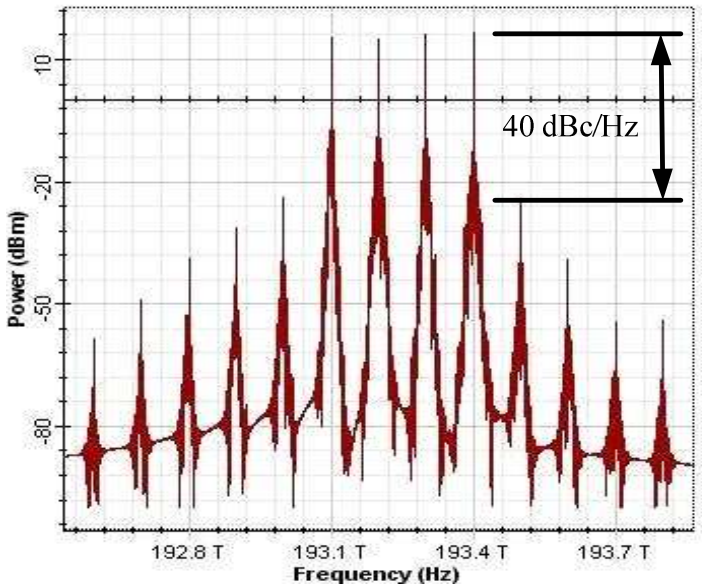

(b)

Figure 5.20 (a): Signal spectrum before linearization, and (b): signal spectrum after linearization

5.8 Summary

This chapter described a brief introduction of WDM lightwave system and optical networks such as wide area, metro area, and multi access WDM networks. Then the WDM system performance issues briefly was explained such as hetero wavelength linear cross talk, homo wavelength linear cross talk, cross phase modulation, and four wave mixing. The multi modulation (i.e. BPSK, QPSK, 16-QAM, and 64-QAM) system over fibre simulation model with the use of WDM was explained with the detail block diagram in transmitter and receiver for each modulation. The simulation results have been discussed base on the constellation point, eye diagram, OSNR, and spectrum for four channels. Finally the feedforward linearization technique was applied to this system which improved the harmonic distortion more than 29 dBc/Hz.

CHAPTER 6

Conclusion

6.1 Conclusion

The investigation of a radio-over-fibre distribution system with feed-forward and Predistortion feedback linearization of semiconductor optical amplifier (SOA) for communication systems has been proposed. The simulation verified these two linearization techniques for single tone direct modulation, two tone indirect modulation and ultra wideband input to the optical fibre. These techniques uses the ASE noise reduction in two loops of SOA by a feed-forward and Predistortion linearizer and is shown more than 6dB improvement. Also it was investigated linearization for the SOA amplifier to cancel out the third order harmonics or inter-modulation distortion (IMD) or four waves mixing. In this project, two channels have been used and have seen more than 20 dB reductions in the spectral re-growth caused by the SOA. Amplifier non-linearity becomes more severe with two strong input channels leading to inter-channel distortion which can completely mask a third adjacent channel. A reduction of 20 dB in inter-modulation distortion was achieved with the feed-forward and Predistortion compensation. The simulations were performed utilizing optimum settings for the variable gain, phase and delay components in the error correction loop of the feed-forward and Predistortion systems and hence represent the ideal situation of a perfect feed-forward and Predistortion system. Therefore it should be consider that complexity of circuit will increased due to imperfect amplitude, phase and delay matches in practical design. It was also shown that the WDM architecture allows efficient distribution of signals from the

central station to the base stations and vice versa. The limitation of transmission distance for optical feed-forward and Predistortion transmitters are overcome. The results suggest that Feedforward and Predistortion linearization allows successful transmission of multiple channels in a wireless-over-fibre system.

6.2 Future Work

The performance of the RoF access network using Software Defined Radio (SDR) in a central base station (CBS) is one of the most demanded technologies in the next generation mobile communication. The relation between RoF and SDR technologies mainly concerns the infrastructure part of the current and future standards radio access networks. For the deployment of current and the future radio access networks, new technologies like RoF and SDR can be used to allow faster routing of new services, simultaneous provisioning of different radio standards and flexible migration to the future radio air interfaces. Innovative Research, development and proof of concept will be sought in an end-to-end aspect, stretching from user device all the way up to base station end. System will provide a complete set of simulation to associated executable environments for multiple air interfaces which will yield to flexible and scalable infrastructure that optimize resource usage.

Here explained is a design of inter-working between wired and wireless as shown in Fig.6.1. Enabling a design to operate on multiple air interfaces will open up new issues for future research on mobility management across different networks.

The key enabler is all RF transport technology that delivers the full benefits of SDR to all points within urban, suburban and rural service areas. This solution is an application of the Outdoor Long Range Coverage Solution and Indoor Short Range Coverage Solution that are in use today in traditional base stations [140].

To meet the explosive demands of high-capacity and broadband wireless access, increase in the number of cells and utilization of higher frequency bands are proposed which leads to a large number of base stations (BSs) to be deployed; therefore, cost effective BS development is a key to success in the market. In order to reduce the system cost, HFR technology has been proposed since it provides functionally using simple remote antenna units (RAU) that are interconnected to a central base station (BS) via an optical fibre.

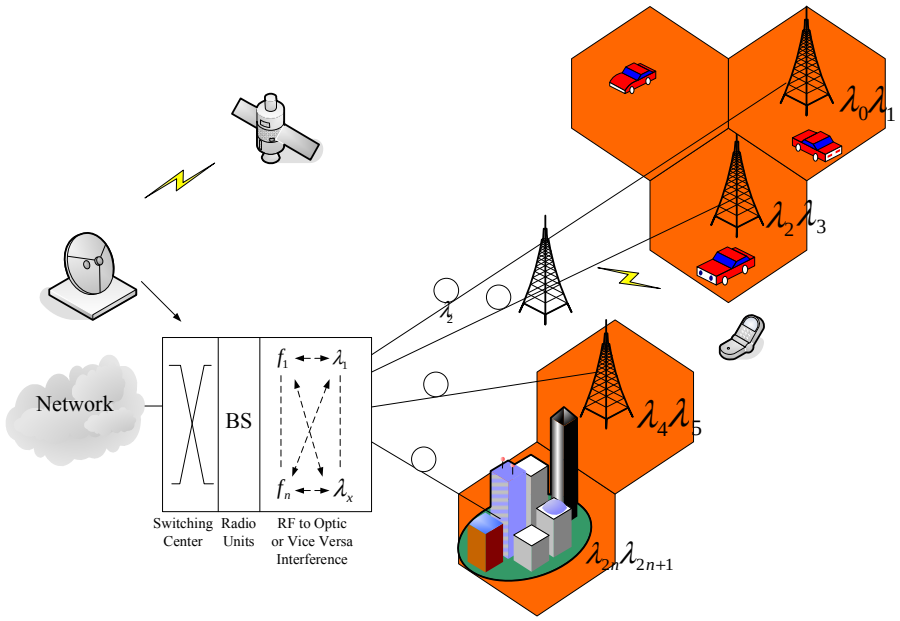

Figure 6.1 End-end network model

For long distance wired communication the fibre causes dispersion and needed for the amplifier, which add non-linearity to the system. The solution to this problem is to implement the linearization technique. But precise control is required for the each wavelength.

To serve users in the order of hundreds/thousands, an area of 5- 10 square miles need to be covered which can't be served from one split point. That is why; multiple split

points in the architecture is needed thus leading to a multistage design. Two possible architectures; Star and Ring are shown in Fig.6.2-3 respectively.

The first structure is star topology, which has easier implementation but less coverage and consists of three major parts as is shown in Fig. 6.11. First the remote antenna unit (RAU) which has multi band antenna to cover all appropriate frequency bands and the electro-absorption modulator to convert the electrical to optical signal and vice versa. Optical part is the next block in the star topology which the main components are multiplexer, demultiplexer and optical amplifier, which has been explained in the previous chapter. Finally the base station which consist of detector to detect the optical signal, tuneable laser and the RF circuitry (filter, amplifier, LNA, and so on), also this part has been described in chapter 5. In up link each RAU dedicate a wavelength to the multiple arrival frequency. This signal is sent to the multiplexer and then to the optical amplifier. The amplified signal is fed to the demultiplexer and then to the detector. Finally the electrical detected signal is filtered, to distinguish the different frequency band and down conversion to the intermediate frequency. For the down link the process is established in the reverse direction as shown in Fig. 6.2.

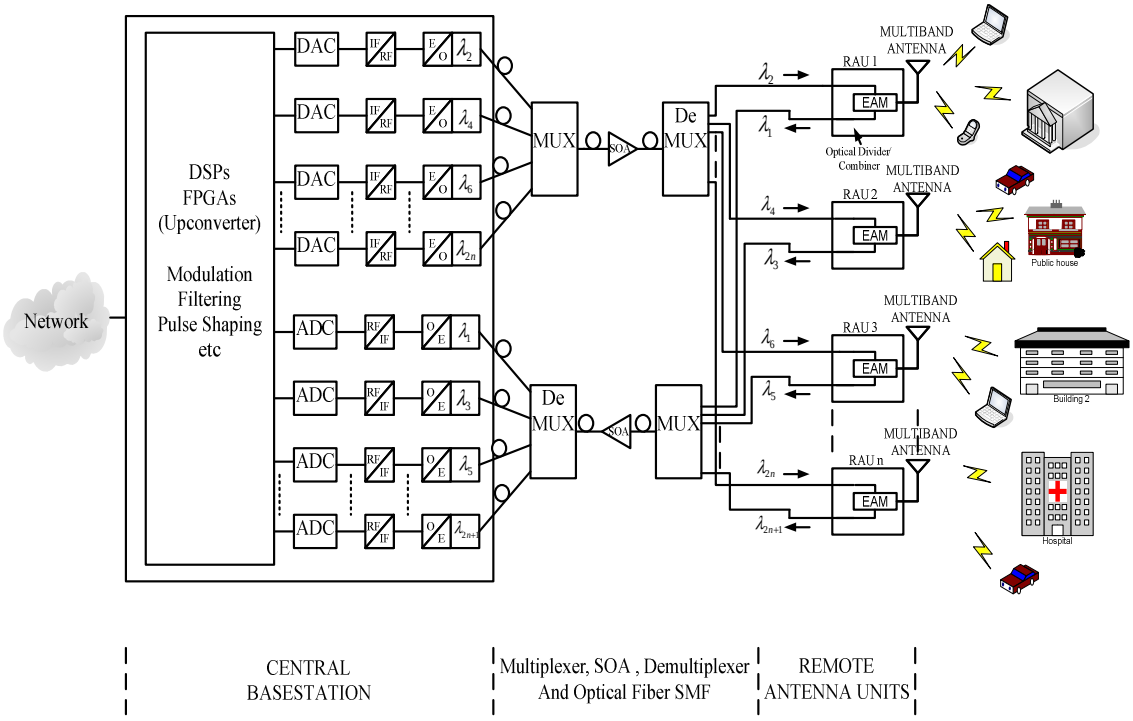

Figure 6.2 RoF system design for up/down link (star topology)

The alternative structure is ring topology, by increasing demand on bandwidth, force the service providers to the development of the re-configurability of optical network mainly relies on the integration of Reconfigurable Optical Add/Drop Multiplexer (ROADM) modules, which the simulation model has been shown in the next section. A reconfigurable device such as, ROADM can be defined as an optical module capable of adding/dropping, or passing through (express) any or all wavelengths present in the Wavelength Division Multiplexed (WDM) signal. ROADM offers pay-as-you grow capability and flexibility on the provisioning of wavelengths regardless of how the network changes. It effectively alleviates the need for service provisioning when new services are added to the network and offers absolute flexibility to the service providers. By using ROADMs, carriers can achieve re-configurability on wavelengths in every corner of their optical network – starting from the core to the

small home network. They would be able to control any set of wavelengths to be added/dropped or forwarded to any part of their network.

Figure 6.3 is shown the design of a ring architecture which has N number of downlink (DL) wavelengths, and N number of uplink (UL) wavelengths. One OADM node consists of a DL, and an UL thus making a total of 20 nodes channel in the network. These 20 nodes channel are distributed in two route one as a main the other as diversity. Each RAU with the dedicated wave length will transmit to or receive from the assigned OADM node pair (main and diversity).

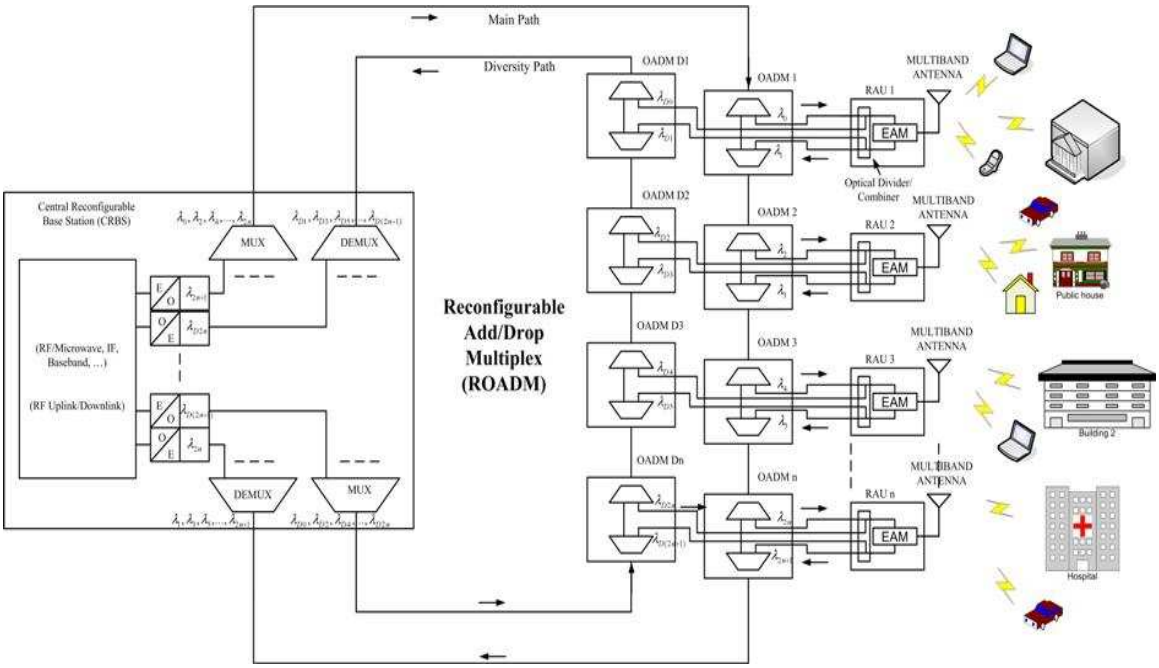

Figure 6.3 HFR system design for up/down link (ring topology)

Currently, there are ten's of Wireless air interfaces available in global wireless communication world. Each air interface has benefits and drawbacks depending on their application scenario. Here the converge is not only the current but also the legacy and next generation radio interfaces to enhance the over all system efficiency in terms of 'best connected and reconfigurable QoS, also the low cost, fast data

transmission on end user demand, 90% of service providers have their backbone based on optical fibre. Optical fibre provides huge bandwidth and also higher capacity to transmit. Fibre has a dedicated power source so by deploying several low cost and simple RAU will result in less power transmission for wireless devices to access points (RAU). Instead of transmitting data to a base station that could be at a distance of 2 Km, devices can transmit it to nearest installed RAU and save huge battery power saving.

The main task is to develop a simulation model with different modulation, which will facilitate the use of an important technology in the next generation systems with the use of ROADM topology. Previous chapter has described the WDM for different modulation scheme by the use of the star topology.

.

References

[1] D. Z. Hsu, S. L. Lee, P. M. Gong, Y. M. Lin, S. W. Lee and M. C. Yuang, "High-efficiency wide-band SOA-based wavelength converters by using dual-pumped four-wave mixing and an assist beam," *IEEE Photon. Technol. Lett.*, Vol. 16, PP. 1903-1905, Aug. 2004.

[2] L. Roselli, V. Borgioni, F. Zepparelli, F. Ambrosi, M. Comez, P. Faccin and A. Casini, "Analog laser predistortion for multiservice radio-overfiber systems," J. Lightw. Technol., Vol. 21, PP. 1211–1223, May. 2003

[3] P. B. Kenington, *High-Linearity RF Amplifier Design*. Norwood, MA: Artech House, 2000.

[4] S. Tanaka, N. Taguchi, T. Kimura, and Y.Atsumi, "A predistortion type equi-path linearizer designed for radio-on-fibre system," *IEEE Trans. Microw. Theory Tech.*, Vol. 54, PP. 938-944, Feb. 2006.

[5] A. H Coskun and S. Demir, "A Mathematical characterization and analysis of a feedforward circuit for CDMA applications," *IEEE Trans. Microw. Theory Tech.*, Vol. 51, PP. 767-777, Mar. 2003.

[6] N. Pothecary, *Feedforward Linear Power Amplifiers*. Norwood, MA: Artech House, 1999

[7] M.; Berger, J.; Ley, A.J.; Levi, I.M.; Kagan, Y.; "Progress in externally modulated AM CATV transmission systems", *Lightw. Technol.*, Vol. 11, PP.82-106, Jan. 1993.

[8] B. Buxton and R. Vahldieck, "Noise and intermodulation distortion reduction in an optical feedforward transmitter", *IEEE MTT-S International*, Vol. 2, PP. 1105-1108, May 1994.

[9] T. Iwai, K. Sato and K. Suto, "Signal distortion and noise in AM-SCM transmission systems employing the feedforward linearized MQW-EA external modulator," *Lightw. Technol.*, Vol. 13, PP.1606-1612, Aug. 1995.

[10] Y. Chiu, B. Jalali, S. Garner and W.Steier, "Broad-band electronic linearizer for externally modulated analog fiber-optic links" *IEEE Photon. Technol. Lett.*, Vol. 11, PP. 48-50, Jan. 1999.

[11] E. I. Ackerman, "Broad-band linearization of a Mach-Zehnder electro-optic modulator," *IEEE Microw. Microw. Theory Tech.*, Vol. 3, PP. 13-19, Jun. 1999.

[12] L. Roselli, V. Borgioni, F. Zepparelli, M. Comez, P. Faccin and A. Casini, "Predistortion circuit design for II and III order simultaneous linearization in multiservice telecommunications apparatuses," *IEEE Microw. Microw. Theory Tech.*,

Vol. 3, PP. 1711-1714, June 2002.

[13] T.R. Clark and M.L. Dennis, "Photonic downconversion and linearization of an X-band fiber optic link using optical I/Q demodulation Clark," *IEEE Lasers & Electro-Optics Society*, PP. 1-2, May 2007.

[14] Lim, C.; Lee, K.-L.; "Investigation of Intermodulation Distortion Reduction Technique for Multi-Channel Fiber-Radio Transmission in Heterogeneous Access Networks," *IEEE Lasers & Electro-Optics Society*, PP. 264-265, Oct. 2006.

[15] Shimoda, T.; Machida, S.; Mukai, T.; Saito, Y.; Kasaba, Y.; Hayakawa, H.; "Evaluation of the Asymmetry in Photoelectron Distribution Around the GEOTAIL Spacecraft," *IEEE Photon. Technol. Lett.* Vol. 36, Issue 5, Part 2, pp. 2253 – 2261, Oct. 2008.

[16] N. A. Olsson, "Light wave signal with optical amplifier," *J. Lightw. Technol.*, Vol. 7, pp. 1071-1082, July 1989.

[17] Yoshihisa Yamamoto, Coherence, Amplification, and Quantom Effects in Semiconductor Lasers. Wiley, 1991.

[18] Govind P. Agrawal, Semiconductor Lasers: Past, Present, and Future (Aip Series in Theoretical and Applied Optics). Amer Inst of Physics, 1995.

[19] I. P. Kamino, T. Li and A.E. Willner, Optical Fiber Telecommunications V A, Academic Press, 2008.

[20] C.E. Zah, J.S. Osinski, C. Caneau, S.G. Menocal, L.A. Reith, J. Salzman, F.K. Shokoohi and T.P. Lee, "Fabrication and performance of 1.5ým GlanAsP travelling-wave laser amplifiers with angled facets," *IEE Electron Lett.*, Vol.23, PP. 990-992, September 1987.

[21] I. Cha, M. Kitamura, H. Honmou and I. Mito, "1.5 mu m band travelling-wave semiconductor optical amplifiers with window facet structure," *IEE Electron Lett.*, Vol. 25, PP. 1241-1242, Aug. 1989.

[22] N.A. Olsson, M.G. Oberg, L.A. Koszi and G. Przyblek, "400 Mbit/s, 372 km coherent transmission experiment using in-line optical amplifiers," *IEE Electron Lett.* Vol. 24, PP. 36-38, Jan. 1988.

[23] S. Cole, D.M. Devlin, W.J. Devlin, A.D. Ellis, D.J. Elton, J.J. Isaac, G. Sherlock, P.C. Spurdens and W.A. Stallard, "Polarisation-insensitive, near-travelling-wave semiconductor laser amplifiers at 1.5 mu m," *IEE Electron Lett.* Vol. 25, PP. 314-315, March 1989.

[24] G. Grobkopf, R. Ludwig, R.G. Waarts and H.G. Weber, "Optical amplifier configurations with low polarisation sensitivity," *IEE Electron Lett.* Vol. 23, PP. 1387-1388, December 1987.

[25] N.A. Olsson, "Polarisation-independent configuration optical amplifier," *IEE Electron Lett.* Vol. 24, PP. 1075-1076, Aug 1988.

[26] M. Sumida and M. Koga, "Practical gain of in-line semiconductor laser amplifiers" ***IEE Electron Lett.*** **Vol 25, PP. 875-877, June 1989.**

[27] M. Koga and T.Matsumoto, "High-gain polarization-insensitive optical amplifier" ***IEE Electronic Lett.*** **Vol. 9, PP. 284-290, Feb. 1991.**

[28] Agrawal, G.P.; "Effect of gain nonlinearities on the dynamic response of single-mode semiconductor lasers," ***IEEEPhoton. Technol. Lett.*** **Vol. 1, Issue 12, . pp. 419 – 421, Dec. 1989**

[29] G. P. Agrawal, Appl. Phys. Lett. 51, 302, 1987; J. Opt. Soc. Am. B5, 147, 1988

[30] G.P. Agrawal, "Amplifier-induced crosstalk in multichannel coherent lightwave systems," ***IEE Electron Lett.,*** **Vol. 23, PP. 1175-1177, October 1987.**

[31] I.M.I. Habbab and G.P. Agrawal, "Asymmetric channel gain and crosstalk in traveling wave optical amplifiers," ***J. Lightw. Technol.,*** **Vol. 7, PP. 1351-1359, Sept. 1989.**

[32] S. Ryu, K. Mochizuki and H. Wakabayashi, "Influence of nondegenerate four-wave mixing on coherent transmission system using in-line semiconductor laser amplifier," ***J.Lightw. Technol.*** **Vol. 7, PP. 1525-1529, Oct. 1989.**

[33] G.P. Agrawal and I.M.I. Habbab, "Effect of a four-wave mixing on multichannel amplifification in semiconductor laser amplifiers" ***IEEE J. Quantum Electron.,*** **Vol. 26, PP. 501-505, March 1990.**

[34] H. Kawaguchi, "Progress in optical functional devices using two-section laser diodes/amplifiers," ***IEE Proc. J.,*** **Vol. 140, PP. 3-15, Feb. 1993.**

[35] Petrantonakis, D.; Zakynthinos, P.; Apostolopoulos, D.; Poustie, A.; Maxwell, G.; Avramopoulos, H.; "All-Optical Four-Wavelength Burst Mode

Regeneration Using Integrated Quad SOA-MZI Arrays," ***IEEE Photon. Lett.*****, Vol 20, Issue 23, pp. 1953 – 1955, Dec. 2008.**

[36] K.E. Stubkjaer, "Semiconductor optical amplifier-basd all-optical processing," ***IEEE J.Quantum Electron.*** **Vol. 6, PP. 1428-1435, Dec. 2000.**

[37] R. E. Slusher and B. J. Eggleton, Nonlinear Photonic Crystals., springer, 2004.

[38] Agrawal, G.P.; Olsson, N.A.; "Self-phase modulation and spectral broadening of optical pulses in semiconductor laser amplifiers," ***IEEE J. Quantun Electron.*****, Vol 25, Issue 11, pp. 2297 – 2306, Nov. 1989.**

[39] G. P. Agrawal, Lightwave Technology: Components and Devices, Wiley, 2004.

[40] V. Petrovic and C. N. Smith, "Reduction of intermodulation distortion by means of modulation feedback," presented at IEE conference on Radio Spectrum Conversion Techniques, 1983.

[41] M. Johnsson and L. Sundstrom, "Linearization of RF multicarrier amplifiers using Cartesian feedback," ***IEEE Electron Device Lett.,*** **Vol. 30, PP. 1110-1112, July 1994.**

[42] M. Bolooran and J. P. McGeehan, "Twin-loop cartesian transmitter (TLCT)," ***IEEE Electron Device Lett.,*** **Vol.32, PP. 971-972, May 1996.**

[43] M.A. Briffa and M. Faulkner, "Stability analysis of Cartesian feedback linearisation for amplifiers with weak nonlineares," ***IEE Proceedings on Communications,*** **Vol. 143, PP. 212-218, Aug. 1996.**

[44] S.I. Mann, M.A. Beach and K.A. Morris, "Digital baseband cartesian loop transmitter," ***IEE Electron Lett.*** **Vol. 37, PP. 1360-1361, Oct. 2001.**

[45] J.Yi, Y. Yang, M. Park, and W.Kang, "analog predistortion linearization for high power RF amplifier," presented at IEEE MTT-S International Microwave Symposium Digest, 2000.

[46] C. Potter, "A 3G Base-Station PA Design Using Load Pull and adaptive Digital predistortion, "Wireless Design Conference, pp. 141-144, 2002.

[47] S. C. Cripps, RF Power Amplifiers for Wireless Communications, Artech House Publisher, 2006.

[48] C. Haskins, T. Winslow and S. Raman, "FET diode linearizer optimization for amplifier predistortion in digital radios," *IEEE Microw. Guided Wave Lett. (until 2002),* Vol. 10, PP. 21-23, Jan. 2000.

[49] K.A. Morris and J.P. McGeehan, "Gain and phase matching requirements of cubic predistortion systems," *IEE Electron Lett.*, Vol.36, PP. 1822-1824, Oct. 2000.

[50] S.C. Cripps, "RF power amplifiers for wireless communications," *IEEE Microw. Mag.*, Vol. 1, PP. 64-64, March 2000.

[51] M. Ghaderi, S. Kumar and D.E. Dodds, "Adaptive predistortion lineariser using polynomial functions," *IEEE*...., Vol. 141, PP. 49-55, April 1994.

[52] S. Kusunoki, K. Yamamoto, T. Hatsugai, H. Nagaoka, K. Tagami, N. Tominaga, K. Osawa, K. Tanabe, S. Sakurai and T. Lida, "Power-amplifier module with digital adaptive predistortion for cellular phones," Vol. 50, PP. 2979-2986, Dec. 2002.

[53] C.G. Rey, 'predistorter linearized CDMA power amplifiers," Microwaves & RF ,pp. 114-123, 1998.

[54] K. J. Muhonen, M. Kavehrad, and R. Krishnamoorthy, " presented at Thirty_Third Asilomar Conference on Signals, Systems and Computers, 1990.

[55] J.K. Cavers, "Amplifier linearization using a digital predistorter with fast adaptation and low memory requirements," *IEEE Trans. Veh. Technol.*, Vol. 39, PP. 374-382, Nov. 1990.

[56] J. Kim and K. Konstantinou, "Digital predistortion of wideband signals based on power amplifier model with memory," *IEE Electron. Lett.*, Vol. 37, PP. 1417-1418, Nov. 2001.

[57] J.K. Cavers, "Optimum indexing in predistorting amplifier linearizers," *IEEE Trans. Veh. Technol.*, Vol. 2, PP. 676-680, May 1997.

[58] J.K. Cavers, "Optimum table spacing in predistorting amplifier linearizers," IEEE Trans. Veh. Technol., Vol. 48, PP. 1699-1705, Sept. 1999.

[59] L. Sundstrom, " Digital RF power Amplifier Linearisers," in Department of Applied Electronics. Lund: Lund University, 1995, pp. 64.

[60] F. Zavosh, M. Thomas, C. Thron, T. Hall, D. Artusi, D. Anderson, D.Ngo, and D. Runton, 'Digital predistortion techniques for RF power amplifiers with CDMA APPLICATIONS," Microwave Journal, pp. 8, 1999.

[61] H. S. Black, "Translating System," U. S. P. Office, Ed., 1928, pp.6

[62] H. Seidel, "AFeedforward Experiment Applied to an L-4 Carrier System Amplifier," *IEEE Trans. Commun. Technol.*, Vol.19, PP. 320-325, June. 1971.

[63] T. Bennett and R. F. Clements, " Feedforward- An alternative approach to amplifier linearization, "RF, Radio and Electronic Engineer, vol. 44, pp. 257-262, 1974.

[64] N. Pothecary, Feedforward Linear Power Amplifiers. Norwood : Artech House Ink. , 1999

[65] A.H. Coskun and S. Demir, "A mathematical characterization and analysis of a feedforward circuit for CDMA applications," *IEEE Trans. Microw. Theory* Tech., Vol. 51, PP. 767-777, March 2003.

[66] N. Pothecary, Feedforward Linear Power Amplifiers. Norwood, MA: Artech House, 1999.

[67] M. Adams, H. Westlake, M. O'Mahony and I. Henning, "A comparison of active and passive optical bistability in semiconductors," *IEEE Quantom Electron.," Vol. 21, PP. 1498-1504, Sep. 1985.*

[68] T.G. Hodgkinson and R.P. Webb, "Application of communications theory to analyse carrier density modulation effects in travelling-wave semiconductor laser amplifiers," *IEE Electron. Lett.,* Vol. 24, PP.1550-1552, Dec 1988.

[69] Yoshishisa Yamamoto, "Characteristics of AlGaAs fabry-perot cavity type laser amplifiers," IEEE J. Quantum Electron., Vol. 16, PP. 1047-1052, Oct. 1980.

[70] Peter B. Kenington, RF and Baseband Techniques for Software Defined Radio. Boston, MA: Artech House, 2005.

[71] K.J. Parsons and P.B. Kenington, "The efficiency of a feedforward amplifier with delay loss," *IEEE Trans. Veh. Technol.,* Vol. 43, PP. 407-412, May 1994.

[72] T. Saitoh and T. Mukai, "Recent progress in semiconductor laser amplifiers," *J. Lightw. Technol.,* Vol. 6, PP. 1656-1664, Nov. 1988.

[73] F. Zeng and J. Yao, "An approach to ultra wideband and pulse generation and distribution over optical fiber," *IEEE Photon. Technol. Lett.,* Vol.18, PP. 823-825, Apr. 2006.

[74] M.Z. Win and R.A. Scholtz, "Impulse radio: how it works," *IEEE Commun Lett.* Vol. 2, PP. 36-38, Feb. 1998.

[75] G.R. Aiello, "Challenges for ultra-wideband (UWB) CMOS integration," *IEEE Radio Frequency Integrated Circuits (RFIC) Symposium*, PP. 497-500, June 2003.

[76] E. Docket, "Revision of part 15 of the commission's rules regarding ultra-wideband transmission systems, first report and order," FCC-2-48, Apr. 2002.

[77] C. M. Tan, L. C. Ong, M. L. Yee, B. Luo, and P. K. Tang, "Direct transmission of ultra wideband signals using single mode radio-over-fiber system," in Proc APMC, 2005,

[78] S. Kim, H. Jang, S. Choi, Y. Kim and J. Jeong, " Performance evaluation for UWB signal transmission with different modulation schemes in multi-cell environment distributed using RoF technology," *IEEE in Proc UWBST*, PP. 187-191, May 2004.

[79] M. Ghavami, L. Michael and R. Kohno, Ultra Wideband Signals and Systems in Communication Engineering, Wiley, 2007.

[80] A.H. Coskun and S. Demir, "A mathematical characterization and analysis of a feedforward circuit for CDMA applications," *IEEE Trans. Microw. Theory Tech.* Vol. 51, PP. 767-777, March 2003.

[81] R.I. Bogya and M.E. Magana, "Linear radio frequency power amplifier design using nonlinear feedback linearization techniques," *IEEE Trans. Veh. Technol.*, Vol. 3, PP. 2259-2263, Sept. 2004

[82] T. Nesimoglu, C.N. Canagarajah and J.P. McGeehan, "Analysis and performance of simple active feedback linearisation scheme," *IEE Electron. Lett.*, Vol. 36, PP. 703-705, April 2000.

[83] J Legarda, "Feedforward Amplifiers for Wideband Communication Systems", Sringer, Netherland, 2006

[84] H. Ishio, J. Minowa and K. Nosu, "Review and status of wavelenght-division-multiplexing technology and its application," *J. Lightw. Technol.*, Vol. 2, PP. 448-463, Aug. 1984.

[85] G. Winzer, "Wavelength multiplexing components--A review of single-mode devices and their applications," *J. Lightw. Technol.*, Vol. 2, PP. 369-378, Aug. 1984.

[86] N.A. Olsson, J. Hegarty, R.A. Logan, L.F. Johnson, K.L. Walker, L.G. Cohen, B.L. Kasper and J.C. Campbell, "68.3 km transmission with 1.37 Tbit km/s capacity using wavelength division multiplexing of ten single-frequency lasers at 1.5 ým," *IEE Electron. Lett.*, Vol. 21, PP. 105-106, Jan. 1985.

[87] C.A. Brackett, "Dense wavelength division multiplexing networks: principles and applications," *IEEE J. Sel Areas Commun.*, Vol. 8, PP. 948-964, Aug. 1990.

[88] J. Zyskind and R. Berry, in Optical Fiber Telecommunications IV, Vol. B, I. P. Kaminov and T. Li, Academic Press, San Diego, CA, 2002

[89] A.R. Chraplyvy, A.H. Gnauck, R.W. Tkach, R.M. Derosier, E.R. Giles, B.M. Nyman, G.A. Ferguson, J.W. Sulhoff and J.L. Zyskind, "One-third terabit/s transmission through 150 km of dispersion-managed fiber," *IEEE Photon. Technol. Lett.*, Vol. 7, PP. 98-100, Jan. 1995.

[90] K. Fukuchi, T. Kasamatsu, M. Morie, R. Ohhira, T. Ito, K. Sekiya, D. Ogasahara and T. Ono, "10.92- Tb/s (273*40-Gb/s) triple-band/ultra-dense WDM optical-repeatered transmission experiment," *Optical fiber commun. Conf.*, Vol.4, PP. PD24-1 - PD24-3, 2001.

[91] N.S. Bergano and C.R. Davidson, "Wavelength division multiplexing in long-haul transmission systems," *J. Lightw. Technol.*, Vol.14, PP. 1299-1308, June 1996.

[92] I. P. Kaminow, Optical Fiber Telecommunication IV-B, Academic Press, 2002.

[93] B. Mukherjee, Optical Communication Networks, Mcgraw-Hill, 1997.

[94] A. Borella, G. Cancellieri, and F. Chiraluce, WDMA Optical Networks, Artec House, Norwood, MA, 1998.

[95] R. A. Barry. Optical Networks and Their Apllications, Optical Society of America, Washington, DC, 1998

[96] T. E. Stern, Georgios and K. Bala, Multiwavelength Optical Networks: Architecture, Design, and Control., Cambridge University Press, 2008.

[97] G. Keiser and G. Keiser, Optical Fiber Communications, McGraw-Hill Science/Engineering/Math., 1999.

[98] K. M. Sivalingam, S. Subramaniam, Optical WDM Network -Principles and Practice, Springer, 2000.

[99] S. Binetti, A. Bragheri, E. Lannone and F. Bentivoglio, "Mesh and multi-ring optical networks for long-haul applications," *J. Lightw. Technol.*, Vol. 18, PP. 1677-1684, Dec. 2000.

[100] A.A.M. Saleh and J.M. Simmons, "Architectural principles of optical regional and metropolitan access networks," *J. Lightw. Technol.*, Vol. 17, PP. 1999, Dec. 1999.

[101] W.T. Anderson, J. Lackel, G.K. Chang, Dai Hongxing, Wei Xin, M. Goodman, C. Allyn, M. Alvarez, A. Tzathas, R. Vora, L. Mercer, H. Dardy, E. Renaud, L. Williard, J. Perreault, R. McFarland and T. Gibbsons, "The

MONET project-a final report," *J. Lightw. Technol.* Vol. 18, PP. 1988-2000, Dec. 2000.

[102] P.E. Green Jr., "Optical networking update," *IEEE J. Sel. Areas Commum.*, Vol. 14, PP. 764-779, June 1996.

[103] I. P. Koch and T. L. Kaminow, Optical Fiber Telecommunications III, academic Pr, 1997.

[104] T. Pfeiffer, J. Kissing, J.-P. Elbers, B. Deppisch, M. Witte, H. Schmuck and E. Voges., "Coarse WDM/CDM/TDM concept for optical packet transmission in metropolitan and access networks supporting 400 channels at 2.5 Gb/s peak rate," *J. Lightw. Technol.* Vol. 18, PP. 1928-1938, Dec. 2000.

[105] N. Ghani, J. Y. Pan, and X. Cheng, in Optical Fiber Telecommunications IV, Vol. A, I. P. Kaminow and T. Li, Eds., Academic Press. San Diego, CA, 2002

[106] E. Harstead and P. H. van Heyningen, in Optical Fiber Telecommunications IV, Vol. A, I. P. Kaminow and T. Li, Eds., Academic Press, San Diego, CA, 2002

[107] P.W. Dowd, "Wavelength division multiple access channel hypercube processor interconnection," *IEEE Trans. Comput.*, Vol. 41, PP. 1223-1241, Oct. 1992.

[108] M.S. Goodman, H. Kobrinski, M.P. Vecchi, R.M. Bulley and J.L. Gimlett, "The LAMBDANET multiwavelength network: architechre, applications, and demonstrations," *IEEE J. Sel. Areas Commun.* Vol. 8, PP. 995-1004, Aug 1990.

[109] E. Hall, J. Kravitz, R. Ramaswami, M. Halvorson, S. Tenbrink and R. Thomsen, "The Rainbow-II gigabit optical network," *IEEE J. Sel. Areas Commun.*, Vol. 14, PP. 814-823, June 1996.

[110] D. Sadot and L.G. Kazovsky, "Power budget optimization of STARNET II: an optically amplified direct-detection WDM network with subcarrier control," *J. Lightw. Technol.* Vol.15, PP. 1629-1635, Sept. 1997.

[111] S.S. Wagner, H. Kobrinski, T.J. Robe, H.L. Lemberg and L.S. Smoot, "Experimental demonstration of a passive optical subscriber loop architecture," *IEE Electron. Lett.*, Vol. 24, PP. 344-346, March 1988.

[112] P.A. Rosher and A.R. Hunwicks, "The analysis of crosstalk in multichannel wavelength division multiplexed optical transmission systems and its impact on miltiplexer design," *IEEE J. Sel. Areas Commun.*, Vol. 8, PP. 1108-1114, Aug. 1990.

[113] G. P. Agrawal, Fiber-Optic Communication Systems, Wiley-Interscience, 2002.

[114] P.A. Humblet and W.M. Hamdy, "Crosstalk analysis and filter optimization of single- and double- cavity Fabry-Perot filters," *IEEE J. Sel. Areas Commun.*, Vol. 8, PP. 1095-1107, Aug. 1990.

[115] E.L. Goldstein and L. Eskildsen, "Scaling limitations in transparent optical networks due to low-level crosstalk," *IEE Photon. Technol. Lett.*, Vol. 7, PP. 93-94, Jan. 1995.

[116] Y. D. Jin, Q. Jiang, and M. Kavehrad, IEEE Photon. Technol Lett. 7, 1210, 1995

[117] D.J. Blumenthal, P. Granestrand and L. Thylen, "BER floors due to heterodyne coherent crosstalk in space photonic switches for WDM networks," IEE Photon. *Technol. Lett.*, Vol. 8, PP.284-286, Feb. 1996.

[118] H. Takahashi, K. Oda and H. Toba, "Impact of crosstalk in an arrayed-waveguide multiplexer on N*N optical interconnection," *J. Lightw. Technol.*, Vol. 14, PP. 1097-1105, June. 1996.

[119] Jingyu Zhou, R. Cadeddu, E. Casaccia, C. Cavazzoni and M.J. O'Mahony, "Crosstalk in multiwavelength optical cross-connect networks," *J. Lightw. Technol.*, Vol. 14, PP. 1423-1435, June 1996.

[120] P.K. Pepeljugoski and K.Y. Lau, "Interferometric noise reduction in fiber-optic links by superposition of high frequency modulation," *J. Lightw. Technol.*, Vol. 10, PP. 957-963, July 1992.

[121] G. P. Agrawal, Nonlinear Fiber Optics, 3rd ed.,Academic Press, San Diego, CA, 2001

[122] A. V. T. Cartaxo,; "Influence of the Channel Number on the Optimal Dispersion Map Due to XPM in WDM Links," *J. Lightw. Technol.*, Vol. 26, Issue 22, pp. 3640 - 3649, Nov.15, 2008.

[123] G. Bellotti and S. Bigo, "Cross-phase modulation suppressor for multispan dispersion-managed WDM transmissions," *IEEE Photon. Technol. Lett.*, Vol. 12, PP. 726-728, June 2000.

[124] R.I. Killey, H.J. Thiele, V. Mikhailov and P. Bayvel, "Prediction of transmission penalties due to cross-phase modulation in WMD systems using a simplified technique," *IEE Photon. Technol. Lett.*, Vol. 12, PP. 804-806, July 2000.

[125] N. Shibata, R. Braun and R. Waarts, "Phase-mismatch dependence of efficiency of wave generation through four-wave mixing in a single-mode optical fiber," *IEEE J. Quantum Electron.*, Vol. 23, PP. 1205-1210, July 1987.

[126] F. Forghieri, R. W. Tkach, and A. R. Chraplyvu, in Optical Fiber Telecommunications III, Vol. A, I. P. Kaminow and T. L. Koch, Eds., Academic Press, San Diego, CA, 1997, Chap.8

[127] J. S. Lee, D. H. Lee, and C. S. Park, IEEE Photon. Technol. Lett. 10, 825, 1998

[128] P.B. Kenington, "Linearized transmitters: an enabling technology for software defined radio," *IEEE Commun Mag.*, Vol. 40, PP. 156-162, Feb. 2002.

[129]

[130]

[131] P.B. Kenington, "Emerging technologies for software radio," *IEE...*, Vol. 11, PP.69-83, April 1999.

[132] J.A. Wepman, "Analog-to-digital converters and their applications in radio receivers," *IEEE Commun Mag.*, Vol. 33, PP. 39-45, May 1995.

[133] P.B. Kenington, "Power consumption of A/D converters for software radio applications," *IEEE Trans. Veh. Technol.*, Vol. 49, PP. 643-650, March 2000.

[134] J. R. Smith, Modern Communication Circuits, McGraw-Hill Science/Engineering/Math, 1997.

[135] Kwang Young Kim, N. Kusayanagi and A.A. Abidi, "A 10-b, 100-MS/s CMOS A/D converter," *IEEE J. Solid-State Circuits*, Vol. 32, PP. 302-311, March 1997.

[136] Moore, G. E., "Cramming More Components onto Integrated Circuits", Electronics, Vol. 38, No. 8, April 19, 1965.

[137] A. Wiesler and F. K. Jondral, "A software radio for second- and third-generation mobile systems," *IEEE Trans. Veh. Technol.*, Vol. 51, PP. 738-748, July 2002.

[138] F.M Colebrook and Homodyne, "Wireless and radio review," No. 13, PP.774.

[139] L. Lessing, Man of High Fidelity: Edwin Howard Armstrong, a Biography, Bantam Books, 1969.

[140] P. Kenington, Rf and Baseband Techniques for Software Defined Radio, Artech House Publishers, 2005.